Available online at www.sciencedirect.com
ScienceDirect
Progress in Oceanography 76 (2008) 217–285
Progress in Oceanography
www.elsevier.com/locate/pocean

Particulate organic carbon fluxes to the ocean interior and factors controlling the biological pump: A synthesis of global sediment trap programs since 1983

Susumu Honjo [a,*], Steven J. Manganini [a], Richard A. Krishfield [a], Roger Francois [b]

[a] *Woods Hole Oceanographic Institution, Woods Hole, MA 02543, USA*
[b] *Department of Earth and Ocean Sciences, University of British Columbia, Vancouver, Canada*

Received 8 January 2007; received in revised form 5 May 2007; accepted 9 November 2007
Available online 18 January 2008

Abstract

Particulate organic carbon (POC) is vertically transported to the oceanic interior by aggregates and their ballasts, mainly $CaCO_3$ and biogenic opal, with a smaller role for lithogenic aerosols through the mesopelagic zone. Diel migrating zooplankton communities effect vertical transport and remineralization of POC in the upper layers of the ocean. Below 1.5 km, the presence of zooplankton is reduced and thus the aggregates travel mainly by gravitational transport. We normalized the fluxes of POC, $CaCO_3$, and biogenic opal from data published on samples collected at 134 globally distributed, bottom-tethered, time-series sediment trap (TS-trap) stations to annual mole fluxes at the mesopelagic/bathypelagic boundary (m/b) at 2 km and defined them as $F_{m/b}C_{org}$, $F_{m/b}C_{inorg}$, and $F_{m/b}Si_{bio}$. Using this global data set, we investigated (1) the geographic contrasts of POC export at m/b and (2) the supply rate of $\sum CO_2$ to the world mesopelagic water column. $F_{m/b}C_{org}$ varies from 25 (Pacific Warm Pool) to 605 (divergent Arabian Sea) mmolC m^{-2} yr^{-1}; $F_{m/b}C_{inorg}$ varies from >8 (high latitude Polar Oceans) or 15 (Pacific Warm Pool) to 459 (divergent Arabian Sea) mmolC m^{-2} yr^{-1}; and $F_{m/b}Si_{bio}$, the most spatially/temporally variable flux, ranges from 6 (North Atlantic Drift) to 1118 (Pacific Subarctic Gyre) mmolSi m^{-2} yr^{-1}. The oceanic region exhibiting the highest POC flux over a significantly large region is the area of the North Pacific Boreal Gyres where the average $F_{m/b}C_{org} = 213$, $F_{m/b}C_{inorg} = 126$, and $F_{m/b}$ $Si_{bio} =$ 578 mmol m^{-2} yr^{-1}. $F_{m/b}C_{org}$ and $F_{m/b}C_{inorg}$ are particularly high in large upwelling margins, including the divergent Arabian Sea and off Cape Verde. One of the data sets showing the lowest flux over a significant region/basin is $F_{m/b}$ $C_{org} = 39$, $F_{m/b}C_{inorg} = 69$, and $F_{m/b}Si_{bio} = 22$ mmol m^{-2} yr^{-1} in the North Pacific subtropical/tropical gyres; Pan-Atlantic average fluxes are similar except $F_{m/b}Si_{bio}$ fluxes are even lower. Where C_{org}/C_{inorg} and Si_{bio}/C_{inorg} are <1 defines the "Carbonate Ocean", and where these ratios are ⩾1 defines the "Silica Ocean". The Carbonate Ocean occupies about 80% of the present world pelagic ocean between the two major oceanographic fronts, the North Pacific Polar Front and the Antarctic Polar Front, and the Silica Ocean is found on the polar sides of these fronts. The total global annual fluxes of $F_{m/b}C_{org}$, $F_{m/b}C_{inorg}$, and $F_{m/b}Si_{bio}$ at m/b calculated by parameterizations of the export flux data from 134 stations are surprisingly similar; 36.2, 33.8, and 34.6 teramol yr^{-1} (120, 112, and 114 mmol m^{-2} yr^{-1}), respectively, resulting in a near uniform binary ratio between the above three elements of about one. The global ternary % ratios estimated from 152 TS-trap samples of the three elements are 35:32:33. From our global $F_{m/b}C_{org}$ and a published model estimate of the global export production, we estimate the regeneration rate of CO_2 through the mesopelagic zone by the biological pump is 441 teramolC yr^{-1}.

* Corresponding author. Tel.: +1 508 540 1162; fax: +1 508 540 9439.
E-mail address: shonjo@whoi.edu (S. Honjo).

0079-6611/$ - see front matter © 2008 Elsevier Ltd. All rights reserved.
doi:10.1016/j.pocean.2007.11.003

Based on our global $F_{m/b}C_{inorg}$ and recently estimated global primary production of PIC, 36–86 teramolC yr^{-1} of PIC is assumed to be dissolved within the upper 2 km of the water column.
© 2008 Elsevier Ltd. All rights reserved.

Keywords: Biological pump; POC; Global particle fluxes; Vertical transport; Remineralization; Mesopelagic CO_2 sink

1. Introduction

The "biological pump" (Volk and Hoffert, 1985) is a complex ecosystem process that efficiently and consistently transports large amounts of carbon molecules in the form of particulate organic carbon (POC) from the epipelagic zone to the deep interior of the world ocean and further to the abyssal floor. The biological pump begins in the euphotic zone where primary producers sequester dissolved CO_2 to produce POC and oxygen through photosynthesis [$CO_2 + H_2O \Leftrightarrow CH_2O$ (POC) $+ O_2$], that is, oceanic primary production (PP) (e.g., Berger et al., 1987, 1989; Antoine, 1996; Behrenfeld and Falkowski, 1997). The majority of POC, which occurs in both living and nonliving forms, is remineralized by metabolic processes in the epipelagic ecosystem that reverse the above reaction through respiration, and the resulting CO_2 is recycled within the mostly thermodynamically driven epipelagic pool. The remaining POC, roughly a fifth of the PP, penetrates the pycnocline as the export production of carbon (EP). However, on its own, unaggregated, nonliving POC detritus would not sink because its density is close to that of seawater, and it is metabolized before settling any significant depth. Two major processes for exporting this POC have been identified: transport by the zooplankton ecosystem, particularly by the diel migrators, and by gravitational settling of biogenic aggregates that are ballasted by heavy biomineral and aerosol lithogenic particles. Most POC thus delivered to the depths of the ocean is remineralized by the zooplankton community to form total CO_2 ($\sum CO_2$) sinks in the world ocean's interior and at the seafloor. Depending upon depth, these sinks retain CO_2 for a relatively long period (decadal to millennial) compared with the epipelagic CO_2 residence time. This grander cycle of carbon in the ocean, the biological pump, is a critical process in regulating Earth's climate by preventing runaway accumulation of CO_2 in the atmosphere.

The objectives of this article are as follows. First, to review existing observations and hypotheses regarding how the biological pump removes POC from upper ocean layers and transports it to the oceanic interior. Second, to clarify the regional and global characteristics of the biological pump by using published annual flux data from 134 moored sediment trap stations normalized to the annual flux at 2 km, the boundary between the mesopelagic and bathypelagic zones. Third, to provide the global geographic distribution, global total, and average fluxes of POC and major ballast particles ($CaCO_3$ and biogenic opal) at a standard depth using a statistical parameterization process and the data sets described in the Sections below. Fourth, to calculate the total rate of POC remineralization that contributes to the mesopelagic $\sum CO_2$ sink by gravitational settling and active transport by zooplankton through the mesopelagic zone.

The term "mesopelagic" (used as a noun) was first introduced by Hedgpeth (1957) but not clearly defined except for identifying this zone to be below the "epipelagic" and above the "bathypelagic". No upper and lower boundaries were specifically defined by depth or oceanographic function, but the mesopelagic is located between approximately 1.0 and 1.7 km in Hedgpeth's original figures. In this paper, we redefine the mesopelagic as below the pycnocline and above the lower limit of zooplankton/micronekton habitat. The depth of this lower limit is generally recognized as shallower than 1.5 km (e.g., Angel, 1989a,b; Angel and Baker, 1982; Angel et al., 1982; Arístegui et al., 2005; Kikuchi and Omori, 1985; Madin et al., 2006; Vinogradov and Tseitlin, 1983; Wiebe et al., 1979). The mesopelagic/bathypelagic boundary zone extends from 1.5 to 2 km. The epipelagic zone occupies the pelagic ocean from the surface to the pycnocline and includes the euphotic layer whose lower limit is defined by the depth of solar penetration.

As one of the results of this investigation, we present a compilation and synthesis of published observational results regarding settling particle export in the pelagic ocean measured by bottom-tethered, time-series sediment traps (TS-traps) over the past approximately 25 years. TS-trap deployments began in 1983 with completion of default design criteria for TS-traps and attendant deep-sea trap moorings (Honjo and Doherty, 1988). Since then, at least 436 TS-traps have been moored at 240 stations for the diverse objectives of international research groups working in all ocean regions and basins for varying periods. Data from most

of these deployments include analysis of collected particles for organic carbon and $CaCO_3$, and many also include assessments of biogenic opal and lithogenic particle flux. The geographic breadth of the data sets provides a global picture of the operation of the biological carbon pump system.

There could, of course, never be enough TS-traps moored in the pelagic oceans to produce definitive data on the worldwide export scheme or precise global total fluxes of POC. However, the distribution of the 134 stations included in this study (Tables 1 and 2 and Fig. 1) should be sufficient to draw a useful interpretation of these fluxes. Despite the coarse approach of this synthesis, clear contrasts can be discerned in the POC flux of different regions of the world's ocean. The analysis shows substantial differences among oceanic basins and regions in the basic function of the biological pump as it removes and transports carbon molecules from the epipelagic zone to the oceanic interior. However, our parameterization statistics surprisingly reveal that the average total global export fluxes of mole POC, particulate inorganic carbon (C in $CaCO_3$; PIC), and biogenic SiO_2 at the mesopelagic/bathypelagic boundary are about equal, a discovery that demands further research toward its explanation.

Efficient gravitational removal of POC and other fine and chemically labile particles by sinking relies on aggregates that contain dense biological and crustal mineral particles as ballast (e.g., Honjo, 1976; Armstrong et al., 2001; Fischer et al., 2003). The critical role of the heaviest common biomineral in the ocean, $CaCO_3$, in removing carbon molecules to the ocean interior has been clarified recently (Francois et al., 2002; Klaas and Archer, 2002). This hypothesis adds a new paradigm to the previously understood role of $CaCO_3$, that is, the sequestration of this material by ubiquitous plankton and the consequent export of alkalinity from the epipelagic zone to the deep oceanic interior and the seafloor. Another recent finding concerns the generation of alkalinity in the upper mesopelagic zone (e.g., Millero et al., 1998a; Feely et al., 2004; Sabine et al., 2004) which may be explained, at least in part, by the supralysoclinal dissolution of labile carbonate minerals (e.g., Milliman et al., 1999). We believe that by constraining fluxes of $CaCO_3$ at the base of the mesopelagic layer, this paper contributes to answering critical questions about the global alkalinity pump.

An extraordinary lesson we learned during the course of this study concerns the significant impact of the zooplankton ecosystem on the entire water column, including operation of the biological pump and the biogeochemical setting of the ocean interior. Progress toward answering fundamental questions, such as defining the sources of $CaCO_3$ that dissolves in the supersaturated upper mesopelagic zone, requires better definition of zooplankton ecology as well the ocean's physical chemistry and biogeochemistry. It is important to continue worldwide, seagoing research to accomplish these broad objectives (e.g., Buesseler et al., 2007).

Although we made a vigorous attempt to obtain all published or disclosed information on TS-trap deployment and related analytical data, some useful data may have been excluded by our unintentional oversight. Furthermore, the co-authors take full responsibility for errors caused by our recompilation, normalization, and unit conversion of previously published data, and we acknowledge that our interpretation of other researchers' published data may be different from that expressed in the original publications.

2. Removal and transport of POC from upper ocean layers

The essential role of the oceanic biological pump is to remove particulate organic carbon (POC) from the euphotic zone and transport it to the oceanic interior sink (Section 6) where it is cached as biogenic carbon molecules in dissolved CO_2 (e.g., Volk and Hoffert, 1985). On its own, POC with particulate organic matter (POM) would not sink because its density is close to that of seawater, and POC is metabolized before it can sink to a significant depth. POC must be ballasted to settle or delivered by organisms. Several processes are known to deliver POC to the pelagic ocean interior and the seafloor. The more significant processes include:

1. Gravitational transport of POC by ballasted biogenic amorphous aggregates (Sections 2.1 and 2.2).
2. Active transport of POC by the zooplankton ecosystem (Section 2.3).
3. Downward transport of labile dissolved organic carbon (DOC) by overturning (Section 2.4).
4. "Terminal gravitational transport" of POC in the mesopelagic/bathypelagic boundary zone and the deeper layers (Sections 2.5 and 5.3).

As summarized in the following subsections, these four processes are intertwined, with POC transitioning from one transport mode to another among the first three processes before culminating in the fourth during its

Table 1
Distribution of $F_{m/b}$ stations in the oceanic domains and biogeochemical provinces (Longhurst et al., 1995)

Oceanic domains	BGC codes	Biogeochemical provinces	m/b norm. stations
Polar	ANTA	Antarctic	9
	APLR	Austral Polar	7
	ARCT	Atlantic Arctic	7
	BERS	North Pacific Epicontinental Seas	3
	BPLR	Boreal Polar	2
	SARC	Atlantic Subarctic	2
Westerlies	GFST	Gulf Stream	
	KURO	Kuroshio Current	5
	MEDI	Mediterranean-Black Sea	2
	NADR	North Atlantic Drift	12
	NAST	North Atlantic Subtropical Gyre	14
	NPPF	North Pacific Polar Front	1
	NPST-E	North Pacific Subtropical Gyre-East	3
	NPST-W	North Pacific Subtropical Gyre-West	
	OCAL	Off-shore California Current	5
	PSAG-E	Pacific Subarctic Gyre-East	2
	PSAG-W	Pacific Subarctic Gyre-West	6
	SANT	Subantarctic	3
	SPSG	South Subtropical Gyre	2
	SSTC	South Subtropical Convergence	
	TASM	Tasman Sea	
Trade wind	ARCH	Western Pacific Archipelagic Deep Basin	
	CARB	Caribbean	
	ETRA	Eastern Tropical Atlantic	11
	ISSG	Indian Ocean South Subtropical Gyre	
	MONS	Indian Ocean Monsoon Gyre	6
	NATR	North Atlantic Tropical Gyre	
	NPTG	North Pacific Tropical Gyre	2
	PEQD	Pacific Equatorial Divergence	2
	PNEC	North Pacific Equatorial Countercurrent	6
	SATL	South Atlantic Tropical Gyre	4
	WARM	Western Pacific Warm Pool	7
	WTRA	Western Tropical Atlantic	1
Coastal	ALSK	Alaska Downwelling Coastal	
	ARAB	Northwest Arabian Upwelling	5
	AUSE	Eastern Australia Coastal	
	AUSW	Australia–Indonesia Coastal	
	BENG	Benguela Current Coastal	
	BRAZ	Brazil Current Coastal	
	CAMR	Central American Coastal	
	CCAL	California Upwelling Coastal	
	CHIL	Chile-Peru Current Coastal	1
	CHIN	China Seas Coastal	3
	CNRY	Canary Current Coastal	
	EAFR	East Africa Coastal	
	FKLD	Southwest Atlantic Continental Shelf	
	GUIA	Guiana Current Coastal	
	GUIN	Guinea Current Coastal	
	INDE	Eastern India Continental Shelf	
	INDW	Western India Continental Shelf	
	NECS	Northwest Atlantic Continental Shelf	
	NEWZ	New Zealand Coastal	
	NWCS	Northwest Atlantic Continental Shelf	
	REDS	Red Sea and Persian Gulf	
	SUND	Sunda-Arafura Seas Coastal	
Total			**134**

Table 2
Normalized annual fluxes of POC-C, C in $CaCO_3$, and Si in opal at 134 individual stations, along with other biogeochemical indices

Station i.d.	BGC province	Station degrees		Year	Biological pump indices (mol m^{-2} yr^{-1}), 250 km^2				Norm. flux at m/b (mmol m^{-2} yr^{-1})			Binary element ratios (mol/mol)			References
		Latitude	Longitude		PP	EP	TE	d*F*Co	*F*Co	*F*Ci	*F*Si	Co/Ci	Co/Si	Si/Ci	
High Arctic Seas															
1	BPLR	81.0	−138.5	95	2[a]				88[b]	5	49	18.0	1.8	10.0	Fahl and Nöthig (2007)
2	BPLR	75.0	150.0	04	2[a]				15[b]	1.5	1.6	13.0	13.0	1.1	WHOI (2007, unpublished)
Atlantic Ocean															
3	ARCT	78.9	1.4	84	7.8	4.6	0.5	4.5	23	8	10	2.8	2.3	1.2	Honjo et al. (1987) and Honjo (1990)
4	ARCT	75.9	11.5	84	23.7	14.6	0.8	14.5	122	53	31	2.3	3.9	0.6	Honjo et al. (1988) and Honjo (1990)
5	ARCT	74.6	−6.7	85	19.1	11.7	0.4	11.7	45	32	44	1.4	1.0	1.4	Honjo et al. (1987) and Honjo (1990)
6	ARCT	73.0	19.0	89	26.5	15.7	0.3	15.6	52	67	79	0.8	0.7	1.2	Manganini et al. (2003)
7	ARCT	72.5	−8.0	90	19.8	12.1	0.0	12.1	3	28	15	0.1	0.2	0.5	von Bodungen et al. (1995)
8	ARCT	70.0	−2.0	85	20.2	11.0	0.5	10.9	55	82	24	0.7	2.3	0.3	von Bodungen et al. (1995)
9	ARCT	70.0	0.0	86+	23.9	13.2	0.8	13.1	101	59	39	1.7	2.6	0.7	von Bodungen et al. (1995)
10	SARC	69.5	10.0	83	28.4	16.3	0.5	16.2	89	97	18	0.9	4.9	0.2	Honjo et al. (1987) and Honjo (1990)
11	SARC	65.5	−0.1	91	27.4	14.1	0.4	14.1	62	87	28	0.7	2.2	0.3	Honjo et al. (1987) and Honjo (1990)
12	NARD	54.7	−21.2	92	25.8	7.6	0.8	7.5	63	92	39	0.7	1.6	0.4	Kuss and Kremling (1999) and Scholten et al. (2001)
13	NARD	54.5	−21.1	92	25.6	7.2	1.1	7.1	83	89	33	0.9	2.5	0.4	Kuss and Kremling (1999) and Scholten et al. (2001)
14	NARD	49.2	−12.8	97	25.9	4.2	3.8	4.0	161	96	43	1.7	3.7	0.4	Scholten et al. (2001) and Antia et al. (2001a)
15	NARD	49.1	−13.4	97	26.0	4.0	9.2	3.7	373	117	107	3.2	3.5	0.9	Scholten et al. (2001) and Antia et al. (2001a)
16	NARD	49.0	−13.8	98	25.8	3.9	9.6	3.5	375	218	71	1.7	5.3	0.3	Scholten et al. (2001); Antia et al., 2001a
17	NARD	47.9	−19.7	92	20.9	2.3	6.3	2.1	143	254	83	0.6	1.7	0.3	Kuss and Kremling (1999)
18	NARD	47.8	−19.5	89	20.8	2.3	10.1	2.0	230	116	61	2.0	3.8	0.5	Jickells et al. (1996)
19	NARD	47.8	−19.7	92	20.9	2.3	1.2	2.3	27	63	6	0.4	4.5	0.1	Scholten et al. (2001)
20	NARD	47.8	−19.8	94	20.9	2.3	4.8	2.2	110	85	34	1.3	3.2	0.4	Kuss and Kremling (1999) and Scholten et al. (2001)
21	NARD	47.8	−19.8	93	20.9	2.3	8.4	2.1	191	215	61	0.9	3.1	0.3	Scholten et al. (2001)
22	NARD	47.8	−19.8	93	18.1	2.0	7.4	1.9	149	168	43	0.9	3.5	0.3	Kuss and Kremling (1999)
23	NARD	47.7	−20.9	89	21.8	2.5	5.9	2.3	147	190	133	0.8	1.1	0.7	Honjo and Manganini (1993)
24	NAST	33.8	−21.0	89	11.5	1.5	0.8	1.4	97	158	39	0.6	2.5	0.2	Honjo and Manganini (1993)
25	NAST	33.2	−22.0	94	10.8	1.4	1.1	1.3	74	119	30	0.6	2.5	0.3	Scholten et al. (2001)
26	NAST	33.0	−22.0	94	10.6	1.4	3.8	1.3	42	100	10	0.4	4.2	0.1	Scholten et al. (2001)
27	NAST	32.1	−64.3	84+	10.2	1.4	9.2	1.3	67	70	29	1.0	2.3	0.4	Deuser et al. (1995) and Conte et al. (2001)
28	NAST	31.6	−24.7	89	10.2	1.4	9.6	1.3	87	88		1.0			Lampitt and Antia (1997) and Jickells et al. (1996);
29	NAST	31.5	−55.9	76s	9.0	1.3	6.3	1.2	43	40	8	1.1	5.1	0.2	Honjo et al. (1982)
30	NAST	29.1	−15.4	91	12.8	1.6	10.1	1.5	100	85	12	1.2	8.5	0.1	Scholten et al. (2001) and Neuer et al. (1997)
31	NAST	28.0	−22.0	90	8.9	1.2	1.2	1.2	68	61	8	1.1	8.7	0.1	Jickells et al. (1996)

(*continued on next page*)

Table 2 (*continued*)

Station i.d.	BGC province	Station degrees		Year	Biological pump indices (mol m^{-2} yr^{-1}), 250 km^2				Norm. flux at m/b (mmol m^{-2} yr^{-1})			Binary element ratios (mol/mol)			References
		Latitude	Longitude		PP	EP	TE	d*F*Co	*F*Co	*F*Ci	*F*Si	Co/Ci	Co/Si	Si/Ci	
32	NAST	25.3	−79.5	89	17.2	2.7	4.8	2.6	39	174	37	0.2	1.1	0.2	Pilskaln et al. (1989)
33	NAST	24.6	−22.8	94	11.6	1.5	8.4	1.4	107	74	16	1.4	6.9	0.2	Jickells et al. (1996)
34	NAST	21.2	−20.7	94	52.0	11.3	5.9	11.1	227						Fischer et al. (2000)
35	NAST	21.2	−20.7	94	52.7	11.5	7.4	11.3	229	287	40	0.8	5.7	0.1	Wefer and Fischer (1993b) and Fischer et al. (2000)
36	NAST	20.9	−19.7	88	72.8	19.4	1.3	19.2	244	287	90	0.8	2.7	0.3	Wefer and Fischer (1993b) and Fischer et al. (2000)
37	NAST	13.5	−54.0	77s	8.2	1.3	6.1	1.2	78	92	27	0.8	2.9	0.3	Honjo et al. (1982)
38	ETRA	1.8	−11.1	93	12.4	1.7	11.1	1.6	112	131	52	0.9	2.2	0.4	Wefer and Fischer (1993b) and Fischer and Wefer (1996)
39	ETRA	1.8	−11.3	95	12.3	1.7	11.3	1.6	123	130	43	0.9	2.8	0.3	Wefer and Fischer (1993b) and Fischer and Wefer (1996)
40	ETRA	0.0	−10.8	95	19.9	2.6	3.2	2.5	83						Fischer et al. (2000)
41	ETRA	0.0	−23.5	98	13.4	1.9	4.6	1.8	86						Fischer et al. (2000)
42	ETRA	−2.2	−9.90	90	17.2	2.2	2.8	2.2	62	53	12	1.2	5.3	0.2	Wefer and Fischer (1993b) and Fischer and Wefer (1996)
43	ETRA	−2.2	−10.10	91	17.2	2.2	2.6	2.2	58	81	13	0.7	4.4	0.2	Wefer and Fischer (1993b) and Fischer and Wefer (1996)
44	ETRA	−2.2	−9.53	90	17.3	2.2	3.6	2.1	80	113	23	0.7	3.4	0.2	Fischer et al. (2000)
45	ETRA	−4.0	−25.7	92	7.9	1.2	5.2	1.1	63						Fischer et al. (2000)
46	ETRA	−4.3	−10.3	91	15.7	2.0	3.1	2.0	62						Fischer et al. (2000)
47	ETRA	−5.8	−9.4	91	13.6	1.8	3.6	1.7	65						Fischer et al. (2000)
48	ETRA	−7.5	−28.0	92	5.6	0.9	3.0	0.9	28						Fischer et al. (2000)
49	WTRA	−10.9	−36.2	95	5.9	0.9	13.8	0.8	126	158	42	0.8	3.0	0.3	Jennerjahn et al. (1996)
50	SATL	−20.0	9.2	89	29.6	5.3	3.1	5.2	165						Fischer et al. (2000)
51	SATL	−20.1	9.2	90	28.6	4.7	5.7	4.4	268	242	52	1.1	5.2	0.2	Wefer and Fischer (1993b)
52	SATL	−20.1	9.2	91	28.6	4.7	9.1	4.3	429	329	137	1.3	3.1	0.4	Wefer and Fischer (1993b)
53	SATL	−28.9	14.6	92	36.5	15.3	1.1	15.2	163						Fischer et al. (2000)
Indian Ocean, Arabian Sea															
54	ARAB	16.0	60.0	87	22.9	3.0	12.8	2.6	380	304	237	1.2	1.6	0.8	Nair et al. (1989) and Haake et al. (1996)
55	ARAB	17.7	57.9	94	36.9	5.7	2.9	5.5	164	226	161	0.7	1.0	0.7	Honjo et al. (1999)
56	ARAB	17.4	58.8	94	30.5	4.1	13.7	3.5	559	422	276	1.3	2.0	0.7	Honjo et al. (1999)
57	ARAB	17.2	59.6	94	28.2	3.7	13.4	3.2	495	390	255	1.3	1.9	0.7	Honjo et al. (1999)
58	ARAB	15.3	61.5	94	18.2	2.4	25.3	1.8	605	459	263	1.3	2.3	0.6	Honjo et al. (1999)
59	INDE	17.5	89.6	90	11.7	1.7	12.4	1.5	209	136	173	1.5	1.2	1.3	Ittekkot (1991) and Schäfer et al. (1996)
60	MONS	14.0	64.0	87	17.4	2.3	9.5	2.1	218	196	61	1.1	3.6	0.3	Nair et al. (1989) and Haake et al. (1996)
61	MONS	15.0	68.0	87	10.8	1.6	14.8	1.3	234	171	94	1.4	2.5	0.5	Nair et al. (1989) and Haake et al. (1996)
62	MONS	10.0	65.0	94	9.5	1.4	7.5	1.3	107	140	42	0.8	2.5	0.3	Honjo et al. (1999)
63	MONS	15.2	89.2	90	10.2	1.5	9.8	1.4	149	123	116	1.2	1.3	0.9	Ittekkot (1991) and Schäfer et al. (1996)
64	MONS	13.2	84.4	90	9.5	1.4	19.2	1.2	277	166	201	1.7	1.4	1.2	Ittekkot (1991) and Schäfer et al. (1996)
65	MONS	4.5	87.3	90	7.4	1.2	21.0	0.9	247	186	120	1.3	2.1	0.6	Ittekkot (1991) and Schäfer et al. (1996)

Pacific Ocean															
66	BERS	58.0	179.0	91	12.3	2.2	11.1	2.0	248	66	579	3.8	0.4	8.8	Honjo (1996)
67	BERS	53.5	−177.0	91	15.0	4.7	6.5	4.3	300	100	804	3.0	0.4	8.0	Takahashi et al. (1997, 2000)
68	BERS	53.0	149.0	90	11.4	3.2	2.3	3.1	72	91	355	0.8	0.2	3.9	Honjo (1996)
69	CHIN	39.7	132.4	94	23.6	6.1	5.3	5.8	327	157	697	2.1	0.5	4.4	Hong et al. (1997)
70	CHIN	14.6	115.1	90	7.6	1.2	6.3	1.1	74	109	118	0.7	0.6	1.1	Wiesner et al. (1996)
71	CHIN	18.5	116.0	87	9.2	1.4	3.7	1.3	51	125		0.4			Wiesner et al. (1996)
72	PSAG-W	51.5	−145.0	91	18.8	9.2	3.0	9.0	273	139	1229	2.0	0.2	8.8	Wong et al. (1999) and Wong (unpublished)
73	PSAG-W	50.0	165.0	97	17.1	7.2	1.9	7.1	134	131	343	1.0	0.4	2.6	Wong et al. (1999) and Wong (unpublished)
74	PSAG-W	46.1	175.3	93	15.0	2.0	9.1	1.8	183	141	779	1.3	0.2	5.5	Kawahata et al. (1997) and Kawahata et al. (2000)
75	PSAG-W	45.0	165.1	91	16.8	3.8	5.3	3.6	202	88	619	2.3	0.3	7.1	Wong et al. (1999)
76	PSAG-W	44.1	155.0	89	20.0	6.6	2.8	6.4	188	136	511	1.4	0.4	3.8	Noriki and Tsunogai (1986)
77	PSAG-W	44.0	155.0	97	19.9	6.5	3.6	6.3	233	138	568	1.7	0.4	4.1	Honda (2001)
78	KURO	42.3	145.1	97	23.9	12.5	1.9	12.2	233	131	770	1.8	0.3	5.9	Honda (2001)
79	KURO	40.0	165.0	97	16.6	1.8	9.0	1.7	163	128	292	1.3	0.6	2.3	Honda (2001)
80	NPST(E)	37.4	175.0	93	14.8	1.7	8.9	1.6	151	152	95	1.0	1.6	0.6	Kawahata et al. (1997) and Kawahata et al. (2000)
81	NPST(E)	34.4	177.7	93	14.8	1.8	6.7	1.7	119	121	34	1.0	3.5	0.3	Kawahata et al. (1997) and Kawahata et al. (2000)
82	KURO	34.2	142.0	92	15.5	1.9	5.5	1.8	105	175	173	0.6	0.6	1.0	Nozaki (1989) and Handa et al. (1989)
83	NPST(E)	30.0	175.0	93	9.2	1.3	11.3	1.1	143	110	23	1.3	6.3	0.2	Kawahata et al. (1997) and Kawahata et al. (2000)
84	KURO	27.0	127.0	93	11.7	1.6	6.6	1.5	103	184	32	0.6	3.2	0.2	Honda (2001) (part 2)
85	KURO	25.0	127.0	94	8.9	1.3	4.3	1.2	56	52	16	1.1	3.4	0.3	Honda (2001) (part 2)
86	WARM	12.0	134.3	88	4.4	0.7	3.5	0.7	25	15	7	1.7	3.5	0.5	Kempe and Knaack (1996)
87	WARM	7.9	175.0	92	4.7	0.8	3.9	0.7	30	28	14	1.1	2.2	0.5	Kawahata et al. (1999)
88	WARM	5.0	138.8	88	5.4	0.9	3.6	0.9	32	33	12	1.0	2.6	0.4	Kempe and Knaack (1996)
89	WARM	4.1	136.3	91	6.3	1.0	17.9	0.8	184	158	169	1.2	1.1	1.1	Kawahata et al. (1999)
90	WARM	3.0	135.0	95	6.7	1.1	21.5	0.9	233	248	222	0.9	1.1	0.9	Kawahata et al. (1999)
91	WARM	1.2	160.6	92	4.9	0.8	4.6	0.8	37	61	17	0.6	2.2	0.3	Kawahata et al. (1999)
92	WARM	0.0	175.2	92	7.9	1.2	4.3	1.2	53	102	27	0.5	2.0	0.3	Kawahata et al. (1999)
93	PSAG-E	50.0	−145.0	83+	15.9	1.9	8.7	1.7	163	171	253	1.0	0.6	1.5	Wong et al. (1994)
94	PSAG-E	49.0	−174.0	95+	15.7	4.1	6.7	3.8	274	99	294	2.8	0.9	3.0	Takahashi et al. (2000)
95	OCAL	48.0	−128.1	84	25.9	9.4	1.0	9.3	91	117	121	0.8	0.7	1.0	Dymond and Lyle (1985)
96	NPPF	45.1	−176.9	91	18.2	2.1	4.8	2.0	99	36	161	2.8	0.6	4.5	Wong et al. (1994)
97	OCAL	42.2	−127.6	87	22.1	4.0	3.2	3.9	129	91	278	1.4	0.5	3.0	Lyle et al. (1992) and Dymond and Lyle (1985)
98	OCAL	42.1	−125.8	87	38.8	18.9	1.4	18.6	257	149	796	1.7	0.3	5.3	Lyle et al. (1992) and Dymond and Lyle (1985)
99	OCAL	41.6	−132.0	87	14.1	1.6	4.0	1.5	63	42	55	1.5	1.1	1.3	Lyle et al. (1992) and Dymond and Lyle (1985)
100	OCAL	39.5	−127.7	83	18.9	2.3	6.7	2.1	150	55	142	2.7	1.1	2.6	Dymond and Lyle (1985)
101	NPTG	31.7	−124.6	82	9.9	1.2	3.8	1.2	46	23	18	2.0	2.6	0.8	Noriki and Tsunogai (1986)
102	NPTG	15.4	−151.5	78	5.2	0.9	3.1	0.8	27	30	10	0.9	2.6	0.3	Honjo et al. (1982)
103	PNEC	11.0	−140.0	82	7.2	1.1	4.3	1.1	49	78	67	0.6	0.7	0.9	Dymond and Collier (1988) and Dymond and Lyle (1985)
104	PNEC	9.0	−140.0	92	7.6	1.2	4.3	1.1	50	53	27	1.0	1.8	0.5	Honjo et al. (1995)
105	PNEC	5.4	−81.9	89	12.0	1.7	18.1	1.4	307	156	161	2.0	1.9	1.0	Honjo et al. (1982)
106	PNEC	5.0	−139.8	92	8.6	1.3	11.0	1.2	143	179	86	0.8	1.6	0.5	Honjo et al. (1995)
107	PNEC	2.0	−140.1	92	9.9	1.5	8.0	1.3	116	180	101	0.6	1.1	0.6	Honjo et al. (1995)
108	PNEC	1.0	−140.0	92	10.4	1.5	10.6	1.3	158	297	342	0.5	0.5	1.2	Dymond and Collier (1988) and Dymond and Lyle (1985)

(*continued on next page*)

Table 2 (*continued*)

Station i.d.	BGC province	Station degrees		Year	Biological pump indices (mol m^{-2} yr^{-1}), 250 km^2				Norm. flux at m/b (mmol m^{-2} yr^{-1})			Binary element ratios (mol/mol)			References
		Latitude	Longitude		PP	EP	TE	d*F*Co	*F*Co	*F*Ci	*F*Si	Co/Ci	Co/Si	Si/Ci	
109	PNEC	0.6	−86.1	76	11.9	1.6	11.9	1.4	194	273	187	0.7	1.0	0.7	Cobler and Dymond (1980)
110	PEQD	0.0	−140.0	92	10.7	1.5	10.1	1.4	156	233	112	0.7	1.4	0.5	Honjo et al. (1995)
111	PEQD	−5.0	−140.0	92	8.4	1.3	7.1	1.2	91	147	85	0.6	1.1	0.6	Honjo et al. (1995)
112	SPSG	−12.0	−135.0	92	6.9	1.1	3.1	1.1	34	66	15	0.5	2.2	0.2	Honjo et al. (1995)
113	CHIL	−29.5	−73.2	93	21.0	4.2	6.3	3.9	263	310	189	0.8	1.4	0.6	Hebbeln et al. (2000)
Southern Ocean															
114	ANTA	−50.1	−5.9	90	6.8	0.7	16.0	0.6	116						Fischer et al. (2000)
115	ANTA	−50.2	−5.9	92	6.8	0.7	13.3	0.6	97	101	255	1.0	0.4	2.5	Wefer and Fischer (1991)
116	ANTA	−54.3	−3.4	92	4.6	0.6	10.8	0.5	62						Fischer et al. (2000)
117	ANTA	−57.0	−37.0	85	9.0	3.9	0.2	3.9	8	10	118	0.8	0.1	11.8	Honjo (1990)
118	ANTA	−62.3	−57.5	83	9.9	5.4	0.9	5.3	51						Wefer et al. (1988)
119	APLR	−62.4	−34.8	85	1.3	0.2	0.4	0.2	1	0	5	7.7	0.2	44.4	Wefer and Fischer (1991)
120	APLR	−64.9	−2.6	87	2.3	0.3	14.1	0.3	43	28	397	1.6	0.1	14.2	Wefer and Fischer (1991)
121	APLR	−64.9	−2.5	87	2.3	0.3	9.4	0.3	28	10	67	2.8	0.4	6.7	Wefer and Fischer (1991)
122	ANTA	−52.0	61.5	99	5.1	0.5	13.5	0.5	73	55	652	1.3	0.1	11.8	Tréguer (unpublished)
123	APLR	−62.0	73.0	98	2.6	0.5	8.9		42	7	308	6.3	0.1	46.2	Pilskaln et al. (2004)
124	APLR	−63.0	71.0	94	1.8	0.2	6.4	0.2	14	2	43	8.4	0.3	25.6	Tréguer (unpublished)
125	SANT	−46.8	142.1	97	14.9	1.6	10.6	1.4	170	204	108	0.8	1.6	0.5	Trull et al. (2001) and Bray et al. (2000)
126	SANT	−51.0	141.7	97	7.0	0.8	22.3	0.6	173	312	254	0.6	0.7	0.8	Trull et al. (2001) and Bray et al. (2000)
127	SANT	−53.8	141.8	97	5.8	0.6	7.7	0.6	49	85	348	0.6	0.1	4.1	Trull et al. (2001) and Bray et al. (2000)
128	ANTA	−56.9	−170.2	96	6.0	0.7	11.8	0.6	76	121	251	0.6	0.3	2.1	Honjo et al. (2000)
129	ANTA	−60.3	−170.1	96	7.7	0.8	13.2	0.7	108	128	460	0.8	0.2	3.6	Honjo et al. (2000)
130	ANTA	−63.1	−169.9	96	6.6	0.9	12.9	0.8	117	82	915	1.4	0.1	11.2	Honjo et al. (2000)
131	APLR	−66.2	−168.7	96	5.5	1.7	4.9	1.6	84	7	269	12.6	0.3	40.4	Honjo et al. (2000)
132	APLR	−73.5	176.9	96	1.8	0.3	7.8	0.3	22	53	79	0.4	0.3	1.5	Collier et al. (2000)
Inland Sea; Black Sea															
133	MEDI	42.2	32.5	82	27.3	6.9	3.7	6.6	257	101	53	2.5	4.8	0.5	Izdar et al. (1984) and Hay et al. (1990)
134	MEDI	41.9	30.4	86	30.3	8.5	1.3	8.4	110	38	58	2.9	1.9	1.5	Hay et al. (1990) and Buesseler et al. (1987)

BGC provinces: Biogeochemical provinces defined by Longhurst et al. (1995). *Year*: Calendar year when the sampling began. *PP*: Average annual primary production in the 250 × 250-km area above a time-series sediment trap (TS-trap) mooring calculated from the ocean-color-based model in molC m^{-2} yr^{-1} by Behrenfeld and Falkowski (1997). *EP*: Average annual export production in the 250 × 250-km area above a TS-trap mooring in molC m^{-2} yr^{-1} calculated from an ecosystem model by Laws et al. (2000). *TE*: Transfer efficiency (%) of POC using the formula from Francois et al. (2002). FC_{org}: Normalized value to 2 km ($-b = 0.86$) applied to calculate POC in mmolC m^{-2} yr^{-1}. Two sets of FC_{org} from the High Arctic were not corrected for depth because the vertical transport of POC in this extremely high-latitude, ice-covered environment with minimum primary production (PP) appears radically different from other world oceans.

[a] The High Arctic PP listed in this table, 2 molC m^2 yr^{-1}, is the average of three reports by Macdonald and Carmack (1991). Cota et al. (1996) and Gosselin et al. (1997) for the High Arctic basins (Sakshaug, 2004, in Stein and Macdonald, 2004).

[b] Because biological pump operation in the High Arctic basins appears radically different from other oceans, we present these numbers without normalizing FC_{org} for depth.

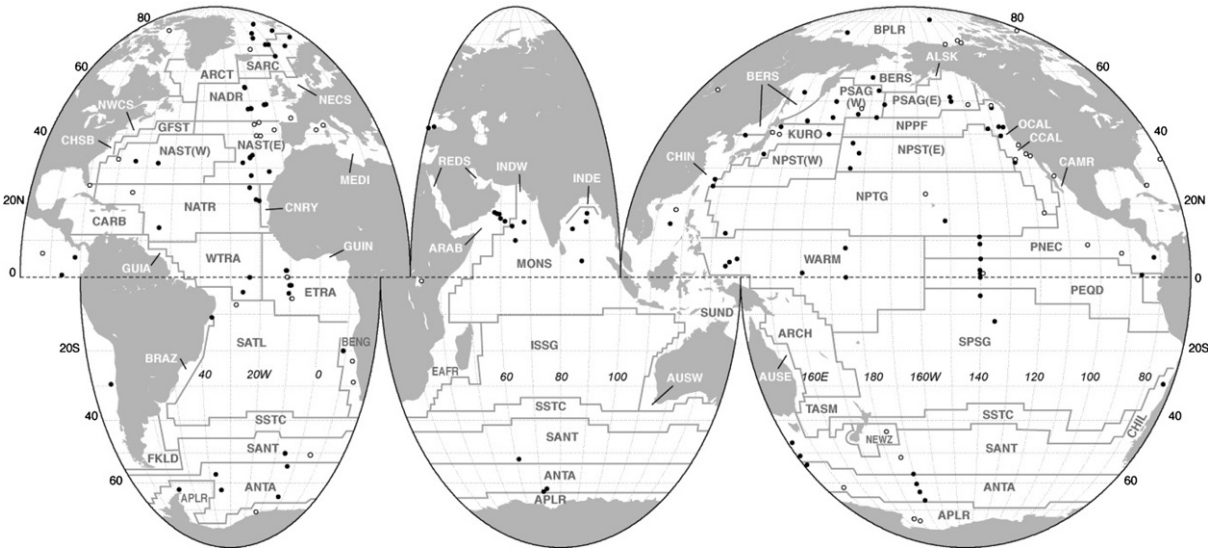

Fig. 1. Plot showing distribution of 134 TS-trap stations utilized for this paper (solid circles) and the global biogeochemical (BGC) provinces proposed by Longhurst et al. (1995) listed in Table 2. We assigned TS-trap stations located near or on the boundaries of BGC provinces according to our best judgment. The large number of stations in NADR and NAST-E were deployed close together and some stations appear to overlap one another in the plot so that the map represents fewer stations than we included in our analysis. A more detailed projection of TS-trap locations in the northeast sector of NAST-E can be found in Fig. 1 of Guieu et al. (2005), and a detailed projection of the University of Bremen's TS-trap stations between 20°N and 80°S in the Atlantic is presented in Fig. 1 of Fischer et al. (2000). For this paper, the south boundary of the North Pacific Polar Front across the the East Sea/Japan Sea area is shifted to approximately 36.5°N, which is about 100 km south of Longhurst's original proposed location. In addition to the 134 stations included in Table 2, there are 49 other major TS-trap stations (open circles), including some long-term, multidisciplinary time-series stations whose TS-trap data from deeper layers have not been published (e.g., HOT, Karl (unpublished), and The Iceland Plateau Station, Olafsson (unpublished).), continental margin projects along the North American West Coast (OCAL and CAMR) (Thunell et al., 2007), and stations in deep lakes (Kempe and Schaumburg, 1996; Pilskaln, 2004), and TS-trap samples too shallow to apply to this paper (some in Fischer et al., 2000). The trap depth of Station M (Smith et al., 2006) is too deep for inclusion in this paper.

downward transport to the interior. In deeper layers where there is no photosynthetic production, POC contained in ballasted aggregates and fecal pellets with colonized microbes provides metabolic energy to the ecosystem beneath the photic zone. Zooplankton consume aggregates (including fecal pellets), repackaging the POC through multi-coprophagy. Zooplankton and micronekton carcasses are converted to aggregates by microbial heterotrophy (see Section 2.3). Further exploration of the quantitative, spatial/temporal relationship between particles and zooplankton communities will yield greater understanding of vertical transport of POC through the water column.

The assumption that zooplankton and micronekton metabolism is minimal at the mesopelagic/bathypelagic boundary (that is, about 2 km deep) and virtually all POC settling is driven by gravity in the lower mesopelagic and submesopelagic zone (Section 2.5) is critical to constraining export fluxes of POC to the oceanic interior. With the disappearance of the settling complexities caused by the zooplankton community in this boundary zone, particle fluxes can be compared among stations with known biases. Thus, we normalized published export flux data to 2 km in order to further understand (1) the global comparative biogeochemical geography (Sections 6–8), (2) to estimate the total and average global export fluxes of POC and other critical elements needed to maintain the biological pump (Section 10), and (3) to constrain the rate of total mesopelagic CO_2 sink in the world pelagic ocean (Section 12).

2.1. Gravitational transport of POC by settling aggregates

2.1.1. Ballasted amorphous aggregates

Amorphous aggregates that are ubiquitous in any productive ocean environment are often called "marine snow" after Suzuki and Kato (1953). Measuring several hundred micrometers to a few millimeters, these

Table 3
Normalized annual fluxes of POC-C, C in $CaCO_3$, and Si in opal calculated for 153 individual TS-trap samples and their ternary ratios

Trap ID	Project	BGC province	Trap location		Year	Depth (m)	*F*Co-uncorr. (mmol m^{-2} yr^{-1})	*F*Co-2 km (mmol m^{-2} yr^{-1})	Ternary ratio (%)			References
			Latitude	Longitude					Co-2 km	Ci	Si	
Arctic												
HA-1	Wrangel Abyssal Plain	BPLR	81.0	−138.5	95	1550	87.5		62	3.5	34.5	Zernova et al. (2000), Nöthig and Shevchenko (2004)
HA-2	Canada Abyssal Plain	BPLR	75.0	150.0	04	3067	15		81	8	11	WHOI (2007, unpublished)
Atlantic Ocean												
A-1	PARFLUX-Fram Strait-C	ARCT	78.9	1.4	84	2400	20	23	56	20	24	Honjo et al. (1987) and Honjo (1990)
A-2	PARFLUX-Bear Island	ARCT	75.9	11.5	84	1700	141	122	59	25	15	Honjo et al. (1988) and Honjo (1990)
A-3	PARFLUX-Greenland B.	ARCT	74.6	−6.7	85	2823	33	45	37	26	36	Honjo et al. (1987) and Honjo (1990)
A-4	PARFLUX-Barents Sea	ARCT	73.0	19.0	89	372	220	52	26	34	40	Manganini et al. (2003)
A-5	Von Bodungen-NS-70N	ARCT	70.0	0.0	86	1000	151	83	50	44	6	von Bodungen et al. (1995)
A-6	Von Bodungen-NS-70N	ARCT	70.0	0.0	87	1000	144	79	49	45	6	von Bodungen et al. (1995)
A-7	Von Bodungen-NS-70N	ARCT	70.0	0.0	88	1000	255	140	51	42	7	von Bodungen et al. (1995)
A-8	PARFLUX-Jan Mayen	ARCT	70.0	−2.0	85	2749	42	55	34	51	15	Honjo et al. (1987) and Honjo (1990)
A-9	Von Bodungen-NS-70N	ARCT	70.0	0.0	86	3000	273	387	66	29	5	von Bodungen et al. (1995)
A-10	Von Bodungen-NS-70N	ARCT	70.0	0.0	87	3000	290	411	56	37	7	von Bodungen et al. (1995)
A-11	Von Bodungen-NS-70N	ARCT	70.0	0.0	88	3000	328	464	74	23	3	von Bodungen et al. (1995)
A-12	PARFLUX-Lofoten	SARC	69.5	10.0	83	2760	68	89	44	47	9	Honjo et al. (1987) and Honjo (1990)
A-13	PARFLUX-Aegir Ridge	SARC	65.5	−0.1	85	2630	49	62	35	49	16	Honjo et al. (1987) and Honjo (1990)
A-14	L3-92-55N	NARD	54.5	−21.1	93	2200	160	173	29	58	13	Kuss and Kremling (1999) and Scholten et al. (2001)
A-15	OMEX-3	NARD	49.2	−12.8	93	1020	281	157	53	32	15	Scholten et al. (2001); Antia et al. (2001b)
A-16	OMEX-4	NARD	49.1	−13.4	93	3220	247	373	57	25	17	Scholten et al. (2001) and Antia et al. (2001b)
A-17	OMEX-4	NARD	49.0	−13.8	92	4000	207	375	60	36	5	Scholten et al. (2001) and Antia et al. (2001b)
A-18	L2-A-92-48N	NARD	47.9	−19.7	92	3500	88	143	52	37	11	Scholten et al. (2001) and Antia et al. (2001b)

A-19	BOFS-48N	NARD	47.8	−19.5	89	3100	158	230	56	28	15	Jickells et al. (1996)
A-20	L2-B-92-48N	NARD	47.8	−19.8	92	1030	70	40	38	44	18	Kuss and Kremling (1999) and Scholten et al. (2001)
A-21	L2-B-92-48N	NARD	47.8	−19.8	92	2030	108	110	48	37	15	Kuss and Kremling (1999) and Scholten et al. (2001)
A-22	L2-B-92-48N	NARD	47.8	−19.8	92	3530	54	88	45	45	10	Kuss and Kremling (1999) and Scholten et al. (2001)
A-23	L2-94	NARD	47.8	−19.8	94	3500	87	141	53	37	10	Scholten et al. (2001)
A-24	L2-93-48N	NARD	47.8	−19.8	93	2000	149	149	41	47	12	Kuss and Kremling (1999)
A-25	JGOFS-NABE-48N	NARD	47.7	−20.9	89	1018	129	72	28	46	25	Honjo (1992, 1993)
A-26	JGOFS-NABE-48N	NARD	47.7	−20.9	89	2018	146	147	31	40	28	Honjo (1992, 1993)
A-27	JGOFS-NABE-48N	NARD	47.7	−20.9	89	3718	83	141	36	40	24	Honjo (1992, 1993)
A-28	JGOFS-NABE-34N	NAST	33.8	−21.0	89	1070	78	45	24	62	13	Honjo (1992, 1993)
A-29	JGOFS-NABE-34N	NAST	33.8	−21.0	89	2067	94	97	33	54	13	Honjo (1992, 1993)
A-30	JGOFS-NABE-34N	NAST	33.8	−21.0	89	4564	78	158	48	41	11	Honjo (1992, 1993)
A-31	L1-94	NAST	33.0	−22.0	94	1050	43	24	32	66	2	Scholten et al. (2001)
A-32	L1-94	NAST	33.0	−22.0	94	2000	42	42	28	66	7	Scholten et al. (2001)
A-33	Sargasso Sea-OFP	NAST	32.1	−64.3	84+	1500	73	57	38	44	18	Deuser et al. (1995) and Conte et al. (2001)
A-34	Sargasso Sea-OFP	NAST	32.1	−64.3	84+	3200	52	77	43	41	17	Deuser et al. (1995) and Conte et al. (2001)
A-35	PARFLUX-Sohm AP	NAST	31.5	−55.9	76	3694	27	45	72	23	5	Honjo et al. (1982)
A-36	ESTOC	NAST	29.1	−15.4	91	1021	37	21	42	50	9	Scholten et al. (2001) and Neuer et al. (1997)
A-37	ESTOC	NAST	29.1	−15.4	91	3075	69	100	51	43	6	Scholten et al. (2001) and Neuer et al. (1997)
A-38	BOFS-28N	NAST	28.0	−22.0	90	3600	41	68	50	45	6	Jickells et al. (1996)
A-39	BOFS-25N	NAST	24.6	−22.8	90	3870	60	107	54	38	8	Jickells et al. (1996)
A-40	U. Bremen-CB1	NAST	21.2	−20.7	88	3502	141	229	41	52	7	Wefer and Fischer (1993)
A-41	U. Bremen-CB2	NAST	20.9	−19.7	89	2195	225	244	39	46	15	Wefer and Fischer (1993)
A-42	BOFS-19N	NAST	19.0	−20.2	90	2190	648	701	59	34	8	Jickells et al. (1996)
A-43	PARFLUX-Demerara AP	NAST	13.5	−54.0	77	3755	53	90	44	44	11	Honjo et al. (1982)
A-44	U. Bremen-EA2	ETRA	1.8	−11.1	90	3921	167	297	71	22	7	Fischer and Wefer, 1996 and Wefer and Fischer (1993)
A-45	U. Bremen-EA2	ETRA	1.8	−11.3	91	953	233	123	41	44	15	Fischer and Wefer, 1996 and Wefer and Fischer (1993)
A-46	U, Bremen-EA4	ETRA	−2.2	−10.1	91	1068	100	58	38	53	9	Fischer and Wefer, 1996 and Wefer and Fischer (1993)
A-47	U.Bremen-GB5	ETRA	−2.2	−9.5	90	3382	175	275	46	39	15	Fischer and Wefer, 1996 and Wefer and Fischer (1993)
A-48	E. Brazil	WTRA	−10.9	−36.2	95	1500	161	126	39	49	13	Jennerjahn et al. (1996)
A-49	U. Bremen-WR	SATL	−20.1	9.2	89	1648	317	268	48	43	9	Wefer and Fischer (1993)
A-50	U. Bremen-WR	SATL	−20.1	9.2	89	1648	506	428	48	37	15	Wefer and Fischer (1993)
Indian Ocean, Arabian Sea												
I-1	JGOFS-Arabian Sea M1	ARAB	17.7	57.9	94	998	345	190	31	42	27	Honjo et al. (1999)
I-2	Bengal Bay-17N	INDE	17.5	89.6	87	1727	101	89	40	26	33	Ittekkot (1991) and Schäfer et al. (1996)
I-3	JGOFS-Arabian Sea M2	ARAB	17.4	58.8	94	903	511	258	27	45	28	Honjo et al. (1999)
I-4	JGOFS-Arabian Sea M3	ARAB	17.2	59.6	94	1857	497	466	41	35	23	Honjo et al. (1999)
I-5	I-G-Arabian Sea W	ARAB	16.0	60.0	87	3020	267	380	41	33	26	Nair et al. (1989) and Haake et al. (1996)
I-6	JGOFS-Arabian Sea M4	ARAB	15.3	61.5	94	2229	496	544	43	36	21	Honjo et al. (1999)
I-7	Bengal Bay-15N	MONS	15.2	89.2	90	1717	237	208	38	32	30	Ittekkot (1991) and Schäfer et al. (1996)
I-8	I-G-Arabian Sea E	MONS	15.0	68.0	87	2800	174	233	47	34	19	Nair et al. (1989) and Haake et al. (1996)
I-9	I-G-Arabian Sea C	MONS	14.0	64.0	87	2900	158	218	46	41	13	Nair et al. (1989) and Haake et al. (1996)
I-10	Bengal Bay-13N	MONS	13.2	84.4	87	2282	170	190	43	26	31	Ittekkot (1991) and Schäfer et al. (1996)
I-11	JGOFS-Arabian Sea M5	MONS	10.0	65.0	94	2363	100	116	37	49	14	Honjo et al. (1999)

(*continued on next page*)

Table 3 (*continued*)

Trap ID	Project	BGC province	Trap location		Year	Depth (m)	*F*Co-uncorr. (mmol m^{-2} yr^{-1})	*F*Co-2 km (mmol m^{-2} yr^{-1})	Ternary ratio (%)			References
			Latitude	Longitude					Co-2 km	Ci	Si	
I-12	Bengal Bay-SN	MONS	4.5	87.3	90	2203	227	247	45	34	22	Ittekkot (1991) and Schäfer et al. (1996)
Pacific Ocean												
P-1	PARFLUX-Bering Sea	BERS	58.0	179.0	91	3137	168	248	28	7	65	Honjo (1996)
P-2	Takahashi-Aleutian – AB	BERS	53.5	−177.0	91	3193	161	241	29	7	64	Takahashi et al. (1997) and Takahashi et al. (2000)
P-3	Takahashi-Aleutian – AB	BERS	53.5	−177.0	93	3200	195	292	25	9	66	Takahashi et al. (1997) and Takahashi et al. (2000)
P-4	Takahashi-Aleutian – AB	BERS	53.5	−177.0	93	3200	213	319	32	10	59	Takahashi et al. (1997) and Takahashi et al. (2000)
P-5	PARFLUX-Okhotsk Sea	BERS	53.0	149.0	90	1061	124	72	14	18	69	Honjo (1996)
P-6	Wong-GD	PSAG	51.5	165.0	91	4500	136	273	17	8	75	Wong et al. (1999) and Wong (unpublished)
P-7	Honda-50N	PSAG	50.0	165.0	97	1230	195	128	20	21	59	Honda (2001)
P-8	Honda-50N	PSAG	50.0	165.0	97	1230	85	56	17	20	63	Honda (2001)
P-9	Honda-50N	PSAG	50.0	165.0	97	3260	97	148	19	18	63	Honda (2001)
P-10	Wong-IOS-OSP	PSAG	50.0	−145.0	83	1000	402	221	21	25	53	Wong et al. (1999) and Wong (unpublished)
P-11	Wong-IOS-OSP	PSAG	50.0	−145.0	85	1000	246	135	20	31	49	Wong et al. (1999) and Wong (unpublished)
P-12	Wong-IOS-OSP	PSAG	50.0	−145.0	89	1000	138	76	13	32	54	Wong et al. (1999) and Wong (unpublished)
P-13	Wong-IOS-OSP	PSAG	50.0	−145.0	90	1000	145	80	14	47	40	Wong et al. (1999) and Wong (unpublished)
P-14	Wong-IOS-OSP	PSAG	50.0	−145.0	93	1000	200	110	25	34	41	Wong et al. (1999) and Wong (unpublished)
P-15	Takahashi-SA	PSAG	49.0	−174.0	94	4826	103	220	46	22	32	Takahashi et al. (2000)
P-16	Takahashi-SA	PSAG	49.0	−174.0	95	4806	134	284	42	12	46	Takahashi et al. (2000)
P-17	Takahashi-SA	PSAG	49.0	−174.0	96	4833	94	201	41	14	44	Takahashi et al. (2000)
P-18	Takahashi-SA	PSAG	49.0	−174.0	97	4822	173	369	42	15	43	Takahashi et al. (2000)
P-19	Takahashi-SA	PSAG	49.0	−174.0	98	4774	140	295	36	13	51	Takahashi et al. (2000)
P-20	NORPAC-8-46N	PSAG	46.1	175.3	93	1412	247	183	17	13	71	Kawahata et al. (1997) and Kawahata et al. (2000)
P-21	Wong-GA	PSAG	45.1	176.9	91	5300	88	202	22	10	68	Wong et al. (1999)
P-22	KNOT-97	PSAG	44.0	155.0	97	2960	186	260	29	17	55	Honda (2001)
P-23	KNOT-99	PSAG	44.0	155.0	99	2960	183	256	26	14	60	Honda (2001)
P-24	Ca. Current-MW	OCAL	42.2	−127.6	87	1333	183	129	26	18	56	Dymond and Lyle (1985) and Lyle et al. (1992)
P-25	Ca. Current-NS	OCAL	42.1	−125.8	87	1167	408	257	21	12	66	Dymond and Lyle (1985) and Lyle et al. (1992)
P-26	C. Current-Gyre	OCAL	41.6	−132.0	87	1625	75	63	39	26	34	Dymond and Lyle (1985) and Lyle et al. (1992)

P-27	Honda-40N	KURO	40.0	165.0	97	953	128	68	19	33	48	Honda (2001)
P-28	Honda-40N	KURO	40.0	165.0	97	950	183	96	27	27	46	Honda (2001)
P-29	Honda-40N	KURO	40.0	165.0	97	2986	110	155	28	24	48	Honda (2001)
P-30	Honda-40N	KURO	40.0	165.0	97	2990	122	172	28	20	52	Honda (2001)
P-31	Hong-East-Sea	CHIN	39.7	132.4	94	2800	245	327	28	13	59	Hong et al. (1997)
P-32	Ca. Current-Mendocino	OCAL	39.5	−127.7	83	3000	106	150	43	16	41	Dymond and Lyle (1985)
P-33	NORPAC-7-37N	KURO	37.4	175.0	93	1482	196	151	38	38	24	Kawahata et al. (1997) and Kawahata et al. (2000)
P-34	NORPAC-5-34N	KURO	34.4	177.7	93	1342	92	65	37	51	12	Kawahata et al. (1997) and Kawahata et al. (2000)
P-35	NORPAC-5-34N	KURO	34.4	177.7	93	2848	130	176	46	41	12	Kawahata et al. (1997) and Kawahata et al. (2000)
P-36	Nozaki-Jp. T	KURO	34.2	142.0	92	5429	54	126	49	24	26	Handa et al. (1997)
P-37	Nozaki-Jp. T	KURO	34.2	142.0	92	8431	139	478	63	7	30	Handa et al. (1997)
P-38	Noriki-EP7	NPTG	31.7	−124.6	82	1250	82	55	38	35	27	Noriki and Tsunogai (1986)
P-39	NORPAC-6-30N	KURO	30.0	175.0	93	3873	81	143	52	40	8	Kawahata et al. (1997) and Kawahata et al. (2000)
P-40	Okinawa Trough	KURO	27.0	127.0	93	1547	125	100	39	55	5	Honda (2001) (part 2)
P-41	Ryukyu Trench	KURO	25.0	127.0	94	3160	38	56	45	42	13	Honda (2001) (part 2)
P-42	PARFLUX-E. Hawaii AP	NPTG	15.4	−151.5	78s	978	17	9	24	54	22	Honjo et al. (1982)
P-43	Weisner-SCS	CHIN	14.6	115.1	90	1190	116	74	25	36	39	Wiesner et al. (1996)
P-44	Kempe-NEC	WARM	12.0	134.3	88	1200	11	7	35	54	11	Kempe and Knaack (1996)
P-45	MANOP-S-1600	PNEC	11.0	−140.0	82	1600	72	59	28	40	32	Dymond and Collier (1988) and Dymond and Lyle (1985)
P-46	MANOP-S-3400	PNEC	11.0	−140.0	82	3400	49	78	36	34	30	Dymond and Collier (1988) and Dymond and Lyle (1985)
P-47	JGOFS-Arabian Sea M5	MONS	10.0	65.0	94	2363	116	134	41	46	14	Honjo et al. (1999)
P-48	JGOFS-EqPac-9N	PNEC	9.0	−140.0	92	2250	47	52	40	39	22	Honjo et al. (1995)
P-49	JGOFS-EqPac-9N	PNEC	9.0	−140.0	92	2150	46	49	37	42	20	Honjo et al. (1995)
P-50	NORPAC-4-8N	WARM	7.9	175.0	92	1637	35	30	42	39	19	Kawahata et al. (1999)
P-51	PARFLUX-Panama	PNEC	5.4	−81.9	89	2265	276	307	51	24	25	Honjo et al. (1982)
P-52	PARFLUX-Panama	PNEC	5.4	−81.9	89	2869	330	451	54	23	23	Honjo et al. (1982)
P-53	JGOFS-EqPac-5N	PNEC	5.0	−139.8	92	2100	137	143	35	44	21	Honjo et al. (1995)
P-54	Kempe-ECC	WARM	5.0	138.8	88	1130	11	7	40	44	16	Kempe and Knaack (1996)
P-55	Kempe-ECC	WARM	5.0	138.8	88	3130	17	25	52	34	14	Kempe and Knaack (1996)
P-56	NORPAC-2-4N	WARM	4.1	136.3	91	1769	204	184	36	31	33	Kawahata et al. (1999)
P-57	NORPAC-1-3N	WARM	3.0	135.0	95	1590	284	233	33	36	31	Kawahata et al. (1999)
P-58	JGOFS-EqPac-2N	PNEC	2.0	−140.1	92	2203	107	116	29	45	25	Honjo et al. (1995)
P-59	NORPAC-10-1N	WARM	1.2	160.6	92	1164	59	37	32	53	15	Kawahata et al. (1999)
P-60	MANOP-C	PNEC	1.0	−140.0	82	1895	129	123	29	35	36	Dymond and Collier (1988) and Dymond and Lyle (1985)
P-61	Galapagos	PEQD	0.6	−86.1	76	2570	138	171	29	43	28	Cobler and Dymond (1980)
P-62	NORPAC-3-EQ	WARM	0.0	175.2	92	1357	74	53	29	60	10	Kawahata et al. (1999)
P-63	JGOFS-EqPac0	PEQD	0.0	−140.0	92	2284	139	156	31	47	22	Honjo et al. (1995)
P-64	JGOFS-EqPa-5S	PEQD	−5.0	−140.0	92	2099	83	87	28	47	25	Honjo et al. (1995)
P-65	JGOFS-EqPa-5S	PEQD	−5.0	−140.0	92	2209	83	90	27	45	28	Honjo et al. (1995)
P-66	JGOFS-EqPa-5S	PEQD	−5.0	−140.0	92	2316	85	96	29	45	26	Honjo et al. (1995)
P-67	JGOFS-EqPa-12S	SPSG	−12.0	−135.0	92	1292	46	31	27	61	12	Honjo et al. (1995)
P-68	JGOFS-EqPa-12S	SPSG	−12.0	−135.0	92	3594	22	36	31	54	15	Honjo et al. (1995)
P-69	Hebbeln Chile	CHIL	−29.5	−73.2	95	3700	191	325	49	39	12	Hebbeln et al. (2000)
P-70	Hebbeln Chile	CHIL	−29.5	−73.2	97	3700	264	448	42	33	24	Hebbeln et al. (2000)

(*continued on next page*)

Table 3 (*continued*)

Trap ID	Project	BGC province	Trap location		Year	Depth (m)	*F*Co-uncorr. (mmol m^{-2} yr^{-1})	*F*Co-2 km (mmol m^{-2} yr^{-1})	Ternary ratio (%)			References
			Latitude	Longitude					Co-2 km	Ci	Si	
P-71	Hebbeln Chile	CHIL	−29.5	−73.2	97	2300	233	263	35	41	25	Hebbeln et al. (2000)
Southern Ocean												
S-1	SAZ-47S	SANT	−46.8	142.1	97	2050	167	170	35	42	22	Trull et al. (2001) and Bray et al. (2000)
S-2	SAZ-5S	SANT	−51.0	141.7	97	3080	119	173	23	42	34	Trull et al. (2001) and Bray et al. (2000)
S-3	Treguer-M2	ANTA	−52.0	61.5	99	1300	88	60	7	7	87	Tréguer (unpublished)
S-4	SAZ-54S	SANT	−53.8	141.8	97	1500	63	49	11	16	72	Trull et al. (2001) and Bray et al. (2000)
S-5	JGOFS-AESOPS-M2	ANTA	−56.9	−170.2	96	982	141	76	17	27	56	Honjo et al. (2000)
S-6	JGOFS-AESOPS-M3	ANTA	−60.3	−170.1	96	1003	195	108	15	18	66	Honjo et al. (2000)
S-7	Pilskaln-62S	APLR	−62.0	73.0	98	1000	77	42	12	2	86	Pilskaln et al. (2003)
S-8	U. Bremen-WS-62S	APLR	−62.4	−34.8	85	863	2	1	15	2	84	Wefer and Fischer (1991)
S-9	Treguer-M3	APLR	−63.0	71.0	94	1300	9	6	15	2	83	Tréguer (unpublished)
S-10	Treguer-M3	APLR	−63.0	71.0	94	3500	13	22	29	3	68	Tréguer (unpublished)
S-11	JGOFS-AESOPS-M4	ANTA	−63.1	−169.9	96	1031	207	117	10	7	82	Honjo et al. (2001)
S-12	U. Bremen-WS-65S	APLR	−64.9	−2.5	87	4456	14	28	27	10	64	Wefer and Fischer (1991)
S-13	JGOFS-AESOPS-M5	APLR	−66.2	−168.7	96	937	162	84	23	2	75	Honjo et al. (2000)
S-14	JGOFS-AESOPS-7a	ROSS-S	−76.5	−177.9	96	465	878	250	40	26	33	Collier et al. (2000)
S-15	JGOFS-AESOPS-7b	ROSS-S	−76.5	−178.0	96	481	1015	298	36	33	31	Collier et al. (2000)
Inland Sea; Black Sea												
M-1	BS-83	MEDI	42.2	32.5	83	1200	398	257	62	25	13	Izdar et al. 1987 and Hay et al. (1990)
M-2	BS-86	MEDI	41.9	30.4	86	1200	170	110	53	18	28	Hay et al. (1990)

Project: Arbitrary names abbreviated from the references by the authors. *Trap depth*: Provided by the cited references. FC_o-*uncorr.*: Non-depth-corrected FC_{org}. FC_{org}: Normalized value to 2 km ($b = -0.86$) applied to calculate POC in mmolC m^{-2} yr^{-1}. *Ternary mol %*: ternary percentage of FC_{org}, FC_{inorg}, and FSi_{bio} calculated for each trap.

aggregates include fecal pellets of mesozooplankton, remains of organisms, polysaccharide flocculates of various origins, and ecosystem components such as larvacean houses. Aggregates are usually strongly colonized by microbes particularly in the surface waters (e.g., Smith et al., 1992). Aggregate sizes and configurations vary widely in the near-surface layers and are likely changed as they encounter turbulence in shallow waters. As they descend through the water column, aggregates attract and entangle fine suspended particles and microbes (e.g., Tsujita, 1953; Milliman et al., 1967; Alldredge, 1976; Shanks and Trent, 1980; Alldredge and Cox, 1982; Alldredge and Silver, 1988; Alldredge et al., 1990; Silver and Gowing, 1991).

Camera images have been used to estimate standing crop, sizes, and settling speeds of aggregates (Honjo et al., 1984; Asper et al., 1992; Davis and Pilskaln, 1993). These observations so far show that (1) aggregates are found in all oceanic zones, wherever cameras are lowered; (2) epipelagic aggregates exhibit random configurations and sizes that become more homogenous as they descend into the mesopelagic and bathypelagic zones; (3) the abundance of aggregates in the lower mesopelagic and bathypelagic zones fluctuates but maintains a constant bulk average (Asper, 1987; Gardner and Walsh, 1990; Asper et al., 1992; Walsh and Gardner, 1992; Walsh et al., 1997; Diercks and Asper, 1997; McCave et al., 2001); (4) large aggregates are not always net scavengers but they can be net suppliers (McCave et al., 2001), and (5) trap measured fluxes and fluxes estimated from camera data are not yet comparable (Walsh and Gardner, 1992; Pilskaln et al., 1998), possibly because of the involvement of too many assumptions. There has been no compilation of aggregate standing stock over larger ocean regions, mainly because the practical image resolution of existing cameras is unconstrained and statistical standards are inconsistent among published data sets. An exception was the OMEX transect where full ocean depth aggregate properties were profiled (McCave et al., 2001). Use of cameras for this research will be improved by higher image resolution and standardization of the image processing routine using recent *in situ* automated plankton identification technology (e.g., Benfield et al., 2007; Pilskaln, 2007, personal communication).

Laboratory measurements using a settling cylinder (e.g., Gorsky et al., 1984) and adaptation of the cylinder concept to *in situ* measurements (e.g., Asper, 1987; Diercks and Asper, 1997) indicate that the short-distance settling speed of a single aggregate ranges from a few to 368 m day^{-1} (e.g., review in Alldredge and Silver, 1988; Diercks and Asper, 1997). However, these short-term measurements cannot be extrapolated to the full water column because of changing aggregate transport modes. Tracking offsets of distinct particle-flux "peaks and valleys" (marking events) between pairs of synchronized shallow and deep TS-traps provides gross settling velocity for POC (and other mass flux constituents) regardless of settling mode (e.g., Honjo, 1996; Honjo and Weller, 1997; Honjo et al., 1999; Berelson, 2002). Previous estimates based on the offset marker method indicate settling speeds between 80 and 200 m day^{-1}. Comparison of simultaneous primary production (Dickey et al., 1998) and high-resolution export flux measurements (with a 4.25-day sampling period) made over a year's time in the Arabian Sea indicates an average POC settling time from epipelagic primary production to upper bathypelagic waters (2.2 km) as approximately 17 days or 130 m day^{-1} (Honjo et al., 1999; Honjo and Weller, 1997). At an Antarctic Circumpolar Current station where a diatomaceous mat served as POC ballast (Honjo et al., 2000) (Section 6.5), the POC settling speed was as high as 200 m day^{-1}. Broerse (2000) investigated the details of offset arrival of coccoliths at many JGOFS depth-series sediment trap arrays and the Sea of Okhotsk and found similar speeds as above mentioned. Using lithogenic Al contents of aggregates as the conservative tracer, gross settling speed of ocean particles is approximately 100 m day^{-1}, and the speed increases in deeper layers (Berelson, 2002) (Section 12.2).

2.2. Ballast particles (Sections 7 and 8)

Several qualities render ballast particles effective for vertical transport of POC, including the following. (1) The particles should be small and uniform in size and readily grazed, filtered, or adhered to aggregates. (2) The in-water gravity of the particles must be high enough so that they add significant extra weight to the particles. (3) The ballast particles should be resistant to *in situ* dissolution and *in vivo* destruction or digestion. Exhaustive microscopy and chemical analysis of particles collected by sediment traps indicates that two common biominerals, *biogenic calcite and opal*, both the byproducts of primary production, play an essential role as ballast in the transport of POC to the interior sink layers (e.g., Honjo, 1996, 1997b).

2.2.1. Biogenic $CaCO_3$ (Section 7.2)

Calcite and aragonite biominerals constitute coccoliths, planktonic foraminiferal tests, and pteropod shells. Calcite is one of the heaviest biominerals found in ocean water, and it is more resistant to dissolution in seawater than other pelagic biominerals, including biogenic opal, aragonite, and magnesium-rich calcite (e.g. Milliman, 1974). Coccoliths, composed of calcite, are a byproduct of primary production. Coccoliths are scales that cover the surface of an individual coccolithophorid cell (e.g., Klaveness and Paasche, 1971). They are continuously released to the seawater as new coccoliths are produced in the cell's interior and added to the exterior while adjusting buoyancy. The per-life-span production rate and number of coccoliths retained within a coccolithophorid cell (a coccosphere) are not well enough constrained to allow estimation the production rate of coccolith-PIC (e.g., Yang and Wei, 2003). Coccolithophorids inhabit broad areas of the ocean's euphotic zone (e.g., Okada and Honjo, 1973; Okada and McIntyre, 1979) and are universally found in TS-traps (Steinmetz, 1991; Broerse, 2000) except in the high polar seas (where noncalcifying species are found; Thomsen et al., 1988). Coccoliths are arguably the most suitable ballast particles because of their small and uniform size, supply directly from the euphotic zone, and high resistance to dissolution (e.g., Honjo, 1997b; Broerse, 2000) (Section 12.2). In laboratory cultures, individual coccolithophorids have been observed to suddenly secrete a mucus, form an aggregate, and sink to the bottom of the culture vessel. This extreme mode of gravitational transport (e.g., Smayda, 1971) may not happen often in nature, though mass sinking of *Umbilicosphaera sibogae* was observed in an early TS-trap experiment in the Panama Basin (Honjo, 1982). Triggers for this mass sinking or "self removal" from the surface in the open sea are not well understood. In contrast to coccolith-$CaCO_3$, celestite ($SrSO_4$) skeletons of Acantharia, relatively common planktonic sarcodines that inhabit the euphotic zone (Bernstein et al., 1987; Caron et al., 1995), do not participate in transporting POC to the oceanic interior despite the fact that their secretetions are likely to be the heaviest biomineral hard tissue produced in the pelagic ocean (specific gravity: 4.0). The celestite skeleton is highly soluble in seawater and seldom preserved in the TS-traps deployed even in the upper mesopelagic zone.

A question remains as to the effectiveness of mature planktonic foraminiferal tests and pteropod shells as POC ballast. Foraminiferal tests are almost never found in mesozooplankton fecal pellets except as gamete shells. Mature foraminifera settle at a rate of 1 km/day (Berger and Piper, 1972; Takahashi and Bé, 1984), and modestly sized pteropod shells settle as fast as a few km per day (Vinogradov, 1961; Byrne et al., 1984), while aggregates normally settle at a rate of only 0.1–0.2 km/day. Aggregates are fragile structures that would quickly disintegrate upon encountering hydrodynamic shear at the high settling speeds of tests and shells. Also, the population of adult foraminifera is far smaller than that of coccoliths and diatoms. Thus, it appears that, in contrast to coccoliths, large tests and shells do not have a role as ballast for transporting POC, except for their large contribution to the total export flux of PIC (molC in $CaCO_3$) in removing alkalinity from upper layers to the interior (Section 12). Laboratory methods developed by Ziveri et al. (2000) and Ramaswamy and Gaye (2006) to constrain the ratio between zooplankton and phytoplankton $CaCO_3$ in trap samples provide an avenue for studying this phenomenon.

Pteropods, which are pelagic snails (Lalli and Gilmer, 1989), are found in all oceanic provinces (Bé and Gilmer, 1977) and their shells consist of aragonite that is "metastable $CaCO_3$" (Section 12.2). Massive pteropod populations are often collected in epipelagic and upper mesopelagic traps (Betzer et al., 1984; Byrne et al., 1984; Collier et al., 2000; Gardner et al., 2000; Mohan et al., 2006; Harbison and Gilmer, 1986). Pteropods are attracted by any large, solid objects during their diel vertical migration to 600 m or more, and therefore the flux data from the upper mesopelagic layer can be strongly overestimated (Harbison and Gilmer, 1986), presenting a challenge in PIC flux and dissolution research (Section 12.2). Although mature pteropod shells may not contribute ballast for settling POC to the oceanic interior, knowledge about their dissolution could be critical to understanding their role as a possible source of upper mesopelagic alkalinity (Section 12.2).

2.2.2. Biogenic opal (Section 7.3)

Opal, in the form of chalcedony crystals, is almost as dense as calcite (Calvert, 1983). but the frustules are porous, and organic matter is incorporated in their microstructure (Hurd, 1983; Takahashi, 1991a), rendering their specific gravity significantly lower than that of coccoliths. Diatom frustules are the most ubiquitous ocean particles, and, in fact, all the TS-trap samples examined for this study contained diatom frustules regardless of the basin and climatic regime where the traps were deployed (Tables 2 and 3). Diatom frustules

are abundant in the northernmost (Wangel Abyssal Plain, the High Arctic; Zernova et al., 2000) and the southernmost (Ross Sea; Collier et al., 2000) open ocean TS-traps (Section 3). Radiolarian tests are also a part of opal export flux and while they are far more highly diversified than planktonic foraminifera (Gowing and Coale, 1989; Takahashi, 1991a), they render far less opal flux than diatom frustules (Takahashi et al., 2000). Silicoflagellates and Actinicsus (Orr and Conley, 1976) skeletons, which are similar in size to diatom frustules, are found in the pelagic trap samples, but their occurrence is inconsistent (Takahashi, 1991b). Diatom frustules often produce numerous long protrusions (seta) that can entangle floccules and form efficient settling media (diatomaceous mats; Lampitt, 1985; Kemp et al., 1999; Honjo, 2004). Significant dissolution (up to 70%) of biogenic opal has been reported (Nelson et al., 1995; Tréguer et al., 1995) in the epipelagic and upper-mesopelagic zones (Section 12).

2.2.3. Lithogenic particles

Crustal aerosol particles (Duce et al., 1991; Tegen and Fung, 1994; Mahowald et al., 1999) play a critical role as POC ballast (e.g., Armstrong et al., 2001) in oceanic regions where abundant supplies result from proximity to significant areas of dry land and desert on the upwind side of ocean margins, such as the western African margins (e.g., Wefer and Fischer, 1993b; Fischer and Wefer, 1996; Ratmeyer et al., 1999) and the Arabian Sea during both monsoon seasons (e.g., Nair et al., 1989). The combination of upwelling and significant dust fallout in these hemipelagic margins generates an extraordinary capacity for transferring primary production to the ocean interior. However, considering the export fluxes of Al and Ti found in TS-traps (Manganini et al., JGOFS Web site, 2003), the world distribution of atmospheric aerosol (e.g., Duce et al., 1991; Rea, 1994; Prospero, 1996), and oceanic precipitation (Tegen and Fung, 1994), the supply of lithogenic aerosol to the pelagic ocean is significantly smaller than and inconsistent with the availability of biomineral particles. Particularly, TS-traps placed in the equatorial Pacific (Honjo et al., 1995) and the Southern Ocean (Honjo et al., 2000), where the POC flux is often far larger than the global average (Table 5; Section 10) (Figs. 3 and 9 and Table 5), yield only trace amounts of particulate Al and Ti. Thus, from a global perspective, lithogenic particles play only a limited role in POC transport (Francois et al., 2002) except in large upwelling margin environments (Fischer et al., 2000, 2003). During the extended deployment of the autonomous platform "Carbon Explorer" near Station P (Wong et al., 1999), its biogeochemical sensors detected 10 days of significant Asian dust fallout followed immediately by a twofold increase in epipelagic POC standing crop in the same area (Bishop et al., 2002). Although the final effect of this lithogenic fallout on the POC flux to the ocean interior is not yet clear, further use of this new instrument and its sensors could greatly enhance biological pump research in the open ocean. Lithogenic particles supplied by coastal erosion and estuarine transport play a greater supporting role for the biological pump in the productive marginal seas (e.g., Thunell et al., 2007) and nonproductive Antarctic margins (Wefer and Fischer, 1988; Fischer et al., 2000). In the sea-ice-covered High Arctic where net community production is essentially zero, vertical and lateral transport of POC depend almost entirely on terrigenous lithogenic particles supplied by river discharge and coastal erosion even far in the interior of a pelagic basin (O'Brien et al., 2006; Fahl and Nöthig, 2007; Hwang et al., 2007, unpublished). The unique operation of the biological pump in the High Arctic demands further immediate exploration in light of rapid environmental change.

2.2.4. Fecal pellets

Mesozooplankton fecal pellets are large aggregates that play a special role as an effective transporter of POC. Flocculated aggregates are extremely fragile and rarely preserved while mesozooplankton fecal pellets are more robust. They are commonly found even in deep TS-trap samples, allowing researchers to study the packaged particles in detail. Typically a few hundred micrometers in diameter, fecal pellets are often packed with underdigested POC and biomineral ballast (e.g., Gagosian et al., 1983; Staresenic et al., 1983; von Bodungen et al., 1987). Wilson et al. (2006), investigated repacking history of fecal pellets (Section 12.2). Gowing and Silver (1985) and Beaumont et al. (2002) reported small classes of fecal pellets (3–50 μm) from the Antarctic waters. Fecal pellets themselves serve to ballast large aggregates, and their contribution to the POC flux ranges widely from almost none to over 80% (Pilskaln and Honjo, 1987; Lane et al., 1994; Urban-Rich et al., 1998). Pelagic salp feces (Norris, 1971; Iseki, 1981; Madin, 1982; Matsueda et al., 1986) are particularly effective couriers of POC because of salps' high filtering and defecation rates

(Harbison and McAlister, 1979) and their diel migration (to 0.9 km; Madin et al., 2006). Calanoid crustaceans are ubiquitous in the world pelagic ocean (e.g., McGowan, 1971; Marshall and Orr, 1972; Miller et al., 1984) and provide another major source of fecal pellets. Filter feeding and grazing mesozooplankton feces are covered by protective pellicles (Gauld, 1957) that are colonized and consumed by heterotrophic organisms whose activities are temperature dependent, so the disintegration and release of DOC (Urban-Rich, 1999) from these feces is more complete when the thermocline is deep (Honjo and Roman, 1978; Kikuchi and Omori, 1985). The settling speed of mesozooplankton fecal pellets (Smayda, 1971; Small et al., 1979) is similar to that of bulk POC, suggesting that pellets and other aggregates descend synchronously.

2.3. Active downward transport by zooplankton

POC transport by zooplankton includes defecation, predation, and sinking of animal carcasses (e.g., Steinberg et al., 2002). Based on deep tows and wide-band sounding, it is estimated that 15–50% of zooplankton biomass above 500 m migrates vertically into shallow layers at night (e.g., Hardy and Bainbridge, 1954; Vinogradov, 1972; Wiebe et al., 1979; Angel and Baker, 1982; Kikuchi and Omori, 1985; Longhurst and Harrison, 1988; National Astronomical Observatory, Japan, 2006). The latter compiled the day/night depths and vertical migration distances of 31 zooplankton species, listing references to 20 publications.). This diel vertical migration pattern of a large zooplanktonic population transports POC (and DOC) across the pycnocline to the ocean interior (e.g., Wiebe et al., 1979; Longhurst and Harrison, 1988; Steinberg et al., 2002; Madin et al., 2006; Buesseler et al., 2007). Diel migration of zooplankton is potentially capable of removing one to two orders of magnitude more POC to the deeper layers than is the case for animals of a similar standing crop that exhibit low-frequency seasonal or ontogenetic migrations with periodicities of months (Angel and Baker, 1982). In upwelling equatorial Pacific waters, Zhang and Dam (1997) estimate cross-pycnocline POC flux by mesozooplankton mortality as $34 \pm 9\%$ and $38 \pm 8\%$ of total active POC flux during spring and fall cruises, respectively. We will review the impact of vertical zooplankton migration more extensively in later discussions of the oceanic interior sink of CO_2 and of upper mesopelagic carbonate chemistry (Sections 11 and 12).

2.4. Downward transport of DOC

There is no evidence that the huge reservoir of highly refractory carbon transported by rivers and distributed in the deep ocean (Cauwet, 2002) (more than all the carbon contained in plants on land; IPCC, 2001) plays a significant part in the biological pump process (Hansell et al., 2004). The labile DOC content of the upper ocean was described by Sambrotto et al. (1993) and Williams (1995), and by Hansell and Carlson (1998) who demonstrated that the net production of labile DOC largely takes place during periods of net community production. Labile DOC excreted by migratory zooplankton provides immediately available food resources to the heterotrophic community in the mesopelagic zone (Doval and Hansell, 2000). Thus, labile DOC is a byproduct of biogenic settling particles such as fecal pellets (Honjo and Roman, 1978; Urban-Rich, 1999), and production of labile DOC at depth can be understood as an extension of the biological pump. Labile DOC can be overturned to the deeper layers (e.g., Talley, 2003; Church, 2007) as well as transported by current systems. Hansell and Carlson (2001) estimate that global labile DOC production is 15–20% of the new production and supports 10% of the metabolism in layers below 500 m. However, Arístegui et al. (2002) argue that the bulk of respiration within the mesopelagic zone is managed by gravitational transport of POC.

2.5. "Terminal" gravitational transport of POC in lower- and submesopelagic zones

As discussed in Section 2.4, the deeper limit for migrant zooplankton is generally recognized as approximately 0.9 km (e.g., Wiebe et al., 1979; Angel and Baker, 1982). The realistic limit of zooplankton habitat appears to be 1.5 km, although trace numbers of resident zooplankton are found throughout the bathypelagic and abyssopelagic zones (e.g., Wishner, 1980; Angel and Baker, 1982; Kikuchi and Omori, 1985). Below the zooplankton habitat, POC is pumped almost solely by the gravitational settling of aggregates, fecal pellets,

and carcasses. We call this form of settling "terminal" gravitational transport (Section 5.3). In theory, aggregates descending here are unaffected by ecosystem activity, though they may be rearranged by slow heterotrophic remineralization, mechanical disintegration, and crashing. However, there is still a question regarding why the particle size and population remain quasi-constant throughout the mid-, lower-, and submesopelagic water column (Section 2.1) while the particle flux decreases with depth. It calls for *in situ* investigation of aggregates at these depths using improved large-volume cameras, collection of intact aggregates by ROV/submersible, or other innovative new methods.

3. Existing global data on settling particle export fluxes: an overview

The vast amount of data available on export fluxes of POC and other oceanic particles were collected by independent, cooperative, international research programs that deployed sediment traps along bottom-tethered mooring platforms in all the world oceanic basins and major marginal inland seas. The northernmost and southernmost open sea TS-moorings with published data sets were located on the Wrangel Abyssal Basin (81.0°N, 138.5°E; Fahl and Nöthig, 2007) and the Ross Sea Shelf (76.5°S, 178.0°E; Collier et al., 2000), respectively. Many of these moorings included more than one trap, some as many as seven traps set at a series of depths (e.g., Honjo et al., 1999, 2000). Moorings were deployed repeatedly over many years, more than 15 years at some time-series stations as described later in this section. We estimate that, through 2006, the oceanographic community has gathered data from at least 426 TS-traps moored at 240 locations. Many of the TS-traps were programmed to operate in a 12-month, time-series sampling mode divided into 12–22 time fractions (Section 4.1). A compilation of minimally edited global TS-trap data obtained from the published literature is posted on a JGOFS Web site (Manganini et al., 2003).

The US JGOFS field program provided annual oceanic export flux data sets from a total of 47 TS-traps set at 22 stations from 1989 to 2001. The program's cooperative studies included a number of institutions and were associated with other related field observations including hydrography, biology, and physical oceanography. The US JGOFS TS-traps were deployed in linear-transect, deep-ocean arrays of multiple traps arranged for 3D coverage and programmed for synchronized open/close sequences. These moorings were set in four oceanic regions:

(1) The North Atlantic (North Atlantic Bloom Experiment [NABE]) in NADR and NAST-E provinces beginning in 1989 (Honjo and Manganini, 1993). (The four-and five-letter acronyms such as NADR and NAST-E indicate global biogeochemical provinces defined by Longhurst et al. (1995), and shown in our Table 1 and Fig. 1.)
(2) The equatorial Pacific (EqPac Program) in PEQD and SPSG, 1992 (Honjo et al., 1995).
(3) The Arabian Sea (Arabian Sea Expedition [ASE]; Smith et al., 1998) in ARAB and MONS, where investigations were conducted jointly with the Indian National Institute of Oceanography and the University of Hamburg. (Many exciting findings have resulted from these pre-JGOFS and JGOFS joint investigations; e.g., Nair et al., 1989; Haake et al., 1996; Lee et al., 1998; Honjo et al., 1999.)
(4) The Southern Ocean (Antarctic Environment and Southern Ocean Process Study [AESOPS] Smith et al., 2000) in SANT and ANTA, 1996 (Honjo et al., 2000).

Over a 20-year period, a University of Bremen program published export particle flux data collected by 40 TS traps from 16 stations set along a quasi-meridional transect from the Cape Verde area (21°N, 21°E) in NATRA to the Weddell Sea (Kapp Norvegia; 71°S, 12°E) in ANTA, with particularly detailed stations in Cape Blanc, off Mauritania (4-year time series stations from 1988 to 1991; e.g., Fischer et al., 1996; Ratmeyer et al., 1999) and Gulf of Guinea (from 1983 to 1985; Wefer and Fischer, 1993b; Fischer and Wefer, 1996; Fischer et al., 1996). The review of this program was published in Fischer et al. (2000). The Nordic Seas were covered by a network of 11 TS-trap stations beginning as early as 1984 (Honjo and Manganini, 1987). These stations were initially operated by a joint University of Kiel–Woods Hole Oceanographic Institution (WHOI) project onboard R/V *Polarstern* (e.g., Wefer and Honjo, 1985; Honjo et al., 1988; Honjo, 1990), and a multi-year, multi-depth TS-trap program was later deployed by von Bodungen et al. (1995), in the central basin of the Nordic Seas. European consortium projects, including the Ocean Margin Exchange

(OMEX; Wollast and Chou, 2001) and Biogeochemical Ocean Flux Study (BOFS) programs, deployed many TS-trap stations in the northeast Atlantic Westerlies domain, particularly in NADR and NAST-E beginning in 1989 (Kuss and Kremling, 1999; Antia et al., 1999; Antia et al., 2001a,b; McCave et al., 2001; Scholten et al., 2001). Antia et al. (2001b) reviewed the results of export flux programs undertaken in northwestern Atlantic margins.

TS-traps have been deployed in European inland seas since the early days of biological pump studies. Multi-year TS-trap stations were set in the southern Euxine Abyssal Plain beginning in 1983 by University of Izmir, University of Hamburg, and WHOI scientists (Izdar et al., 1984; Hay et al., 1990). Buesseler et al. (1987) successfully monitored the fallout rates of Chernobyl radionuclides in the deep interior of the Black Sea after the 1986 reactor incident. Three TS-trap stations each were set in the Ligurian Sea and the Gulf of Lion, and two were deployed for reference in the Bay of Biscay in the period from 1988 to 1991 (Monaco et al., 1990; Etcheber et al., 1996).

In the Pacific, from 1995 to 1998, NOPACCS (Northwest Pacific Carbon Cycle Study; Tsubota et al., 1999) deployed 13 TS-traps at eight mooring stations spaced at quasi-equal distances from 46.1°N (PSAG) to 0.0° (WARM) along a cross-basin meridional transect at 175°W (e.g., Kawahata et al., 1999, 2000). The NOPACCS transect covered Arctic/subarctic and tropical and subtropical gyres in the North Pacific at the widest part of this basin over a 3-year time span. The boreal Pacific is particularly well covered by TS-trap stations. As early as 1982 to 1984, a Hokkaido University program deployed six TS-trap stations in the North Pacific and one in the Antarctic Zone for short periods (e.g., Noriki and Tsunogai, 1986; Tsunogai and Noriki, 1987). Takahashi et al. (1997, 2000) successfully collected deep-flux data at two Aleutian stations (designated AB and SA; PSAG-W) between 1994 and 1999. TS-trap stations were jointly deployed in the central Sea of Okhotsk (1990) and the northern Bering Sea (1991) by the Japan Marine Science and Technology Center (JAMSTEC) and WHOI; these stations provide the northernmost marginal-sea data (Honjo, 1997a; Broerse, 2000). The ongoing Japanese KNOT-HiLat Project in the Northwest Pacific (Honda et al., 1997, 2002) has collected multiyear export records since 1996. A review of this program was published in Honda et al. (2002). Hong et al. (1997) have deployed TS-traps in the East Sea/Japan Sea (ES/JS) since 1994 as a part of a continuing Korean ES/JS investigation. The western Pacific warm-water pool (AWRM) was studied by University of Hamburg scientists in 1988 and 1989, providing critical information from a large oceanic region of depleted export particle flux (Kempe and Knaack, 1996).

Despite great interest in the biological pump that operates in the pelagic, ice-covered High Arctic Ocean, only a few programs have acquired annual TS-trap data from this region. O'Brien et al. (2006) successfully deployed several TS-traps for a full year on the Canadian Beaufort Shelf to study the terrestrial supply of POC. The sea-ice-covered High Arctic is the remaining challenge for a year-long deployment. However, two TS-trap moorings were successfully deployed on the Wrangel Abyssal Plain (Zernova et al., 2000; Fahl and Nöthig, 2007) and most recently on the Canada Abyssal Plain (Honjo et al., 2007, unpublished). The University of Bremen program covered the Atlantic sector of the Southern Ocean from 1983 to 1995 (e.g., Fischer et al., 2000). In the Pacific sector, as mentioned above, the JGOFS AESOPS program deployed 7 stations with 23 synchronized TS-traps along approximately 170°W from 76.5°S (Ross Sea shelf) to 53.0°S in 1997 (Collier et al., 2000; Honjo et al., 2000). A long term TS-trap array between Tasmania and Antarctica has been maintained by the Australian Subarctic Zone Program (e.g., Trull et al., 2001) since 1997 (Bray et al., 2000), and US and French investigators have placed TS-trap stations in the Indian Ocean sector of the southern Ocean, Prydz Bay area, at 62°S/63°S and 71°W/73°W (Pilskaln et al., 2004; Tréguer, 2003, unpublished).

Several TS-trap stations at fixed locations have been maintained for more than 15 years (and are continuing as of this writing). These include: (1) Ocean Station P located in the eastern North Pacific since 1983 at 50°N, 145°E (e.g., Wong et al., 1999), (2) BAT (Bermuda Atlantic Time-series) station in the Sargasso Sea in the North Atlantic at 32.1°N, 64.3°E, initiated by W. Deuser in 1984 (Deuser, 1987; Deuser et al., 1995; Deuser, 1996; Conte et al., 2001), (3) the Indo-German Arabian Sea and Bay of Bengal stations since 1987 (Nair et al., 1989; Ittekkot et al., 1991; Haake et al., 1996), (4) the IMS (Institute of Marine Science, Iceland) station on the Icelandic Plateau in the Nordic Seas at 68°N, 12, 7°E since 1987 (Olafsson et al., 2001, unpublished), and (5) Ocean Station M in the eastern North Pacific (Smith and Kaufmann, 1999; Smith et al., 2006). In addition, the ongoing Hawaii Ocean Time-series (HOT) station north of Hawaii initiated

in 1996 (TS-trap data have not been disclosed; Karl, personal communication), the OMEX North Pacific station (Antia et al., 2001a,b; Scholten et al., 2001), and the ongoing Japanese KNOT-HiLat Project in the Northwest Pacific (Honda et al., 1997, 2002) have collected multi-year export records since 1996.

The deepest TS-trap, set at 8431 m for a 12-period time series, was successfully recovered after a 1-year continuous deployment from the 8931-m Japan Trench seafloor at 34.2°N, 142°E in 1992–1993 (Nozaki, 1989; Handa, 1989; Nozaki and Oba, 1995; Handa et al., 1997; Saito et al., 1997). Itou and Noriki (1997) also deployed a mooring in deep Japan Trench slope water with three TS-traps at 40°26'N, 144°28'E in 1994–1995. The lowest TS-trap was set 6800 m deep, approximately 400 m above the bottom. The mass flux of the deepest trap surged during the collection period beginning December 27, 1994, to as much as >9 above the average flux during the previous collection periods. The mass flux decreased to the pre-surge level after 6 months in a linear mode. The authors suspect the surge to be an effect of the Mw 7.7 Sanriku-Oki Earthquake (Tanioka et al., 1996) that occurred on December 28, 1994, with its epicenter at 40°52'N, 143°42'E. Programs that have set long-term coastal zone stations along the North American West Coast have made unique contributions to the understanding of the biological pump in upwelling-dominated coastal zones and high-volume estuaries (e.g., Thunell et al., 1994; Thunell, 1998a; Thunell, 1998b, 2007; Pilskaln et al., 1996; Pena et al., 1999; Lyle et al., 1992; O'Brien et al., 2006). Thunell et al. (2007) review the POC fluxes and processes in the upwelling-dominated subtropical and tropical continental margins of the Americas. Highly productive anoxic basins, including the Cariaco Basin, have been investigated by multi-year time-series TS-trap deployments (Thunell et al., 2000). A number of articles have been published on the export fluxes of biogenic particles in large lakes such as Lake Baikal (at 1582 m; e.g., Kemp et al., 1996) and Lake Malawi (at 300–350 m; Pilskaln, 2004) (Fig. 1). Though these studies on the biological pump in deep lakes contribute stimulating results for comparison with the oceanic biological pump, we did not include them in this article. However, their data are available on a US JGOFS Web site (Manganini et al., 2003).

4. TS-trap methodology and possible biases in flux data

4.1. TS-trap technology: a short summary

4.1.1. TS-trap technology

Most TS-traps that provided particle flux data for this synthesis are approximations of the WHOI PARFLUX Mark 6 Time-series sediment trap (Honjo and Doherty, 1988). The trap design has evolved over the last 25 years to the most recent model, the McLane Mark 78H-21 (the operating manual may be found at: <http://www.mclanelabs.com/manuals/trap-revE.pdf>). However, the principle design and hydrodynamic profile of the original trap have been preserved as much as possible based on the model that was tested during the 1979 Panama Basin Intercomparison Experiment (Honjo et al., 1992). The default specifications include: (1) a 0.25 m^2 (or 0.5 m^2) round aperture covered by a honeycomb baffle whose individual cells have an aspect ratio of 2.5, (2) a 16° funnel slope, and (3) accommodations for in-line attachment to a mooring.

4.1.2. Long-term, deep-ocean TS-trap platforms

The TS-trap mooring is based on the WHOI-Heinmiller mooring that supports a heavily instrumented mooring cable while maintaining uniformly distributed tension throughout the line and providing optimum stability against deep-sea advection. Distribution of flotation is calculated on a model that balances the weight of both the mooring line and the instruments against the anchor. An acoustic release mechanism allows efficient retrieval of the TS-traps and their samples. Since Heinmiller (1979), numerous engineering improvements have steadily increased instrument stability on the mooring. More recent TS-traps are equipped with precision tilt-gauge/compass combinations or acoustic current meters to detect abnormal advection events. In general, currents do not exceed several cm s^{-1} in the lower mesopelagic zone and the turbulent benthic layers. However, an onboard tilt-gauge with an accuracy of 0.5° (in recent models) continuously monitors a TS-trap's aperture plane. Rarely, a mooring encounters a "deep ocean storm" (e.g. Gardner and Sullivan, 1981) lasting for days or weeks; for example, one storm tilted a TS-trap we moored at 1 km in the New Zealand sector of the Subantarctic Zone (SAZ) as much as 35° from the horizon for several weeks (Honjo et al., 2000). The particle flux data from such periods should be discarded.

4.2. Possible biases in export data collected by moored TS-traps

4.2.1. Effects of advection

The effects of advection have been discussed and studied experimentally since the inception of particle flux research in aquatic environments (e.g., Gardner, 1980, 1989; Butman, 1986; Baker et al., 1988; Buesseler, 1991; Gust et al., 1992; Buesseler et al., 1994, 2000; Siegel and Deuser, 1997). There are still unanswered questions about exactly how settling particles behave when they encounter a trap. Discrepancies between oxygen utilization measurements on the deep seafloor and POC flux found in data from sediment traps in the water column above have led to questions about the reliability of sediment trap measurements of POC (e.g., Christensen, 2000). One good example is the set of decadal time-series observations from the Station M > 4-km-deep station in the CCAL province of the North Pacific (Smith and Kaufmann, 1999; Smith et al., 2006). These questions can only be answered by further research on the complex but intriguing relationship between benthic community respiration and POC supply. The major difficulty in simulating the process of entrapment of aggregates is our inability to create a very small advection field in the laboratory and to produce synthetic ballasted aggregates that behave exactly the same as their extraordinarily fragile natural counterparts. Use of neutrally buoyant traps may offer a promising approach for acquiring vertical particle flux in relatively shallow layers such as the upper mesopelagic zone (e.g., Buesseler et al., 2007).

4.3. Sample preservation

Preservation of collected samples to protect them from degradation and disintegration is critical to measuring the export flux of all biogenic particles, particularly POC. Remineralization of POC in a sampling container lowers the pH and dissolves trapped $CaCO_3$ (e.g., Gardner et al., 1983; Lee et al., 1992; Knauer et al., 1984; Cole et al., 1985, 1987; Hedges et al., 1993; Christensen, 2000). Two commonly used preservatives, sodium borate-buffered formalin (often formaldehyde) for the *in situ* deep-water samples (obtained from bottle casts prior to trap deployment) and $HgCl_2$ for the filtered surface water with slightly elevated salinity, were used in the majority of deployments included in this synthesis. Field intercomparison experiments using buffered formalin and $HgCl_2$ solutions in the lower mesopelagic zone indicated no detectable difference in preservation capacities for POC and biominerals (e.g., Honjo et al., 1995); however, formalin and formaldehyde interfere with carbon isotope measurements, and $HgCl_2$ solution interferes with some trace-metal and clay-mineral analyses. Sodium azide solution was used in a number of shorter pre-1985 deployments (e.g., Honjo et al., 1979). The effectiveness of this organic nitrogen compound for a full-year deployment has not been established. TS-trap sampling containers must be securely sealed against seawater intrusion before and after their collecting periods. A preservation anomaly is indicated by the lowering of pH in the supernatant of samples at recovery. Information on preservation conditions, particularly the pH levels of the supernatant, was missing in many published reports. In this synthesis, we assume that most of the TS-trap deployments successfully preserved POC and $CaCO_3$, as long as the deployment conditions of a TS-trap followed the US JGOFS protocol on preservatives (US JGOFS Planning Committee, 1989).

4.4. Zooplankton effects

As discussed above, the zooplankton community, particularly in a migrant ecosystem, is one of the essential means by which the biological pump removes and transports POC from the upper layers to the oceanic interior. Zooplankton on the order of millimeters to centimeters in size constantly consume and repack particles, prey upon other animals, and reproduce while migrating vertically in a diel pattern. Some pteropods, decapods, and salps shuttle 500–900 m/day (e.g., Kikuchi and Omori, 1985; Lampitt et al., 1993; Madin et al., 2006) (Section 2). A sediment trap designed only to collect gravitationally settling particles cannot deal properly with this problem. Living zooplankton that actively swim into the open sampling bottle of a trap and are preserved along with the settling particles bias the export flux measurements of POC (e.g., Knauer et al., 1984; Harbison and Gilmer, 1986; Lee et al., 1988). The "swimmer problem" (Knauer et al., 1979; Lee et al., 1988) is particularly severe when a trap is deployed within a zooplankton diel migrating habitat in the upper mesopelagic layer. A sediment trap with an indented rotating sphere (IRS) designed to eliminate living, moving

zooplankton has been developed to cope with this problem (Peterson et al., 2005) but has not yet been broadly used. No TS-traps cited in this paper used the IRS method.

4.5. Systematic errors in laboratory analysis

Most trap-collected samples are sieved through a 1-mm nylon mesh using filtered seawater. Most particles that are larger than 1 mm disintegrate during this sieving process and pass through the mesh. The particles that pass through the 1-mm mesh are recovered on a hole-type membrane filter with a nominal hole diameter of 0.2 μm. This fraction is used for laboratory analysis after rinsing with distilled water and oven drying. Any particles retained on the 1-mm mesh are usually regarded as swimmers (Knauer et al., 1979), though there is a question about whether this process eliminates all swimmers in the TS-traps deployed in the upper mesopelagic zone. However, the amount of >1 mm particles collected in the mesopelagic/bathypelagic boundary constitutes less than 5% of the mass flux and even less in deeper samples, falling within the range of analytical error. In principal, no swimmers are expected in the material delivered to a trap via terminal gravitational transport. Therefore, zooplankton carcasses and remains collected at the mesopelagic/bathypelagic boundary are considered to result from senescence and molting (Section 2.3) and thus are a genuine part of POC flux.

When TS-trap samples are shared with a research project that mandates wet samples (for example, quantitative microscopy of foraminiferal tests and all other biocoenosis research), an original sample with supernatant water is first divided into a number of aliquots (usually 10) by a precision wet-sample divider such as the widely used MRL WAD-10 wet-sample divider. Introduction of this procedure imposes a systematic error of 3–5% when assessing total mass flux.

Interlaboratory analytical error in analyzing POC and PIC is constrained within 5%, based on the results of an intercomparison by several US JGOFS and Japanese laboratories using a standard particle sample. This relatively low interlaboratory error level in carbon analysis is attributed to the universal use of direct elementary analysis under common principals, though there may be some differences among designs of equipment being used for analysis (elementary analyzers for POC and coulometric titration for PIC analysis). In some pre-1986 publications where organic carbon flux is described as "organic matter" flux, it was converted to mole POC flux, applying relational factors between plankton dry weight vs. organic carbon (e.g., Wiebe et al., 1975). The magnitude of error caused by this conversion is not known, but could be substantial.

Biogenic silicon analysis shows greater differences among laboratories and stations/depths. This is due to the difference in methods used to separate Si in biogenic opal and Si in silicate minerals originating in Earth's crust (lithogenic Si). Thus, the discrimination of lithogenic silicate mineral particles from biogenic opal creates additional errors despite common use by most laboratories of the direct Si assessment originally described by Mortlock and Froelick (1989). Two methods are commonly applied to segregate biogenic opal. One is sequential leaching of opal in an alkaline solution to exploit the resistance of crustal minerals to dissolution in diluted alkaline solutions. The other is the total dissolution of a known mass of particles in a lithium metaborate flux followed by atomic-absorption spectrometer analysis of Si and Al (and Ti). Lithogenic particle flux, reconstructed from Al (often Ti as well) contents using the Earth-crust elemental indices, is then subtracted from total Si to obtain biogenic opal Si flux. US JGOFS investigators have employed a total liquidizing method since 1998 (Arabian Sea Process Study and thereafter; Honjo et al., 1999) that significantly reduces the errors compared to the two methods described above. In this method, a known mass of particle sample is liquidized in an HNO_3/HF solution at high temperature and pressure under microwave radiation. Then the total Si and Al (and Ti) contents are determined by an ICP-emission spectrometer or an ICP-mass spectrometer. The fraction of layered and structured silicate minerals (total lithogenic components) is reconstructed from Al (and Ti) concentration and subtracted from total Si to determine biogenic Si flux. Using a standard sample from the Panama Basin Intercomparison Experiment, US, Asian, and European laboratories each conducted a biogenic opal Si analysis and found that their data exhibited apparent error of <10%.

4.6. Radiochemical correction of POC flux

A radiochemical correction method for POC based on scavenging ^{230}Th and ^{231}Pa from the water column was developed in the 1980s (e.g., Brewer et al., 1980; Anderson et al., 1983) and recently expanded and refined

(Yu et al., 2001; Scholten et al., 2001). The fluxes of ^{230}Th and ^{231}Pa intercepted by TS-traps deployed in the upper mesopelagic layer are often erratic in time and space (Yu et al., 2001). We believe that such inconsistencies are caused by variations in behavior of the zooplankton community and its resulting influence on the operation of the biological pump within the upper-ocean ecosystem. However, the efficiency of these traps is consistent with the ^{230}Th/^{231}Pa disequilibrium model in the lower mesopelagic layer. Analyses by Yu et al. (2001) and Francois et al. (2002) estimate the efficiency of TS-traps placed between 1.5 and 2.5 km at 98 ± 13% where the terminal gravitational transport mode prevails (based on annual POC export samples). Recent attempts to predict global POC fluxes by inverse modeling (Usbeck et al., 2003) resulted in large discrepancies in the ^{230}Th/^{231}Pa disequilibrium compared with trap data obtained shallower than 1 km, while fluxes measured at greater depths showed better comparison. These authors stated that the differences between their model and the observed fluxes are consistent with the poor trapping efficiency of shallow traps documented from the intercepted fluxes of ^{230}Th and ^{231}Pa.

5. Data review and normalization procedures

We selected and normalized TS-trap export data sets in order to objectively compare the scales and rates of biological pump operation at 152 individual traps from 134 locations distributed in all basins and regions of the world ocean.

5.1. Review criteria for TS-trap data

Our primary criteria for choosing data to include in this review were the depth range of TS-trap deployments and the length of the period of deployment. Because this study aims to synthesize fluxes reaching the mesopelagic/bathypelagic boundary zone in open ocean basins and major marginal seas, TS-trap stations located on continental margins (for example, Thunell et al., 2007; Pilskaln et al., 1996; Hargrave et al., 1993; O'Brien et al., 2006) were not used as principal sources. Criteria we applied include:

(1) TS-trap data sets were required to supply four essential operational conditions in the original publication: (a) mooring location, (b) trap depths, (c) start/finish dates/years, and (d) open/close schedules.
(2) TS-trap samples must have been collected between approximate depths of 1.5 and 3.5 km.
(3) Results of chemical analysis on (a) total particle mass fluxes, (b) particulate organic carbon (POC) or "organic matter", (c) $CaCO_3$, and (d) biogenic silica or "dehydrated opal" in any flux units associated with the total mass flux were included. Data based on microscopic counting of particles were not used.
(4) We included a number of TS-trap data sets where the annual flux of organic carbon or "organic matter" was presented.
(5) Results of deployments without spring blooms in the Westerlies domain and polar ocean stations were not included.

5.2. Normalization to annual fluxes

Although all 153 TS-traps selected were originally scheduled to operate for a year, many of them actually operated within ±5% of 365 days after all time-series segments were totaled. We used these data as they were published, after depth correction as described in the next subsection. In cases where traps operated through the bloom periods and continued for more than, or close to, half a year, we multiplied estimated daily flux by 365 days (Manganini and Honjo, 1992). Then, "duration-normalized fluxes of POC" were converted to annual mole fluxes expressed in mmolC m^{-2} yr^{-1} (also in molC m^{-2} yr^{-1}); this annual POC flux specific to a discrete TS-trap is called FC_{org} hereafter. The $CaCO_3$ fluxes were converted similarly to mole numbers of carbon in $CaCO_3$ in mmolC m^{-2} yr^{-1} as the annual mole flux of inorganic particulate carbon (PIC) that is called FC_{inorg}. Analytical data for biogenic opal ($SiO_2 \cdot 0.4H_2O$) and biogenic silicate (SiO_2) were reported by approximately 70% of the TS-trap publications. Biogenic opal flux was converted to "biogenic silicon Si", called FSi_{bio}, and expressed in mmolSi m^{-2} yr^{-1}.

5.3. Normalization of depths for station-based particle fluxes at the mesopelagic/bathypelagic boundary (Table 2)

Of the 153 TS-traps included in our study, 32 were deployed at 2 km ±5% and their POC flux data required no depth normalization. Other data collected between 1.5 and 3.5 km (some exceptions, Table 2) were normalized to 2 km using Berelson's empirical POC flux reduction formula (Berelson, 2001) modified from Martin et al., 1987 (reviewed by Bishop, 1989; Francois et al., 2002), with a power constant $[-b]$ of 0.87. With this power constant at these depths, the correction curve is practically a linear function and the compensation value is often insignificant. However, attempts by many authors to represent the reduction of POC fluxes through the entire mesopelagic zone using a single exponential formula are unrealistic considering the very large and highly irregular standard deviations normally found in the PIO fluxes measured in the upper mesopelagic zone. Fluxes in the mid- to lower-mesopelagic layer and deeper zones (Berelson, 2001, 2002) are far more predictable. A more realistic approach would be the early curve fitting by Suess (1980), who used a combination of rapid, quasi-linear reduction in the upper mesopelagic zone and gentle linear reduction in the mid- to lower-mesopelagic zones. The corrected and uncorrected POC fluxes in each TS-trap are listed for comparison in Table 3. Thus, we generated 134 locations that are represented by an annual $F\mathrm{C}_{\mathrm{org}}$ at the boundary zone between the mesopelagic and bathypelagic zones. We call this index $F_{\mathrm{m/b}}\mathrm{C}_{\mathrm{org}}$ in mmolC m^{-2} yr^{-1} (Tables 2 and 3).

5.3.1. Normalization of $CaCO_3$ and opal fluxes

The vertical variability of $F\mathrm{C}_{\mathrm{inorg}}$ and $F\mathrm{Si}_{\mathrm{bio}}$ in the ocean is not well constrained mainly due to the scarcity of "depth series" flux data for $CaCO_3$ and opal. Our moored TS-trap investigation found no clear evidence suggesting that fluxes of $CaCO_3$ and opal particles significantly change with depth in the layer between approximately 1 km and 3.5 km.Therefore, we averaged the flux values from 1 km to 3.5 km for 47 stations where multiple TS-traps were deployed at a series of depths. For the 89 single-trap stations, the $F\mathrm{C}_{\mathrm{inorg}}$ and $F\mathrm{Si}_{\mathrm{bio}}$ were applied between 1.5 km and 3.5 km to represent fluxes in the mesopelagic/bathypelagic boundary zone without corrections, on the assumption that settling $CaCO_3$ and opal dissolves insignificantly between 1.5 and 3.5 km as discussed below. Table 2 shows the $F_{\mathrm{m/b}}\mathrm{C}_{\mathrm{inorg}}$ in mmolC m^{-2} yr^{-1} at 125 locations and $F_{\mathrm{m/b}}\mathrm{Si}_{\mathrm{bio}}$ in mmolSi m^{-2} yr^{-1} at 123 locations.

Of the 153 traps included in the study, 28 were deployed at 2.0 km, and 128 were deployed at other depths ranging from 1.5 km to 3.5 km and normalized to 2.0 km.TS-traps were deployed at multiple depths at 47 stations; there were 25 stations with traps at two depths, and 22 stations with three to six traps deployed in depth series that included the lower mesopelagic zone. Examination of the 47 depth-series flux data sets revealed several patterns in the vertical variability of $F\mathrm{C}_{\mathrm{inorg}}$ and $F\mathrm{Si}_{\mathrm{bio}}$:

(1) On 11 moorings equipped with multiple TS-traps, the $F\mathrm{C}_{\mathrm{inorg}}$ and $F\mathrm{Si}_{\mathrm{bio}}$ varies little with depth. No trend is observed, while the standard deviation (std) varies >10% from the shallow (1.0–1.5 km) to the deeper traps (3.5 km).
(2) Data from 14 moorings indicate that the apparent maximum depths of $F\mathrm{C}_{\mathrm{inorg}}$ and $F\mathrm{Si}_{\mathrm{bio}}$ are around 2 km.
(3) At 15 trap moorings, $F\mathrm{C}_{\mathrm{inorg}}$ and $F\mathrm{Si}_{\mathrm{bio}}$ show a slight increase with depth in the mesopelagic/bathypelagic boundary depth range.
(4) At 7 mooring stations, radical changes in fluxes by depth are evident without an appreciable trend.

The $F\mathrm{C}_{\mathrm{inorg}}$ decreases significantly at great depths in the bathypelagic layers, particularly over 6.5 km. However, resuspended particles from the trench slope appear to increase the flux of all biogenic particles (e.g., 8430 m,Nozaki, 1989).

6. Global biogeochemical geography of annual POC exports at the mesopelagic/bathypelagic boundary (m/b)

6.1. Overview and range of POC fluxes at the mesopelagic/bathypelagic boundary

Annual export fluxes of POC normalized to 2 km ($F_{\mathrm{m/b}}\mathrm{C}_{\mathrm{org}}$) and their global distribution are shown in Table 2 and Fig. 3. In Fig. 2, it appears that the $F_{\mathrm{m/b}}\mathrm{C}_{\mathrm{org}}$ is higher in the Northern Hemisphere. However,

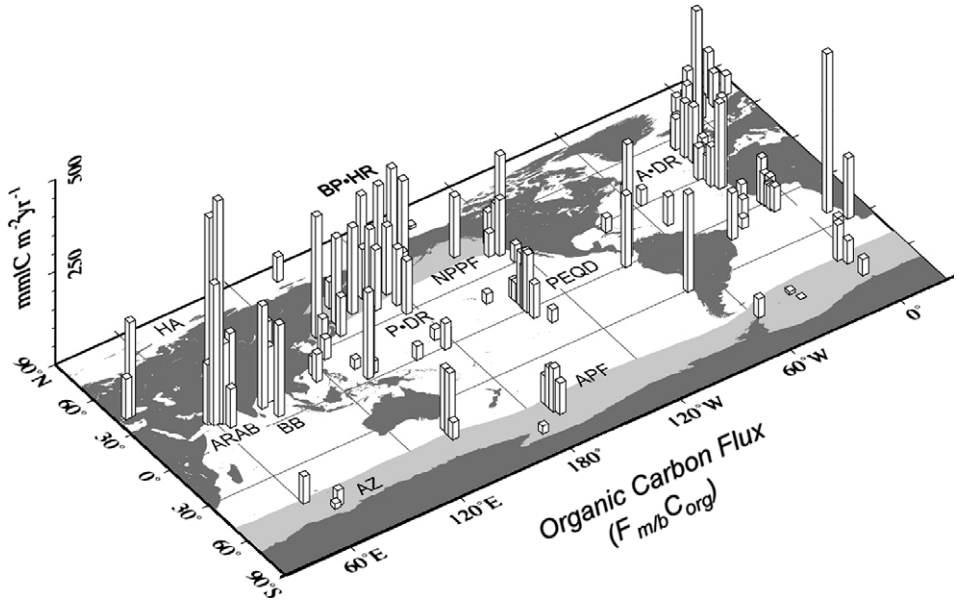

Fig. 2. Annual POC fluxes ($F_{m/b}C_{org}$) at the stations plotted in Fig. 1. Column height represents organic carbon fluxes in mmolC m^{-2} yr^{-1} normalized to 2 km (the bottom of the mesopelagic/bathypelagic boundary zone). Blue areas indicate Silica Ocean conditions and the remainder Carbonate Ocean conditions. The High Arctic Ocean has not been assigned to either category. Some columns in Fig. 2 through Fig. 7 are obscured by taller ones in front of them in the oceanic regions where more stations with high particle flux are concentrated, including the Arabian Sea, the northwest Pacific, and the northeast Atlantic. Letters in this figure indicate the ocean area used to explain the variability of the biological pump in Section 11. They are: *HA*: High Arctic Ocean. *ARAB*: Divergent Arabian Sea or Northwest Arabian Upwelling (Longhurst et al., 1995). *AZ*: Antarctic Zone. *BB*: Bay of Bengal. *BPSO*: Boreal Pacific Silica Ocean. *P-DR*: Pacific Depleted Region. *NPPF*: North Pacific Polar Front. *APF*: Antarctic Polar Front. *PEQD*: Pacific Equatorial Divergence. *A-DR*: Atlantic Depleted Region. *CNRY*: Canary Current Coastal (Longhurst et al., 1995). *NS*: Nordic Seas.

the data are insufficient to draw a firm conclusion on the geographic deviation of the Northern and Southern hemispheres because observations of export fluxes in some large Southern Hemisphere biogeochemical provinces are lacking at this compilation (Table 1 and Fig. 1), and that may affect our global parameterization (Section 9). Fig. 2 indicates that the $F_{m/b}C_{org}$ in the subtropical and tropical gyres in the Atlantic and Pacific are decidedly lower than in the subarctic gyres. If it is assumed that biogenic particle exports in Southern Hemisphere subtropical gyres, including SPSG (South Pacific) and ISSG (Indian Ocean), are similar to those in the Northern Hemisphere, such quasi-asymmetric distribution of $F_{m/b}C_{org}$ in the global ocean might be valid. The $F_{m/b}C_{org}$ in the Southern Ocean is larger than the fluxes in the subtropical and tropical gyres, and markedly smaller than in the Pacific subarctic gyres.

For this paper, we limited our scope to POC fluxes. However, fluxes and fates of particulate organic nitrogen (PON) and phosphorus (POP) with POM in regard to the pumping scheme of nitrogen and phosphorus to the ocean interior are also critically important to further understand oceanic biogeochemical cycles (e.g., Altabet et al., 1991, Altabet 1996, 2006).

$F_{m/b}C_{org}$ ranges from 605 mmolC m^{-2} yr^{-1} at a station in the Arabian Sea (Honjo et al., 1999) to <8 mmolC m^{-2} yr^{-1} in the ice-covered Wangel Abyssal Plain of the High Arctic Ocean (Fahl and Nöthig, 2007) and the seasonally ice-covered Weddell Sea station (1 mmolC m^{-2} yr^{-1}; Wefer and Fischer, 1991). The minimum $F_{m/b}C_{org}$ from a low-latitude open-ocean station is 25–28 mmolC m^{-2} yr^{-1}, reported from the Pacific warm pool (WARM) (Kempe and Knaack, 1996; Kawahata et al., 2000) (Table 2).

Four of the five stations exhibiting the largest $F_{m/b}C_{org}$ (605–380 mmolC m^{-2} yr^{-1}) in the existing data were located in the Arabian Sea (Nair et al., 1989; Haake et al., 1993, 1996; Honjo et al., 1999). The fifth was the Walvis Bay station (429 mmolC m^{-2} yr^{-1}; Wefer and Fischer, 1993b) (Table 2). The next 10 stations include two NARD stations (375 mmolC m^{-2} yr^{-1}; Scholten et al., 2001; Antia et al., 2001a,b), two in the Northwest Pacific Marginal Seas (East Sea/Japan Sea, hereafter referred to as ES/SJ) (327–300 mmolC m^{-2} yr^{-1}; Hong

et al., 1997), several stations in the Southern Bering Sea and Aleutians (273–241 mmolC m^{-2} yr^{-1}; Takahashi et al., 1997, 2000; Wong et al., 1994), and a station in the Bay of Bengal (277 mmolC m^{-2} yr^{-1}; Ittekkot, 1991; Schäfer et al., 1996). TS-traps deployed in shallow coastal zones often record export fluxes of POC that are an order of magnitude larger than the fluxes at the pelagic m/b. For example, Thunell (1998a) and Thunell et al. (2007) reported up to 3–2.4 molC m^{-2} yr^{-1} of POC export in the Santa Barbara Basin and 1 molC m^{-2} yr^{-1} in the San Pedro Basin, both from 0.5 km deep.

6.2. The Atlantic ocean

6.2.1. The Atlantic polar/boreal domain

The Nordic Seas that consist of ARCT and SARC are separated into two oceanic regions: the East Greenland Current and the Norwegian Current (including the West Spitsbergen Current) regions, each bordered by a significant oceanic front. The East Greenland Current is the southern extension of the Transpolar Drift that originates from the High Arctic Seas and conveys ice floes through the western Fram Strait, delivering cold, brackish waters at the surface (Swift, 1986). The Norwegian Current is the northward extension of the Gulf Stream that transports relatively warm water and pushes higher salinity as far north as the Fram Strait (Swift, 1986). The biological pump operates differently in these two areas. For example, in 1988 and 1990, the uncorrected $F_{C_{org}}$ at a station representative of the Greenland Current is as small as 3 mmolC m^{-2} yr^{-1} at 2.2 km deep (72.5°N, 8°E; von Bodungen et al., 1995). This value is only a few percent of the global average flux, 120 mmolC m^{-2} yr^{-1} (Table 5, calculated from the parameterization models in Section 9), comparable to the $F_{m/b}C_{org}$ in the Antarctic zone stations, and possibly a global minimum. However, this station's $F_{C_{org}}$ at 500 m was approximately 300 mmolC m^{-2} yr^{-1} in both years. The $F_{m/b}C_{org}$ in the pelagic Nordic Sea is 42–106 mmolC m^{-2} yr^{-1} and tends to increase to the south (Honjo, 1990; von Bodungen et al., 1995). The mean $F_{m/b}C_{org}$ in the pelagic Eastern Nordic Sea is 79 mmolC m^{-2} yr^{-1} with a std of 24 mmolC m^{-2} yr^{-1}. An exception in this region is $F_{m/b}C_{org}$ as high as 140 mmolC m^{-2} yr^{-1}, larger than the global average at the mesopelagic/bathypelagic boundary, in the deep hemipelagic frontage near a large fjord under the West Spitsbergen Current (Honjo et al., 1988).

6.2.2. The North Atlantic westerlies domains

These areas consist of NADR in the north and NAST that spans the open Atlantic between Iberia/North Africa and the East Coast of North America. NADR is bordered by the Subarctic Front over the Iceland-Faeroe Ridge at its northern edge. Published particle-export data indicate that NADR is characterized by a large $F_{m/b}C_{org}$ that is often more than twice as much as the global annual average (Section 9.4 and Table 5) (Honjo and Manganini, 1993; Jickells et al., 1996: Kuss and Kremling, 1999; Scholten et al., 2001; Antia et al., 2001a,b). Mean $F_{m/b}C_{org}$ of the NADR stations is 171 with a very large std of 110 mmolC m^{-2} yr^{-1} ($n = 20$). In NAST stations distributed along 20°E, $F_{m/b}C_{org}$ is smaller than that at the NADR stations to the north, reaching only about half of the global average.

6.2.3. The Atlantic trade wind domain

This domain spans both sides of the subtropical and equatorial Atlantic. Data from offshore of West Africa, in both NATR and ETRT, were obtained from TS-traps moored by the University of Bremen's long-term projects (e.g., Wefer and Fischer, 1993; Fischer and Wefer, 2000), while WTRA and the vast south Atlantic province (including SATL) are understudied (Fig. 1). The Cape Verde Basin, in the easternmost NATR, is characterized by very high $F_{C_{org}}$. The multi-year mooring stations at 21.15°N, 20.69°E and 20.92°N, 19.74°E show $F_{m/b}C_{org}$ that is not only as large as 237 mmolC m^{-2} yr^{-1} (average) but also more consistent (the std was only 9 mmolC m^{-2} yr^{-1} for 3 years; Fig. 1 and Table 2) (Wefer and Fischer, 1993b). The Demerara Abyssal Plain was occupied by a station at 13.5°N, 54°E with non-time-series traps that opened for 27% of 1977 (Honjo, 1982). An extrapolation of the flux data from this station indicated that $F_{m/b}C_{org}$ is 78 mmolC m^{-2} yr^{-1}. The average $F_{m/b}C_{org}$ in the Guinea Abyssal Plain, which lies in the northeastern ETRA, is 118, close to the global average, with a std of 8 mmolC m^{-2} yr^{-1} (Wefer and Fischer, 1993b; Fischer and Wefer, 1996). Far to the southwest, along both sides of the Mid-Atlantic Ridge, the

$F_{m/b}C_{org}$ (Fischer et al., 2000) is significantly smaller than the global mean. The FC_{inorg} and FSi_{bio} for this area have not been published. The only TS-trap study in WTRA is one reported from the Pernambuco Abyssal Plain, off the east coast of Brazil. At this station, the $F_{m/b}C_{org}$ is 126 mmolC m^{-2} yr^{-1} (Jennerjahn et al., 1996). At the boundary between SATL and BENG, in the northern part of the Benguela Current offshore of the Walvis Bay station around 9°E, 20°S, the $F_{m/b}C_{org}$ is as large as 429-163 mmolC m^{-2} yr^{-1} (1988–1989), indicating this is another high-export area in the South Atlantic (Wefer and Fischer, 1993b; Fischer et al., 2000, 2003).

6.2.4. European inland seas

A Turkish–German–US multiyear biogeochemistry program in the southern Black Sea provided deep trap data as early as 1983 (e.g., Izdar et al., 1984; Buesseler et al., 1987; Hay and Honjo, 1989; Hay et al., 1990). Data from a station at 32.5°E, 42.2°N, in the southern Euxine Abyssal Plain north of Amarsra and at 1.2 km deep under strong anoxic conditions, show that settling particles fluctuate widely by year: the $F_{m/b}C_{inorg}$ is 256 mmolC m^{-2} yr^{-1} in 1983 and 110 mmolC m^{-2} yr^{-1} in 1987. Data is available from a trap station deployed in the Mediterranean Ligurian Sea north of Corsica at 8.5°E, 42.7°N at 1000 m (1987). There, the $F_{m/b}C_{org}$ is smaller than the global mean, 91.3 mmolC m^{-2} yr^{-1}. There is no explanation for the extremely small FC_{inorg} reported from this station (Buat-Ménard et al., 1989; Miquel et al., 1994).

6.3. The Pacific Ocean

6.3.1. The Bering Sea and the Sea of Okhotsk

The $F_{m/b}C_{org}$ at the northern Bering Sea Abyssal Plain station at 58°N, 179°W is 248 mmolC m^{-2} yr^{-1}, twice as large as the global average despite the location's high latitude. The $F_{m/b}Si_{bio}$ is also very large at this station, as much as 579 mmolSi m^{-2} yr^{-1} while the $F_{m/b}C_{inorg}$ is 65.8 mmolC m^{-2} yr^{-1} (Honjo, 1997a), about the same as in the Nordic Seas. Average $F_{m/b}C_{org}$ from the multiple year (1990–1994), single TS-trap station set 3200 m deep at 53.5°N, 177°W on the abyssal plain north of Adak Island, Aleutian Archipelago, is also as large as 300 mmolC m^{-2} yr^{-1}. This substantial POC flux is associated with the huge $F_{m/b}Si_{bio}$ of 804 mmolSi m^{-2} yr^{-1} that is the largest annual export reported in the Northern Hemisphere, while the associated $F_{m/b}C_{inorg}$ is 100 mmolC m^{-2} yr^{-1}, about 80% of the global average (Takahashi et al., 2000).

6.3.2. The North Pacific westerlies domain

This domain consists of three biogeochemical provinces: two large mid-ocean gyre systems and a globally significant oceanic front. They are the Pacific Subarctic Gyre (PSAG), the North Pacific Subtropical Gyre (NPST) (Fig. 1), and the North Pacific Polar Front (NPPF) (e.g., Favorite et al., 1976; Belkin et al., 2002), which separates the two gyres and is not only a significant hydrographic boundary but also a major biogeochemical ocean front. The mode of the biological pump in the biogeochemical province to the north of this front (PSAG) and the one to the south (NPST) show strong differences; thus, the NPPF plays a critical role in formulating the biogeochemical setting of the Pacific, as we elaborate later in this paper.

The northernmost NORPAC TS-trap mooring was deployed in the south of the PSAG-W at 46.1°N, 175°E (Kawahata et al., 1997) (Section 3). The $F_{m/b}C_{org}$ measured at this station is 183 mmolC m^{-2} yr^{-1}. The KNOT program (Honda et al., 2002) provided a cluster of multidepth, multiyear TS-trap moorings around 44°N, 155°E, covering the PSAG and northern Kuroshio province (KURO) from 1997 to 1999. At the KNOT station, the interannual mean $F_{m/b}C_{org}$ was 232 mmolC m^{-2} yr^{-1}, nearly twice as large as the world average. The $F_{m/b}C_{org}$ fluctuates by a factor of 1.8 between 1998 and 1999 at this station. Under the Oyashio Current near the northern Kuril Islands (50°N, 165°E), the $F_{m/b}C_{org}$ in 1997 data is 134 mmolC m^{-2} yr^{-1} (Honda, 2001; Honda et al., 1997, 2002), less than at other PSAC-W stations. Mean $F_{m/b}C_{org}$ in BERS, PSAG-W, PSAG-E, ES/JS, and northern KURO is 214, with a relatively small std of 67 mmolC m^{-2} yr^{-1} (Wong et al., 1994; Honjo and Weller, 1997; Takahashi et al., 2000; Hong et al., 1997; Kawahata et al., 1997; Noriki et al., 1997; Takahashi et al., 2000; Honda et al., 1997, 2002; Honda, 2001). Further south, at the NORPAC station at 37.4°N, 175°E, $F_{m/b}C_{org}$ declines to 151 mmolC m^{-2} yr^{-1} (Kawahata et al., 2002) but is still about 25% greater than the global average. Only 3° to the south of this NORPAC station, but on the south side of

the Polar Front at 34.4°N, 177.4°E, the annual $F_{m/b}C_{org}$ decreases to the level of the global average (119 mmolC m^{-2} yr^{-1}) (Kawahata et al., 2002). A TS-trap mooring located on the north side of the ES/JS front at 39.7°N, 132.4°E in the Ulung Basin exhibits an annual $F_{m/b}C_{org}$ as high as 327 mmolC m^{-2} yr^{-1} (Hong et al., 1997), repeating the distribution pattern of $F_{m/b}C_{org}$ in the open northwest Pacific.

Ocean Station P (50°N, 140°W) presents one of the longest quasi-continuous TS-trap records in PSAG-E beginning in the early1980s (e.g., Wong et al., 1994). The published decadal particle export records from 1983 to 1993 indicate that the annual $F_{m/b}C_{org}$ at this station fluctuates from 76 to 221 mmolC m^{-2} yr^{-1} (normalized from 1 km TS-trap data), with a decadal average of 163 mmolC m^{-2} yr^{-1}. This is significantly larger than the global average, but smaller than the fluxes at PSAG-W stations. A notable anomaly is that the $F_{m/b}C_{org}$ plunged to a range of 76–80 in 1989 and 1990, but recovered to the normal PSAG-E level in later years.

6.3.3. Pacific trade wind domain

This domain consists of large biogeochemical provinces that include the North Pacific Tropical Gyre (NPTG) and encompass the entire width of the North Pacific between 10°N and 30°N, from the South China Sea to offshore of Mexico's Pacific coastal province, CAMP. The Western Pacific Warm Pool (WARM) province occupies the area from 12°N to 15°S in the western equatorial Pacific and from offshore Mindanao, Philippines, at about 158°W (Longhurst et al., 1995) to about 173°W (Figs. 1 and 9). It is the region of least biogenic particle export in the world ocean except for seasonally ice-covered polar seas. Mean $F_{m/b}C_{org}$ in this part of the North Pacific, where the FC_{org} is small and the biological pump is enervated, is 40 with a std of 17 mmolC m^{-2} yr^{-1} (based on seven stations between 15.3°N and 0°). The $F_{m/b}C_{org}$ at the 7.9°N, 175° station, observed by the German Warm Pool Project, is 30 mmolC m^{-2} yr^{-1} (Kempe and Knaack, 1996). At the NORPAC station on the equator at 175.2°E, the $F_{m/b}C_{org}$ is 53 mmolC m^{-2} yr^{-1} (Kawahata et al., 2002). A cluster of several stations in the area bounded by 7.9°N, the equator, 160°E, and 175°E registered 30 to 70 mmolC m^{-2} yr^{-1} (Kempe and Knaack, 1996; Kawahata et al., 1997). NORPAC deployed two TS-traps in 1991 in WARM at 4.1°N, 136.3°E and 3°N, 135.0°E. At these stations, the $F_{m/b}C_{org}$ was as high as 182 and 233 mmolC m^{-2} yr^{-1}, respectively (Kawahata et al., 1999, 2000) (Fig. 2). These anomalous POC fluxes could be explained by vigorous tropical sediment discharges (Milliman and Syvitski, 1992; Milliman, 1995) transported from the high-energy rivers in northeastern New Guinea by the Equatorial Counter Current (ECC) to these mooring locations; these data are not included in the calculation of the average $F_{m/b}C_{org}$ in WARM.

The JGOFS EqPac Program occupied a meridional transect along 140°W in 1992 to collect comprehensive biogeochemical data (Murray et al., 1995). Spanning the Pacific Northern Equatorial Current (PNEC) and the north Pacific Equatorial Divergence (PEQD), five TS-trap moorings were deployed at 9°N, 5°N, 2°N, O°, and 5°S, and a sixth was set at 12°S,135°W. The southernmost moorings extended into the South Pacific Subtropical Gyre (SPDG) (Honjo et al., 1995). The $F_{m/b}C_{org}$ at the northernmost EqPac transect (9°N, 140°W) was 50 mmolC m^{-2} yr^{-1}, equivalent to other NPTG and WARM stations. A MANOP TS-trap deployed at 11°N, 140°W in 1992 also yielded similar $F_{m/b}C_{org}$, 49 mmolC m^{-2} yr^{-1} (Dymond and Lyle, 1985). The $F_{m/b}C_{org}$ along the meridional transect of PNEC from 5°N to 5°S along 140°W varied in quasi-Gaussian distribution with maximum export at 1°N and the equator (158–194 mmolC m^{-2} yr^{-1}) (Honjo et al., 1995). The 5°S station was located on the boundary of the PEQD and the South Pacific Subtropical Gyre (SPSG).

The southernmost station of the EqPac transect was located at 12°S, 135°W in the deep basin east of the Marquesas Islands and well inside the South Pacific Subtropical Gyre (SPSG). The annual $F_{m/b}C_{org}$ from this station was only 34 mmolC m^{-2} yr^{-1} (Honjo et al., 1995), similar to the POC export at the NPTC and WARM stations. We found no other published TS-trap data from the vast SPSG province. To the east of the EqPac transect, there are only a few TS-trap stations in the PNEC and the PEQD. The eastward extent of this highly organic, carbon-rich zone is not well understood because of insufficient distribution of mooring stations in that area. However, the $F_{m/b}C_{org}$ at two stations near the Galápagos Spreading Center area at 0.6°N, 86°W (partially covered by Cobler and Dymond, 1980) and in the Panama Basin at 5.4°N, 82°W (partial time-series in Honjo, 1982) were 194 and 307 mmolC m^{-2} yr^{-1}, suggesting that the zone of vigorous POC export at the mesopelagic/bathypelagic boundary in the eastern equatorial Pacific continues to the east and

extends to Middle American coastal zones (Fig. 2); verification would demand deployment of more TS-traps in this extensive, data-barren region (Fig. 9).

6.4. The Indian Ocean

The border between the Indian Ocean Monsoon Gyre (MONS) to the north and the Indian Ocean South Subtropical Gyre (ISSG) is at 10°S (Longhurst et al., 1995). The northern part of MONS, the offshore convergent zone of the western Arabian Sea (ARAB), and the Bay of Bengal have been well covered by TS-trap stations moored by the Indo-German Ocean Biogeochemistry Program since 1986 (e.g., Ittekkot et al., 1991). In the Arabian Sea, multiple-year time-series stations were designated W, C, and E at 60°E, 16°N; 64°E, 14°M; and 68°E, 15°N, respectively (e.g., Nair et al., 1989; Haake et al., 1996).

The JGOFS Arabian Sea Process Study occupied ARAB and northern MONS in 1994 and 1995 (ASPS; Smith et al., 1998), following the original Indo-German transects. This program collected export POC fluxes at five stations along a northwest/southeast transect from Oman coastal waters (Station MS-1) to a mid-ocean station (MS-5) at 65°W, 10°N (Honjo et al., 1999) (Fig. 1). All stations except the open Indian Ocean station (MS-5) were located in the divergent conditions induced by the monsoonal low-atmosphere, cross-equatorial jet stream (Findlater, 1974). The largest annual $F_{m/b}C_{org}$ (605 mmolC m^{-2} yr^{-1}, nearly five times the global average flux) is observed at station MS-4 located at 15.3°N, 61.5°E from 1998 to 1999. At three stations on the west side of MS-4 (MS-1 at 17.4°N, 58.8°E; MS-2 at 16.0°N, 60.0°E; and MS-3 at 17.2°N, 59.6°E), the annual $F_{m/b}C_{org}$ are also extraordinary high: 605, 559, and 495 mmolC m^{-2} yr^{-1}, respectively. At the nondivergent oligotrophic mid-ocean station MS-5 further southeast, but still in MONS, the $F_{m/b}C_{org}$ was slightly smaller than the global average: 107 mmolC m^{-2} yr^{-1} (Honjo et al., 1999).

The Bay of Bengal (MONS) is a significant marginal sea with respect to the biogenic material cycles in the Indian Ocean (Ittekkot et al., 1991). A transect of TS-trap moorings was set from 17.5°N to 4.5°N along 90°E, the geographic center of the Bay of Bengal. The $F_{m/b}C_{org}$ at 89.6°E, 17.5°N, approximately 310 nautical miles from the Ganges–Brahmaputra estuary, was 209 mmolC m^{-2} yr^{-1}. At the two stations to the south (15.2°N and 13.2°N) along this transect, $F_{m/b}C_{org}$ is also as large as 159 and 277 mmolC m^{-2} yr^{-1}. While the southernmost station at 4.5°N, 87.3°E was located outside of the bay in the open Indian Ocean, the $F_{m/b}C_{org}$ is as much as 247 mmolC m^{-2} yr^{-1} (Ittekkot et al., 1991; Schäfer et al., 1996). Average $F_{m/b}C_{org}$ from this transect is 221 with a std of 55 mmolC m^{-2} yr^{-1}.

6.5. The Southern Ocean

Longhurst et al. (1995) divided the Westerlies-dominated Southern Ocean into the South Subtropical Convergence (SSTC) and the Subantarctic (SANT) biogeochemical provinces. Combined, these zones make up the "Subantarctic Zone (SAZ)" that is bordered by the Antarctic Polar Front (APF) and the Antarctic province (ANTA) to the south. The ANTA is equivalent to the Antarctic Circumpolar Current (ACC) zone and the Austral Polar (APLR) zone in Longhurst et al. (1995) and is a combination of the Permanently Open Ocean Zone or POOZ (Tréguer and Jaques, 1992) and Antarctic Shelf Areas. JGOFS-AESOPS refers to the pelagic region to the south of APF, abutting the shelves, as the Antarctic Zone (AZ). This paper utilizes the Tréguer and Jaques (1992) classification adopted by JGOFS researchers.

The annual $F_{m/b}C_{org}$ determined from the two SAZ stations, deployed in 1997–1998 at 46.8°S and 53.8°S along 142°E, was substantially larger than the global average, 170 and 173 mmolC m^{-2} yr^{-1}, respectively (Bray et al., 2000). Five TS-trap moorings were located from 1996 to 1998 on a JGOFS-AESOPS transect in the New Zealand-Ross Sea (NZRS) sector along 170°W from 53.0°S to 66.1°S (Honjo et al., 2000), but data from the shallow Ross Shelf stations (<0.6 km) (Collier et al., 2000) and the coastal Atlantic Southern Ocean stations (Wefer and Fischer, 1993b; Fischer et al., 2000) are not included in this study. At an AESOPS mooring station (MS-2) to the north of the APF at 57°S, in the Polar Frontal Zone, the $F_{m/b}C_{org}$ was small, 76 mmolC m^{-2} yr^{-1}. The MS-3 station, at 60°S, 170°E, was located at the APF itself, and the meandering polar front passed over it. The $F_{m/b}C_{org}$ at MS-3 was 108 mmolC m^{-2} yr^{-1}. At the station in the Antarctic Circumpolar Current (ACC) to the immediate south of the APF (MS-4, 63°S 170°E), the $F_{m/b}C_{org}$ was 117 mmolC m^{-2} yr^{-1}. However, the $F_{m/b}Si_{bio}$ was as large as 926 mmolSi m^{-2} yr^{-1}—one of the largest opal

exports in the world ocean (elaborated in Section 7.3). In the pelagic Ross Sea Gyre the $F_{m/b}C_{org}$ is 84 mmolC m^{-2} yr^{-1}; $F_{m/b}C_{inorg}$ is as small as 7 mmolC m^{-2} yr^{-1}, while there is a relatively large $F_{m/b}Si_{bio}$ of 269 mmolSi m^{-2} yr^{-1} (Honjo et al., 2000). $F_{m/b}C_{org}$ observed in the New Zealand-Tasmania sector is substantially larger than the global average in the SAZ (Bray et al., 2000), and it is about the global average or smaller in the south of the APF within the Circumpolar Current, and the $F_{m/b}C_{org}$ plunges to merely 5% of the global average in the POOZ, south of the Circumpolar Current.

The zonal characteristics of settling particles observed in the New Zealand and Tasmania sectors are approximately similar to those in the Indian Ocean sector stations. At the French M-2 station at 52°S, 61.5°E, the $F_{m/b}C_{org}$ and $F_{m/b}Si_{bio}$ observed in 1994 equal 73 mmolC m^{-2} yr^{-1} and 651 mmolSi m^{-2} yr^{-1}, respectively (Tréguer, 2003, personal communication). A Prydz Bay station was located slightly further south of the French station at 62°S, 73°E (Pilskaln et al., 2004). Here, the $F_{m/b}C_{org}$ and $F_{m/b}Si_{bio}$ are 42 mmolC m^{-2} yr^{-1} and 308 mmolSi m^{-2} yr^{-1}, respectively. This station appears to be equivalent to the POOZ station in the Ross Sea Gyre along the JGOFS-AESOPS 170°W transect.

7. Annual export of $CaCO_3$ and biogenic opal

7.1. Overview and range of fluxes

The geographic distributions of two major biogenic ballast particles, $CaCO_3$ and $SiO_2 \cdot 0.4H_2O$ at the mesopelagic/bathypelagic boundary zone are presented as annual molar fluxes of carbon and silicon ($F_{m/b}C_{inorg}$ and $F_{m/b}Si_{bio}$) at each mooring station in Figs. 3 and 4 and Table 2. At a glance, Fig. 3 indicates that the $F_{m/b}C_{inorg}$ varies less geographically, and its distribution appears monotonous compared to $F_{m/b}C_{org}$ (Fig. 2) and $F_{m/b}Si_{bio}$ (Fig. 4). Also, the carbonate fluxes in the Pacific Subtropical Gyres are far smaller than the global average, similar to the distribution of $F_{m/b}C_{org}$, while the $F_{m/b}C_{inorg}$ in the Atlantic subtropical gyres is moderately high. Generally, the Atlantic $F_{m/b}C_{inorg}$ is higher than that of the Pacific (Fig. 3). In contrast, $F_{m/b}Si_{bio}$ is strikingly higher in the Pacific than in the Atlantic (Fig. 4). Particularly, the $F_{m/b}Si_{bio}$ in the Subarctic Pacific is tenfold greater than in the boreal Atlantic. It is also noticeable that the $F_{m/b}Si_{bio}$ is very large in the North Pacific and the Southern Ocean, while the biogenic silica fluxes in the Pacific subtropical and tropical gyres are as small as those in all the Atlantic Ocean except for the Atlantic Southern Ocean.

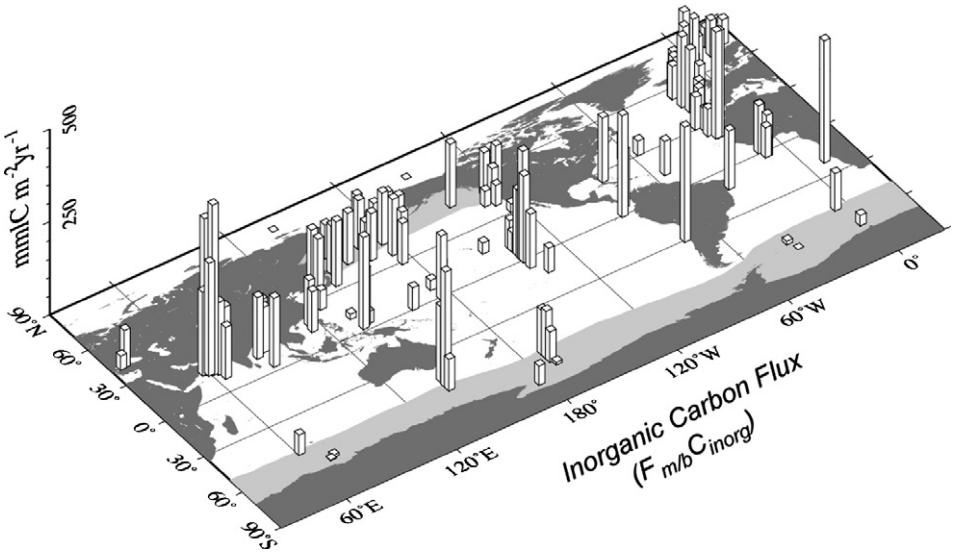

Fig. 3. Column height represents annual flux of biogenic $CaCO_3$–C in mmolC m^{-2} yr^{-1} ($F_{m/b}C_{inorg}$) at the mesopelagic/bathypelagic boundary.

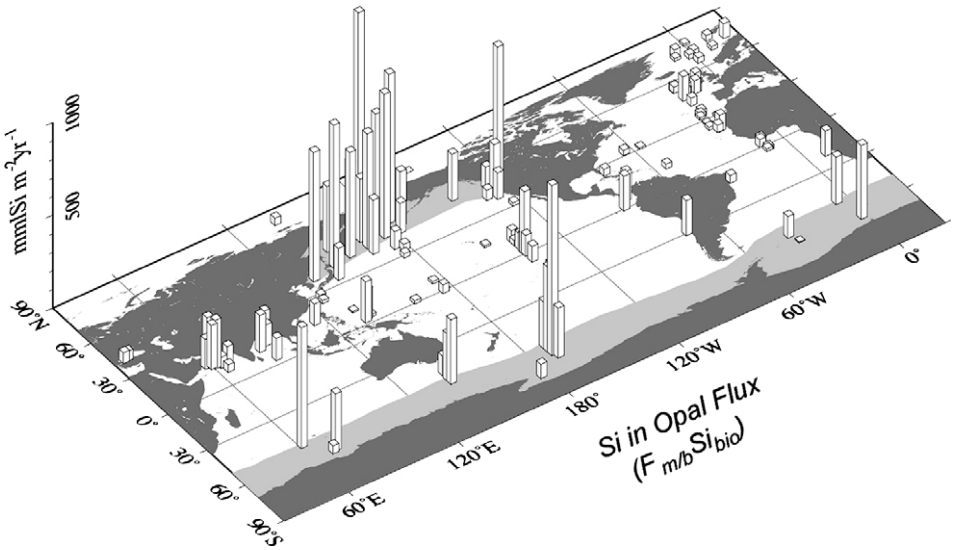

Fig. 4. Column height represents annual flux of biogenic opal-Si in mmolSi m^{-2} yr^{-1} ($F_{m/b}Si_{bio}$) at the mesopelagic/bathypelagic boundary.

The $F_{m/b}C_{inorg}$ ranges from 459 mmolC m^{-2} yr^{-1} observed at the divergent Arabian Sea station in 1995 (Station W at 15.3°N, 61.5°W; Nair et al., 1989) to 8 mmolC m^{-2} yr^{-1} or less in the seasonally ice-covered Southern Ocean (Wefer and Fischer, 1993a; Honjo et al., 2000; Pilskaln et al., 2004; Tréguer, 2003, personal communication) and the High Arctic station (Fahl and Nöthig, 2007). The $F_{m/b}C_{inorg}$ is 8 mmolC m^{-2} yr^{-1} at a station in the Central Fram Strait observed from 1988 to 1989 (Honjo, 1990). The smallest carbonate flux observed in non-ice-covered waters is 15 mmolC m^{-2} yr^{-1} at 12°N, 134.3°W (Kempe and Knaack, 1996) and 28 mmolC m^{-2} yr^{-1} at 7.9°N, 175.0°W (Kawahata et al., 2000); both were reported from the $F_{m/b}C_{org}$-depleted equatorial Pacific WARM province.

The $F_{m/b}Si_{bio}$ observed at 4500 m at 51°N, 165°E, to the south of Kiska Island in the western Aleutians, was 1229 mmolSi m^{-2} yr^{-1} (Wong et al., 1994). This trap was set 460 m above the seafloor in the midst of the Meiji Drift. Resuspended opal particles may contribute to this large annual flux. The next highest $F_{m/b}Si_{bio}$ station in the Northern Hemisphere, 804 mmolSi m^{-2} yr^{-1}, is also in the western Aleutian area (Takahashi et al., 1997, 2000) where the trap was deployed 3.2 km deep and no significant resuspension of bottom sediment would be expected. The highest $F_{m/b}Si_{bio}$ in the Southern Hemisphere is 915 mmolSi m^{-2} yr^{-1} at a station located in the Antarctic Circumpolar Current, Antarctic Zone, New Zealand-Australia sector (Honjo et al., 2000). The minimum annual $F_{m/b}Si_{bio}$ so far observed in the open ocean is 7 mmolSi m^{-2} yr^{-1} (Kempe and Knaack, 1996) at a Philippine Sea station located at 12°N, 134°W in the Trade Wind Domain. Stations with <20 mmolSi m^{-2} yr^{-1} are reported from the Pacific WARM (Kempe and Knaack, 1996; Kawahata et al., 2000), the Atlantic section of the boreal polar provinces (BPLR) (Honjo, 1990; von Bodungen et al., 1995; Fischer and Wefer, 1993a), and the Atlantic gyres such as NAST/NARD (Neuer et al., 1997; Jickells et al., 1996; Scholten et al., 2001).

7.2. $CaCO_3$ fluxes at the mesopelagic/bathypelagic boundary and export of alkalinity

Although $F_{m/b}C_{inorg}$ is less variable in the world ocean in general, a few conspicuous areas with higher $F_{m/b}C_{inorg}$ are found where upwelling and coastal currents prevail. An exceptionally large open ocean $F_{m/b}C_{inorg}$ was observed in the divergent Arabian Sea (Fig. 3 and Table 2) by the Indo-German Arabian Sea Program, ongoing since 1987, and the 1994–1995 JGOFS Arabian Sea Expedition (JGOFS-ASE); $F_{m/b}C_{inorg}$ there ranges from 304 to an extraordinary 459 mmolC m^{-2} yr^{-1} at the station where $F_{m/b}C_{org}$ was 605 mmolC m^{-2} yr^{-1}. The average $F_{m/b}C_{inorg}$ among the divergent Arabian Sea stations is 394 mmolC m^{-2} yr^{-1} with a std of 66 mmolC m^{-2} yr^{-1}, roughly four times that of the global $F_{m/b}C_{inorg}$ average (Nair

et al., 1989; Haake et al., 1993, 1996; Honjo et al., 1999). Lithogenic carbonate mineral aerosol could cause an overestimation of the biogenic $CaCO_3$, especially under areas abutting dry land, including the Cape Verde vicinity (Fischer et al., 2000). However, the input of lithogenic carbonate to the divergent Arabian Sea is limited to certain seasons and does not significantly affect the annual $F_{m/b}C_{inorg}$ estimation (Honjo et al., 1999).

Along the meridional EqPac 145°E TS-trap transect, the variability of $F_{m/b}C_{inorg}$ follows that of $F_{m/b}C_{org}$, forming a quasi-Gaussian distribution (Fig. 3). The maximum $F_{m/b}C_{inorg}$ is 297 mmolC m^{-2} yr^{-1}, which occurs at 1°N, where the $F_{m/b}C_{org}$ (194 mmolC m^{-2} yr^{-1}) is also the largest along this transect (Honjo et al., 1995). $F_{m/b}C_{inorg}$ is far larger than the global average at some upwelling and coastal stations. These include the Walvis Bay and the Cape Verde area stations, where the $F_{m/b}C_{inorg}$ is >300 mmolC m^{-2} yr^{-1} (Wefer and Fischer, 1996). Large $F_{m/b}C_{inorg}$, to which sporadic pteropod-shell exports were thought to contribute, were reported in the Westerlies Domain and the Polar Oceans (e.g., Wefer and Fischer, 1993b; Hong, 2000, personal communication). A very large apparent flux of aragonite to the Ross Sea Shelf (several hundred meters deep) is due to swarming pteropods that actively swam into the TS-traps (Collier et al., 2000; Gardner et al., 2000), verifying a prediction found in Harbison and Gilmer (1986). The mean $F_{m/b}C_{inorg}$ at PSAG and northern Kuroshio stations, where the Kuroshio Current converges with the Oyashio Current (Honda et al., 1997, 2002), is 187 mmolC m^{-2} yr^{-1}, with an elevated std of 88 mmolC m^{-2} yr^{-1} (based on 13 annual samples). Settling large pteropod shells might contribute to the large std in the mean $F_{m/b}C_{inorg}$ in these areas.

There are two regions where the $F_{m/b}C_{inorg}$ is consistently smaller than the global average. One is the Pacific Trade Wind Domain, particularly the NPTC and WARM, and the other is the sea-ice-covered Southern Ocean sandwiched between the ACC and the Antarctic Shelf. Although the number of mooring stations yielding annual data is rather small, the average $F_{m/b}C_{inorg}$ in the NPTC and WARM is 27 mmolC m^{-2} yr^{-1} with a std of 7.5 mmolC m^{-2} yr^{-1}, just one quarter of the global mean $F_{m/b}C_{inorg}$. The smallest $F_{m/b}C_{inorg}$ in the Westerlies and Trade Wind Domains is 15 mmolC m^{-2} yr^{-1} at 12°N, 134.3°E, observed at a station under the North Equatorial Current in the southern Philippine Sea, on the boundary zone of the NPTG and WARM provinces (Kempe and Knaack, 1996). In the Atlantic as a whole, $F_{m/b}C_{inorg}$ is generally high, and are no significantly large depleted areas of $F_{m/b}C_{inorg}$ similar to WARM are observed. The only exception to the "carbonate flux rich Atlantic" is an Atlantic Arctic station in Fram Strait (79.9°N, 1.4°W) where $F_{m/b}C_{inorg}$ was 8 mmolC m^{-2} yr^{-1} in 1984–1985 (Honjo, 1990). However, Hebbeln and Wefer (1991) reported $F_{m/b}C_{inorg}$ as large as 130–246 mmolC m^{-2} yr^{-1} from two nearby stations set 1.1 km deep at 78.79°N, 6.68°/6.74°W.

The operation of the biological pump in the Subantarctic Zone (SAZ; Trull et al., 2001) does not appear to be similar to that in the Southern Ocean. In the New Zealand-Tasmanian sector, $F_{m/b}C_{inorg}$ in the SAZ is 122 mmolC m^{-2} yr^{-1} (Bray et al., 2000). Although only a single observation is available so far, the annual $F_{m/b}C_{inorg}$ is as high as 312 mmolC m^{-2} yr^{-1} at 51°S, 142°W in the southern Tasmanian Sea (Trull et al., 2001). At a JGOFS-AESOPS station in the Polar Frontal Zone, which appears to be the transitional zone between the Southern Ocean and the Westerlies Domain, the $F_{m/b}C_{inorg}$ is 66 mmolC m^{-2} yr^{-1}. Coccolith and planktonic foraminiferal tests are the source of the $CaCO_3$ at this station as at other Westerlies stations. Further south, at the station within the Antarctic Circumpolar Current, $F_{m/b}Si_{bio}$ is extremely large, and the $F_{m/b}C_{inorg}$ is 107 mmolC m^{-2} yr^{-1}, about the global average. However, the majority of $CaCO_3$ here originates from pteropod shells, with a minor-to-trace flux of foraminiferal shells; no coccoliths are found in these zones. In the Antarctic Zone (AZ, Ross Sea Gyre in this sector), the southernmost pelagic Southern Ocean, the $F_{m/b}C_{inorg}$ is present at a trace level of 6 mmolC m^{-2} yr^{-1} and consists of dwarf foraminiferal shells (Honjo et al., 2000; Honjo, 2004). Similar small $F_{m/b}C_{inorg}$, 2.5–7 mmolC m^{-2} yr^{-1}, are also observed in the Indian Ocean AZ stations at 62°S, 73°W (Pilskaln et al., 2004) and 63°S, 71°W (Tréguer, 2003, personal communication). At the APF, the content of the exported particles is a mixture from SAZ and AZ, reflecting meandering of the front.

7.3. Biogenic opal ($SiO_2 \cdot 0.4H_2O$)

The flux of biogenic opal, mostly from diatom frustules, is quite small in the Atlantic, and its distribution is uniform compared to the Pacific (Fig. 4). Average $F_{m/b}Si_{bio}$ from the entire Atlantic is only 39 mmolSi m^{-2} yr^{-1} ($n = 45$) with std of 25 mmolSi m^{-2} yr^{-1}, indicating that the $F_{m/b}Si_{bio}$ is relatively

uniform throughout the Atlantic basins. This Atlantic average $F_{m/b}Si_{bio}$ is only about 8% of the that found in the northeast Pacific Boreal Gyres. These major differences suggest that the biological pump functions significantly differently in the Atlantic and the Pacific oceans.

There are two relatively large and clearly demarcated latitudinal zones where the oceanic interior flux of opal is markedly large. One encompasses the subarctic gyre and the northwestern Asian marginal seas, including the deep Bering Basin (the BERS, the PSAG, the northern KURO provinces, the northern ES/SJ, and the Sea of Okhotsk). The other is the pelagic Antarctic Zone (AZ), including the ACC. The equatorial sides of both high $F_{m/b}Si_{bio}$ regions are demarcated by globally significant oceanic fronts: the North Pacific Polar Front and the Antarctic Polar Front.

Arguably the largest $F_{m/b}Si_{bio}$ measured in the North Pacific Boreal Gyres is 804 mmolSi m^{-2} yr^{-1}, observed in 1997 at a 3.2-km-deep TS-trap during a 5-year program at AB (the Aleutian-Bering Station, Takahashi et al., 2000). The AB Station was located at 53.5°N, 177°E in a 3.7-km-deep basin, located within the central Aleutian Archipelago. Similarly, the largest $F_{m/b}Si_{bio}$ detected in the southern Silica Ocean is 915 mmolSi m^{-2} yr^{-1} at 63.2°S, 140°E in the New Zealand-Tasmanian sector and under the Antarctic Circumpolar Current (Honjo et al., 2000). In the Carbonate Ocean (Section 7), a few stations exhibit elevated $F_{m/b}Si_{bio}$, which is associated with a large $F_{m/b}C_{inorg}$. The divergent Arabian Sea exports opal up to about 2.5 times the global average at the mesopelagic/bathypelagic boundary (Nair et al., 1989; Haake et al., 1996; Honjo et al., 1999). Ittekkot et al. (1991) report large $F_{m/b}Si_{bio}$ (up to 201 mmolSi m^{-2} yr^{-1}) from the Bay of Bengal. In the JGOFS EqPac area (Murray et al., 1995) along the 140°E meridional cross-equator transect, $F_{m/b}Si_{bio}$ registers as high as 342 mmolSi m^{-2} yr^{-1} at 1°N (Dymond and Collier, 1988) and 187 mmolSi m^{-2} yr^{-1} at 0.6°N, but the export of opal quickly declines to the north and south along the 140°E transect. At 2°N and 0°, the $F_{m/b}Si_{bio}$ is 101 and 112 mmolSi m^{-2} yr^{-1}, respectively (Honjo et al., 1995). This sharp-peaked Gaussian distribution of opal export with the maximum at 1°N coincides with the distribution of the buoyant diatom *Rhizosolenia* spp. (Yoder et al., 1994; Archer et al., 1997) along the upwelling center in the South Equatorial Current and Equatorial Undercurrent. In the central and eastern equatorial Pacific, $F_{m/b}Si_{bio}$ is also relatively large as observed only toward the east. For example, the $F_{m/b}Si_{bio}$ was estimated at 161 mmolSi m^{-2} yr^{-1} in the Panama Basin from data taken with partial time coverage (Honjo et al., 1982).

Fig. 4 shows that the $F_{m/b}Si_{bio}$ is prominent in the boreal gyre provinces, PSAG-W, PSAG-E, and the northern Asian marginal seas that include the deep Bering Sea basin, the Sea of Okhotsk, and the northern side of the ES/SJ Subarctic Front. In the North Pacific Boreal Gyres, average $F_{m/b}Si_{bio}$ is as great as 530 mmolSi m^{-2} yr^{-1}, with a high std of 202 mmolSi m^{-2} yr^{-1} (the data from the deep TS-trap deployed at 51.5°N, 165°W are excluded). The mean $F_{m/b}Si_{bio}$ in the North Pacific Boreal Gyres is approximately five times larger than the mean global $F_{m/b}Si_{bio}$ while the $F_{m/b}C_{inorg}$ data are within the global average and far more consistent than $F_{m/b}Si_{bio}$ (except where the Kuroshio and Oyashio currents converge).

7.3.1. Meridional variability of $F_{m/b}Si_{bio}$ in the North Pacific

The $F_{m/b}Si_{bio}$ at the northernmost NORPAC transect (46.1°N, 175.3°E) (Kawahata et al., 1997, 2002) is as large as 779 mmolSi m^{-2} yr^{-1}. This is the second largest annual $F_{m/b}Si_{bio}$ in the North Pacific. The $F_{m/b}Si_{bio}$ at 50°N, 165°W and 44°N, 155°W are 343 and 568 mmolSi m^{-2} yr^{-1}, respectively (Honda, 2001). At the KNOT TS-trap station (45°N, 155°W), to the east of the northern Kuril Archipelago, the $F_{m/b}Si_{bio}$ is again very large, 511 and 568 mmolSi m^{-2} yr^{-1} in 1997–1998 and 568 mmolC m^{-2} yr^{-1} in 1999–2000 (Noriki et al., 1997; Honda et al., 2002). The NORPAC transect data show that the $F_{m/b}Si_{bio}$ decreases significantly in the region immediately south of the North Pacific Polar Front. At 37.4°N, 170°W, about 3° south of the Polar Front, $F_{m/b}Si_{bio}$ is reduced to the global average, 95 mmolSi m^{-2} yr^{-1}, and associated with relatively high $F_{m/b}C_{org}$ and $F_{m/b}C_{inorg}$, 151 and 152 mmolC m^{-2} yr^{-1} (Kawahata et al., 1997), respectively. Further south at 34.4°N, 177.7°W and well inside the subtropical gyre (NPST), the $F_{m/b}Si_{bio}$ decreases drastically to 34 mmolSi m^{-2} yr^{-1}. Both $F_{m/b}C_{org}$ and $F_{m/b}C_{inorg}$ are about 20% less than at the station to the north (Kawahata et al., 1997).The $F_{m/b}Si_{bio}$ is also as small as 34 mmolSi m^{-2} yr^{-1} (Kawahata et al., 2000) at the station located at the boundary between the North Pacific Subarctic Gyre (NPST) and the North Pacific Subtropical Gyre (NPTG) (34.4°N, 174.7°W) and at the approximate boundary between the Westerlies and the Pacific Trade Wind region. Further to the south, in the southern NPTG and the entire WARM, the average $F_{m/b}Si_{bio}$ is further reduced to <20 mmolSi m^{-2} yr^{-1} (19 mmolSi m^{-2} yr^{-1}, with a std of 13 mmolSi m^{-2} yr^{-1}),

forming the most depleted zone for $F_{m/b}Si_{bio}$ in the world ocean. This symmetric distribution of the $F_{m/b}Si_{bio}$ in the North and South Pacific, which shows an increase in the $F_{m/b}Si_{bio}$ from depleted low-latitude gyres to the highly enriched high-latitude regions, is also demonstrated in the ternary graph of mole ratio among POC, PIC, and biogenic Si (Section 8.2; Fig. 8). Although so far there are few observations, the average $F_{m/b}Si_{bio}$ in the Atlantic subtropical gyre, NATR, is 22 mmolSi m^{-2} yr^{-1} ($n = 3$), as small as that of WARM. The $F_{m/b}Si_{bio}$ does not show north-south symmetric distribution around the equator in the Atlantic as it does in the Pacific (Fig. 8).

7.3.2. The PSAG-W vs. the PSAG-E

Multiyear time-series observations from 1995 to 1999 at two Aleutian-Bering Sea stations, Station AB at 53.5°N, 177°E and Station SA at 49°N, 174°E, reveal an extraordinarily high opal flux in this area throughout the data period (Takahashi et al., 1997, 2000), as mentioned above. At Station AB north of the archipelago, the 5-year mean is as large as 804 mmolSi m^{-2} yr^{-1} with a std of 228 mmolSi m^{-2} yr^{-1}. At Station SA, located on the 5.4-km-deep northern slope of the Aleutian Trench and about 4.5° south and 3° east of Station AB, there is a 4-year mean $F_{m/b}Si_{bio}$ of 294 mmolSi m^{-2} yr^{-1} with a std of 88 mmolSi m^{-2} yr^{-1} while $F_{m/b}C_{inorg}$ is about the same as at Station AB. The $F_{m/b}Si_{bio}$ from the decadal time-series mooring Ocean Station P (OS-P; 50°N, 145°E; e.g., Wong et al., 1994), located in PSAG-E from 1983 to 1990 (except in 1994), ranges from 179 to 560 mmolSi m^{-2} yr^{-1}. Mean $F_{m/b}Si_{bio}$ during this period is 321 mmolSi m^{-2} yr^{-1} with a large std of 120 mmolSi m^{-2} yr^{-1}. This indicates that the $F_{m/b}Si_{bio}$ in PSAG-E is generally smaller than its counterpart in PSAG-W.

7.3.3. Kuroshio and Oyashio regions

Although the export data was collected only in 1994, a $F_{m/b}Si_{bio}$ as large as 770 mmolSi m^{-2} yr^{-1} was observed at 42.3°N, 145.1°, off the northern end of Honshu Island, Japan (Honda et al., 2002). Both the $F_{m/b}C_{org}$ and the $F_{m/b}C_{inorg}$ are also quite large at this station, 233 and 131 mmolC m^{-2} yr^{-1}, respectively. This is the area where the Kuroshio and Oyashio current systems converge. Another large $F_{m/b}Si_{bio}$ reading, 294 mmolSi m^{-2} yr^{-1}, occurs at the KURO station located near the end of the main Kuroshio Current at 40°N, 165°W, and it is associated with $F_{m/b}C_{org}$ and $F_{m/b}C_{inorg}$ that are also large, 327 and 152 mmolC m^{-2} yr^{-1}, respectively. At a Japan Trench station at 34°N, 142°W, where the meandering Kuroshio passes, the $F_{m/b}Si_{bio}$ and $F_{m/b}C_{inorg}$ are also relatively large, 173 and 175 mmolC/Si m^{-2} yr^{-1}, while the $F_{m/b}C_{org}$ is 105 mmolC m^{-2} yr^{-1} (Nozaki, 1989; Nozaki and Oba, 1995). At the station immediately south of the North Pacific Polar Front and the eastern termination of the Kuroshio Extension at 37.4°N, 170.0°W, the $F_{m/b}Si_{bio}$ is reduced to the global average, 95 mmolC m^{-2} yr^{-1} (Kawahata et al., 1997; Kawahata et al., 2000).

7.3.4. The Southern Ocean

Along the JGOFS-AESOPS transect, the $F_{m/b}Si_{bio}$ is approximately the global average or slightly less in SAZ than in the large Southern Ocean region to the north of the Polar Frontal Zone (PFZ) (1997–1998; Bray et al., 2000). The $F_{m/b}Si_{bio}$ increases south of the PFZ, from 258 at the PFZ to 486 mmolSi m^{-2} yr^{-1} at the northern boundary of the ACC. The maximum $F_{m/b}Si_{bio}$ along this transect, observed at a southern ACC station (63.1°S, 169.9°E), is 915 mmolSi m^{-2} yr^{-1}, perhaps the largest $F_{m/b}Si_{bio}$ so far observed in the world's pelagic ocean (Honjo et al., 2000). The $F_{m/b}Si_{bio}$ is 269 mmolSi m^{-2} yr^{-1} at the Antarctic Zone (Ross Sea Gyre), smaller than the flux at the ACC station located immediately to the north. Moorings in the ACC in the Indian Ocean sector measured similarly large opal fluxes: 652 mmolSi m^{-2} yr^{-1} in 1994–1995 (Tréguer, 2003, personal communication) and 308 mmolSi m^{-2} yr^{-1} in 1998–1999 (Pilskaln et al., 2004).

8. Biogeochemical ratios in export particles

8.1. Binary ratios of three major biological pump elements at the mesopelagic/bathypelagic boundary

In order to further understand the relationship between the export of POC and the major biogenic ballast materials ($CaCO_3$ and opal particles) and to determine their contribution to the biological pump, we examined the global distribution of three sets of binary molar ratios. These are mole weight ratios of annual fluxes at

2 km (Table 2): (1) organic carbon vs. inorganic carbon in $CaCO_3$ (C_{org}/C_{inorg}) (Fig. 5), (2) Si in biogenic opal vs. organic carbon (Si_{bio}/C_{org}) (Fig. 6), and (3) Si in biogenic opal vs. inorganic carbon in $CaCO_3$ (Si_{bio}/C_{inorg}) (Fig. 7).

8.1.1. Silica Ocean and Carbonate Ocean based on Si_{bio}/C_{inorg} (Fig. 7 and Table 2)

The Si_{bio}/C_{inorg} ratio indicates the mixing conditions of two major ballast particles (essentially diatom frustules, radiolaria shells, and silicoflagellate skeletons versus coccoliths and planktonic foraminifer tests; Section 2.2). In an oceanic area with a high Si_{bio}/C_{inorg} ratio, the biological pump exports POC with little loss of alka-

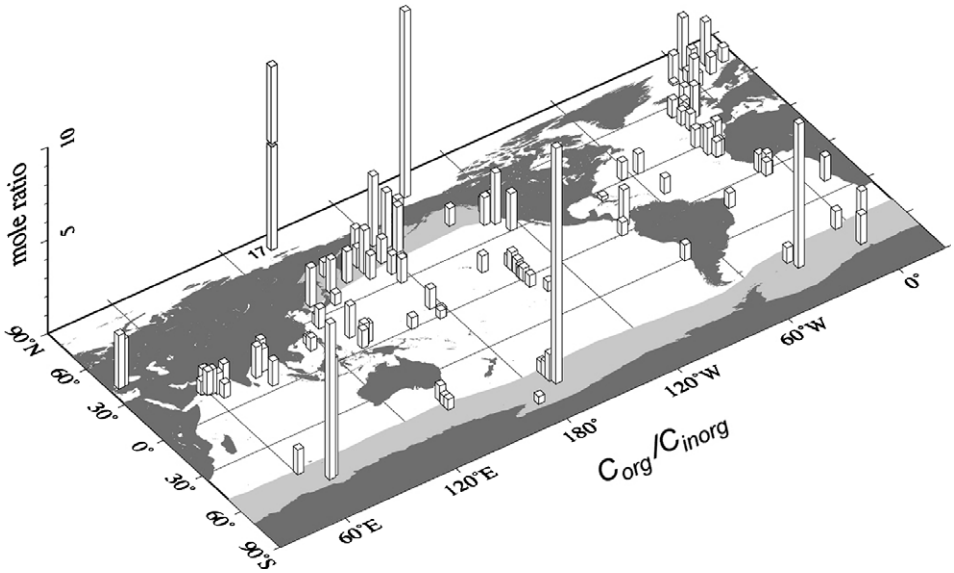

Fig. 5. Global distribution of binary mol-ratio of $F_{m/b}C_{inorg}$ in $F_{m/b}C_{org}$.

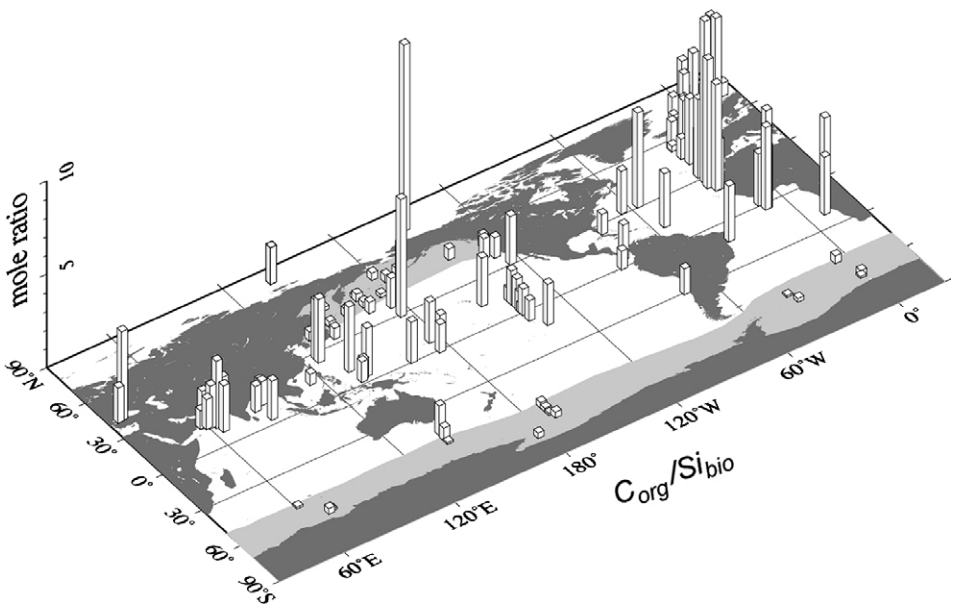

Fig. 6. Global distribution of binary mol-ratio of $F_{m/b}Si_{bio}$ in $F_{m/b}C_{org}$.

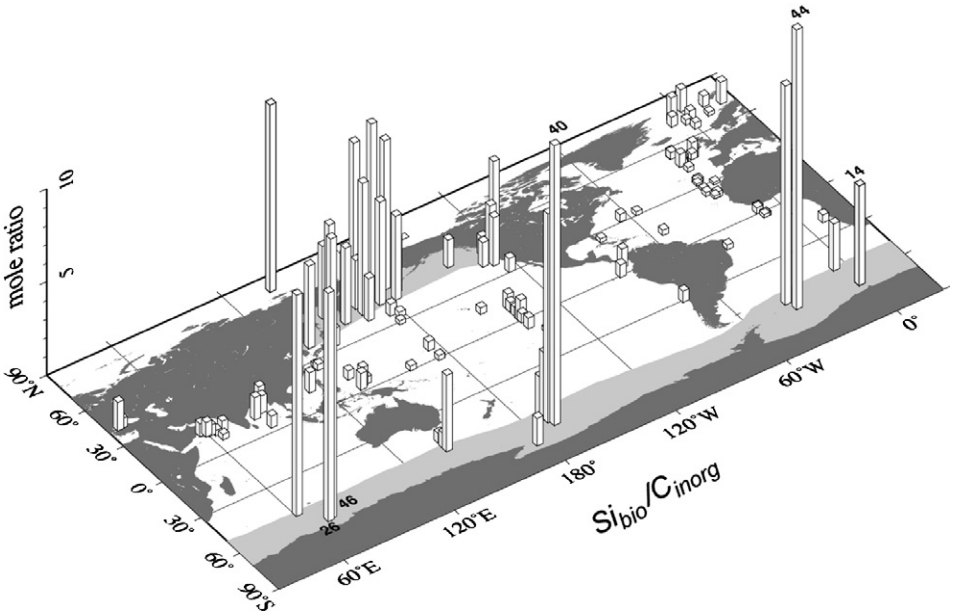

Fig. 7. Global distribution of binary mol-ratio of $F_{m/b}Si_{bio}$ in $F_{m/b}C_{inorg}$.

linity from the surface. The Si_{bio}/C_{inorg} ratios in the world ocean exhibit an important biogeochemical contrast. As Fig. 7 shows, stations where the Si_{bio}/C_{inorg} is > 1 are concentrated in two regions: the North Pacific Boreal Gyres including the large pelagic northern marginal seas (western Bering Sea, the Sea of Okhotsk, and the northern ES/SJ) and the Antarctic Zone in the Southern Ocean. In the rest (majority) of the world ocean, $Si_{bio}/C_{inorg} < 1$. Although the geographic contrasts of highs and lows are modest, the C_{org}/C_{inorg} ratio (Fig. 5) is larger than 1 when the Si_{bio}/C_{inorg} ratio is also larger than 1 and vice versa. The oceanic regions where the C_{org}/C_{inorg} and Si_{bio}/C_{inorg} are $\geqslant 1.0$ constitute what we refer to as the *Silica Ocean*, and the regions where these ratios are <1.0 constitute the *Carbonate Ocean* (Figs. 2–7). Since the global Si_{bio}/C_{inorg} and C_{org}/C_{inorg} ratios are estimated as approximately 1.0 and 1.1, respectively, from the parameterization explained in Section 9 (Table 5), an oceanic region where the mole export of biogenic silica is larger than PIC, and where POC exceeds PIC at the mesopelagic/bathypelagic boundary, is a Silica Ocean, and a region exhibiting the reverse relationship of these elements is a Carbonate Ocean. C_{org}/Si_{bio} is also <1 in the Silica Ocean and >1 in the Carbonate Ocean.

The eight highest Si_{bio}/C_{inorg} ratios were observed in the Southern Ocean south of the APF and range from 46.2 (Pilskaln et al., 2004) to 11.2 (Wefer et al., 1982, 1990; Wefer and Fischer, 1988, 1993a; Honjo et al., 2000; Pilskaln et al., 2004; Tréguer, 2003, personal communication) (Table 2). Among the next 23 stations with Si_{bio}/C_{inorg} ratios between nine and two, 15 were located in the North Pacific Silica Ocean (Wong et al., 1994; Honjo, 1997a; Hong et al., 1997; Kawahata et al., 1997, 2000; Noriki et al., 1997; Takahashi et al., 2000; Honda, 2001; Honda et al., 2002), 5 were in the Southern Ocean (Wefer and Fischer, 1993a; Bray et al., 2000; Honjo et al., 2000; Pilskaln et al., 2004; Tréguer, 2003, personal communication), and 3 were located near coastal upwelling areas (Lyle et al., 1992; Wong et al., 1994).

The pan-Atlantic average Si_{bio}/C_{inorg} is 0.4, with a std of 0.3 ($n = 41$) (stations in the Southern Ocean AZ [e.g., Wefer and Fischer, 1991] are not counted; Table 2). If we exclude three stations where the Si_{bio}/C_{inorg} are 1.2, 1.4, and 1.2 in the Nordic Seas, the mean Si_{bio}/C_{inorg} is as small as 0.3, with std of 0.2 ($n = 38$). Thus, virtually the entire Atlantic is a Carbonate Ocean except for a small fringe area in the Southern Ocean AZ, a few Nordic Sea stations, and perhaps the Labrador Sea (no data; refer to Section 12.1). In contrast, the Si_{bio}/C_{inorg} ratio in the North Pacific Silica Ocean, composed of the western BERS, PSAG (North Pacific Boreal Gyres), northern KURO, and northern ES/JS (Fig. 7), is as large as 5.0 with a std of 2.5 ($N = 14$). Immediately south of the North Pacific Silica Ocean, there is a large $F_{m/b}Si_{bio}$-depleted region, and the Pacific

Carbonate Ocean develops. Average Si_{bio}/C_{inorg} is 0.5 with a std of 0.25 ($n = 25$). The pan-Pacific Si_{bio}/C_{inorg}, combining the Silica and Carbonate oceans, is 2.2 with a large std of 2.4 ($n = 48$) in contrast to the Atlantic mean Si_{bio}/C_{inorg} of 0.4.

The Si_{bio}/C_{inorg} in the Atlantic NAST province, such as at Station L-2 (NARD; 48°N, 19.7°E; Kuss and Kremling, 1999), Station L-1 (NAST; 33°N, 22°E; Scholten et al., 2001), and a station further south in the ETRA (21°N, 20.7°E; Wefer and Fischer, 1993b), is extremely small, such as <0.2. The smallest Si_{bio}/C_{inorg} reported in our data sets is 0.14 at 29.1°N, 15.4°E (Neuer et al., 1997), 28.0°N, 22.0°E (Jickells et al., 1996), and 21.2°N, 20.7°E (Wefer and Fischer, 1993). The smallest Si_{bio}/C_{inorg} in the Pacific Carbonate Ocean is 0.18, observed in the eastern WARM province along the equator from 160.6°W to 175.2°W (Kawahata et al., 1999; Honda et al., 2002).

The largest Si_{bio}/C_{inorg} in the North Pacific Silica Ocean is 8.8, reported from 3200 m at 58.0°N, 179.0°W in the northern Bering Sea (Honjo, 1996). In addition, there are ratios of 8.8 in the deep trap data from northwestern PSAG-W at 51.5°N, 165°W (Wong et al., 1994) and 8.0 at 53.5°N, 177.0°E (Takahashi et al., 1997). Further to the south at 46°N, 175.3°W, near the southern edge of the PSAG, the Si_{bio}/C_{inorg} decreases (Kawahata et al., 1997). In the divergent North Pacific Equatorial Current (NPEC) area, the Si_{bio}/C_{inorg} is elevated slightly to about 1.0 or larger, particularly at the divergent center along the EqPac 140°E transect. For example, Si_{bio}/C_{inorg} is 1.2 at 1°N at the North Equatorial Current/South Equatorial Counter Current transition where a large bloom of the buoyant diatom *Rhizosolenia* spp. (>20 mg chlorophyll-*a* m^{-3}) was observed (Yoder et al., 1994; Archer et al., 1997) (Section 7.3). Some of the opal material may have been transported to the interior depth, thus raising the Si_{bio}/C_{inorg} over 1.0 in the northern EqPac stations.

The Si_{bio}/C_{inorg} in the Arctic Zone (AZ) south of the Antarctic Polar Front (APF) is remarkably high, making this area an extreme Silica Ocean. The $F_{2\,km}Si_{bio}$ increases abruptly in the Polar Frontal Zone to the south, while $F_{2\,km}C_{inorg}$, mostly from pteropod shells, remains relatively constant at the ACC stations. The Si_{bio}/C_{inorg} increases to the south along the 170°W AESOPS transect. At the Ross Sea Gyre station in the POOZ (AZ), the Si_{bio}/C_{inorg} shows a dramatic increase to 40 while the $F_{m/b}C_{inorg}$ declines severely (Honjo et al., 2000). A large Si_{bio}/C_{inorg} of 44.4 is found in the northern Weddell Sea (62.4°S, 34.8°E; Wefer and Fischer, 1991, 1993a). At an Indian Ocean ACC station (52°S, 61.5°W), the Si_{bio}/C_{inorg} is about 12. In the Indian Ocean POOZ at 62°S, 73°W and 63°S, 71°W, the Si_{bio}/C_{inorg} are also as large as 46.2, the highest Si_{bio}/C_{inorg} measured so far (Pilskaln et al., 2004), and 25.6 (Tréguer, 2003, personal communication), respectively (Table 2).

8.1.2. "Rain ratio" or C_{org}/C_{inorg} (Fig. 5 and Table 2)

The PIC/POC ratio is a critical driver of glacial–interglacial pCO_2 variability in linked ocean–atmosphere modeling efforts (e.g., Broecker, 1971; Archer and Maier-Reimer, 1994; Sarmiento et al., 2004). At the same time, this ratio is crucial to understanding the potential efficiency of the gravitational removal of POC from the upper ocean layers to the interior because the abundance and specific gravity of calcite particles make them efficient as ballast (Francois et al., 2002; Klaas and Archer, 2002). Together with the Si_{bio}/C_{inorg} ratio discussed above, the C_{org}/C_{inorg} in settling particles also indicates the volume of carbonate particles required to deliver POC to the ocean interior. Furthermore, C_{org}/C_{inorg} is an important indicator of the removal and transport of alkalinity from the surface ocean to the interior sink. In cases where the C_{org}/C_{inorg} is extremely large and few carbonate particles are available to ballast organic carbon, a massive export of opal assumes the ballasting role for $CaCO_3$. This type of biological pump is advantageous for Earth's CO_2 balance because it constrains the loss of alkalinity from the upper layers.

The distribution of $F_{m/b}C_{org}$ is generally similar to $F_{m/b}C_{inorg}$ (Fig. 3), and therefore C_{org}/C_{inorg} varies only modestly in the world ocean (Fig. 5). For example, the divergent Arabian Sea exhibits particularly high FC_{org}, which varies among TS-trap stations from 233 to 604 mmolC m^{-2} yr^{-1} (Haake et al., 1993; Honjo et al., 1999) as a result of roaming mesoscale eddies (Honjo and Weller, 1997). However, the C_{org}/C_{inorg} is consistently 1.3, slightly larger than the global average (Table 2 and Fig. 5). The data show that C_{org}/C_{inorg} is extremely high in the Southern Ocean POOZ area where $CaCO_3$ particles, either from phytoplankton or zooplankton, are rare (Honjo, 2004). The highest C_{org}/C_{inorg} in our data, 12.6, is observed in the Ross Sea Gyre at 66.2°S, 168.7°E (Honjo et al., 2000), followed by 8.4 and 6.3 from the Indian Ocean POOZ (Pilskaln et al., 2004; Tréguer, 2003, personal communication). Two Atlantic Southern Ocean stations also yield high C_{org}/C_{inorg} values of 7.7 and 2.8. (Wefer and Fischer, 1993a).

A high C_{org}/C_{inorg} ratio itself does not necessarily mean the biological pump is working efficiently. The $F_{m/b}C_{org}$ from the high C_{org}/C_{inorg} stations in the Southern Ocean are as small as 14–84 mmolC m^{-2} yr^{-1} (Table 2). Clusters of stations with high C_{org}/C_{inorg}, comparable to the POOZ stations, are concentrated in the North Pacific Silica Ocean, particularly the North Pacific Boreal Gyre provinces and the Bering Sea Basin (e.g., Honjo, 1997a; Takahashi et al., 2000; Honda et al., 2002) (Fig. 5). At these stations, $F_{m/b}C_{org}$ is far larger than the global average and is associated with very large $F_{m/b}Si_{bio}$ as ballast for POC, with modest to average fluxes of PIC. Thus, the biological pump operating in the North Pacific Silica Ocean may be the most efficient pump system in the global ocean.

Average annual C_{org}/C_{inorg} at the mesopelagic/bathypelagic boundary in the pan-Atlantic is 0.98, with a std of 0.55 ($n = 37$). Three OMEX stations in the eastern NARD province at 49°N, 12.8–13.8°E show an extremely high C_{org}/C_{inorg} of 3.2. The $F_{m/b}C_{org}$ is also very large at this station, >370 mmolC m^{-2} yr^{-1}, but this is also associated with an $F_{m/b}C_{inorg}$ as large as >215 mmolC m^{-2} yr^{-1} (Antia et al., 2001a,b; Scholten et al., 2001). This could be an isolated area with high biological pump activity. Combinations of ratios at these stations are similar to those in the northwest Pacific's PSAG. However, at Station L-2 (48°N, 20°E), just south of the OMEX area, and Station L-1 (33°N, 22°E) (Scholten et al., 2001), the C_{org}/C_{inorg} drops to only 0.4, one of the smallest in the Atlantic. The stations with the smallest C_{org}/C_{inorg} in the Atlantic are a NAST station at 25.3°N, 79.5°E reporting 0.2 (Pilskaln et al., 1989) and a Nordic Sea station at 72.5°N, 8°E reporting 0.1 (von Bodungen et al., 1995).

Mean C_{org}/C_{inorg} from 48 pan-Pacific stations is 1.3, about 23% larger than the pan-Atlantic average. Mean C_{org}/C_{inorg} in the Pacific Silica Ocean is 1.9 with std of 0.85. Particularly, the C_{org}/C_{inorg} in the Bering Sea and the northern PSAG near the Aleutian Arc (Stations AB and SA) are as high as 3.8 (58°N, 179W; Honjo, 1997a), 3.0, and 2.3 (53°N, 177°E; Takahashi et al., 2000). The station on the north of the ES/JS Sub-Polar Front is also high at 2.1 (Hong et al., 1997). The mean annual C_{org}/C_{inorg} from 1983 to 1990 measured at Station P is 0.95 (Wong et al., 1999). The smallest C_{org}/C_{inorg} in the Pacific is about 0.4, found at WARM stations (Kawahata et al., 1999; Honda, 2001) and in the South China Sea (Wiesner et al., 1996), both under the Carbonate Ocean condition.

8.1.3. Contribution of diatoms to C_{org}/Si_{bio} (Table 2 and Fig. 6)

As mentioned above, the mass settling of $CaCO_3$ particles may be too small in parts of the Silica Ocean to effectively remove POC from the surface layers. However, POC must be removed in order to maintain a steady ocean chemistry state. Opal particles assume the major ballast role under such conditions. Combined with Si_{bio}/C_{inorg}, C_{org}/Si_{bio} indicates the quantitative role of opal particles as POC ballast. Published C_{org}/Si_{bio} ranges from 8.7 (NAST; Jickells et al., 1996) to 0.1 at six Southern Ocean stations (Wefer and Fischer, 1993a; Bray et al., 2000; Honjo et al., 2000; Pilskaln et al., 2004; Tréguer, 2003, personal communication). C_{org}/Si_{bio} from the eastern NAST bounded by 24.6° to 28°N and 15.4° to 23°E ranks third highest in C_{org}/Si_{bio} with readings of 8.7, 8.5, and 6.9 (Jickells et al., 1996; Scholten et al., 2001; Neuer et al., 1997). Meanwhile, Si_{bio}/C_{inorg} at these stations are the smallest at 0.1–0.2, and C_{org}/C_{inorg} range from 1.1 to 1.4. Thus, nearly all $F_{m/b}$ C_{org}, 68–109 mmolC m^{-2} yr^{-1}, is removed by carbonate particles, and the role of opal is insignificant in this North Atlantic region. In contrast, the smallest C_{org}/Si_{bio} in the world ocean occurs at six AZ stations in the Southern Ocean, ranging from 0.1 to 0.3. As mentioned above, Si_{bio}/C_{inorg} in the Southern Ocean is as great as 46.2 (Pilskaln et al., 2004), by far the largest in the world ocean. Therefore, opal-particle ballasts are almost exclusively responsible for removing approximately 42–117 mmolC m^{-2} yr^{-1} of POC annually at 2 km depth in this AZ area. The C_{org}/Si_{bio} in the North Pacific Silica Ocean ranges from 0.3 (PSAG-W; Kawahata et al., 2000) to 0.6 (PSAG-E; Wong et al., 1994). C_{org}/Si_{bio} ratios recorded at the North Pacific Silica Ocean stations, along with the Southern Ocean Silica Ocean stations, are among the 35 smallest.

8.2. Ternary percent ratios at the mesopelagic/bathypelagic boundary

The Fig. 8A–E graphic projection shows a ternary percent (T% hereafter) ratio of the essential biogeochemical elements in moles ($\%F_{m/b}C_{org} + \%\ F_{m/b}C_{inorg} + \%\ F_{m/b}Si_{bio} = 100\%$) defined by three figures whose outlines run through one-to-one ratios of the three combinations of $F_{m/b}C_{org}$, $F_{m/b}C_{inorg}$, and $F_{m/b}Si_{bio}$, converging at the geometric center of the triangle. The resulting three equal-volume quadrilaterals on the

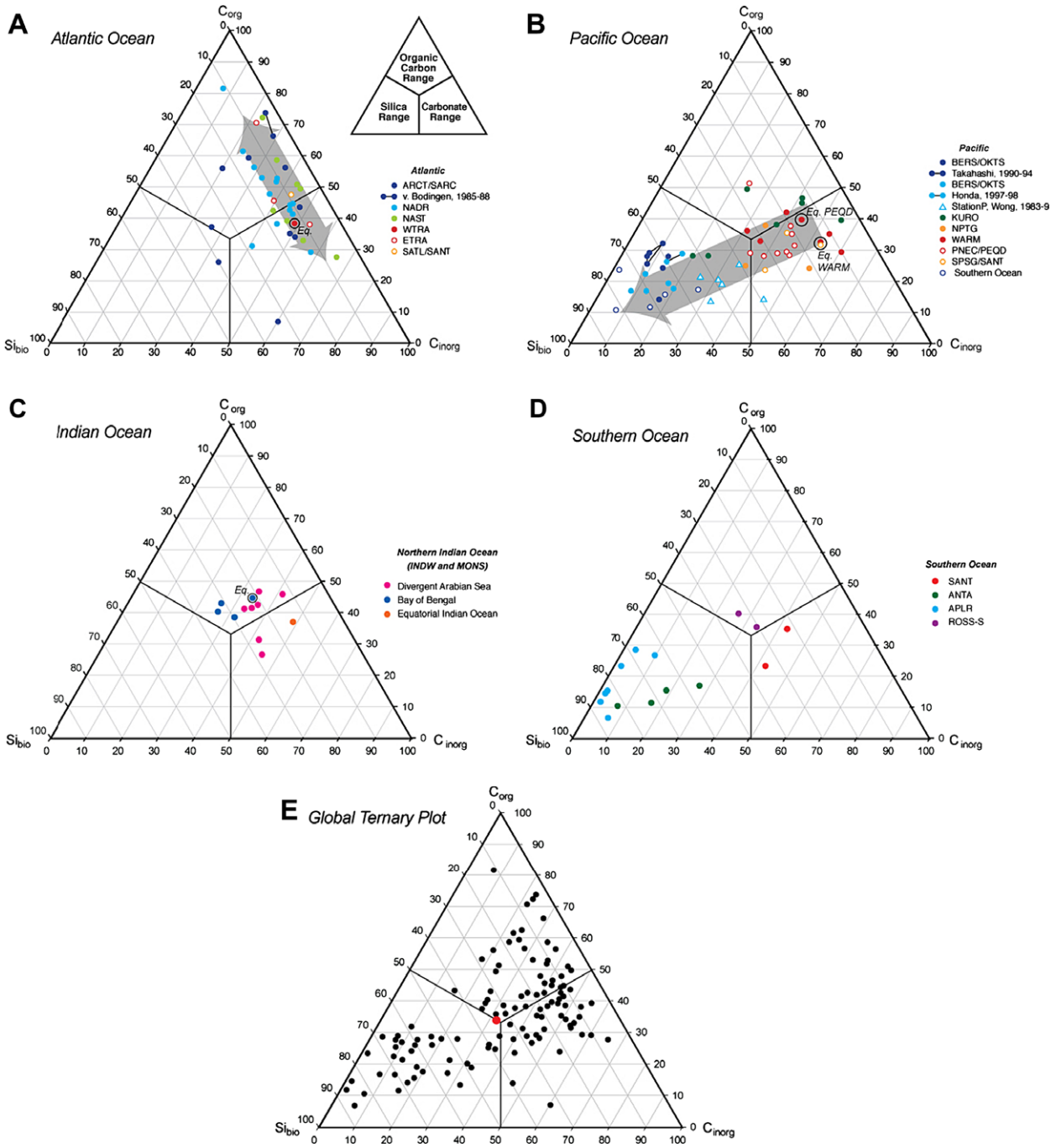

Fig. 8. (A) Ternary mol-percentage projection of $F_{m/b}C_{org}$, $F_{m/b}C_{inorg}$, and $F_{m/b}Si_{bio}$ among the Atlantic stations, including the Atlantic Southern Ocean. The black-outlined solid red circle is the ternary percent (T%) at the station located on the equator in the Atlantic Ocean. (B) Ternary mol-percentage projection of $F_{m/b}C_{org}$, $F_{m/b}C_{inorg}$, and $F_{m/b}Si_{bio}$ among the Pacific Stations, including the Pacific Southern Ocean. The black-outlined solid red circle is the T% at the station located on the equator in the Pacific Ocean. (C) Ternary mol-percentage projection of $F_{m/b}C_{org}$, $F_{m/b}C_{inorg}$, and $F_{m/b}Si_{bio}$ among the Indian Ocean stations, excluding the data from the Indian Ocean sector of the Southern Ocean. (D) Ternary mol-percentage of three biogeochemical elements in the Southern Ocean from the Subantarctic Zone (SAZ) to the Antarctic Zone (AZ). (E) Plot of all ternary ratios in the analytical data from all TS-trap samples in Table 3. The solid red circle near the center of the graph is the nonweighted average of all ternary ratios in Table 3.

graph are designated as the Organic Carbon Range, the Carbonate Range, and the Silica Range (see Fig. 8A inset). This ternary percent projection of the three essential elements at each TS-trap location provides a visual concept of their interrelated roles in the biological pump; Fig. 8A shows the Atlantic TS-traps, Fig. 8B the Pacific traps,; Fig. 8C the Indian Ocean traps including those in the Arabian Sea, and Fig. 8D the Southern Ocean traps.

The distribution patterns of T% in the Atlantic (Fig. 8A) and in the Pacific (Fig. 8B) are quite different. In the Atlantic, T% data points are distributed within a band constrained by Si_{bio}< about 15 T% and > about 5 T%, while the proportions of C_{org} and C_{inorg} change randomly with latitude or biogeochemical province (thick arrow in Fig. 8A). However, in the Pacific, the ratios between C_{org} and C_{inorg} are more constant than in the Atlantic, and the T% data points move toward T% maximum of Si_{bio} (and C_{inorg} minimum) as the mooring locations move poleward in both hemispheres (thick arrow in Fig. 8B). The T% at the equatorial zones in both the Atlantic (ETRA, Fig. 8A) and the Pacific (WARM, Fig. 8B) occupy similar locations on a ternary projection with characteristically small Si T% (9–15%). However Si T% increases to 22% in the Pacific upwelling province (PEQD). The T% data points of the northwest Pacific Silica Ocean and the Southern Ocean Silica Ocean coincide in the extreme Silica Range (Fig. 8B).

The largest T% of $F_{m/b}C_{org}$ among these three elements is found in the TS-trap samples collected at the OMEX-4 mooring in the NARD province of the Northeast Atlantic (Fig. 8A). The combination (T% $F_{m/b}C_{org}$: T% $F_{m/b}C_{inorg}$: T% $F_{m/b}Si_{bio}$) is *82*:7:11 at 49.2°N, 12.8°E in 1993 (original data from Antia et al., 2001a,b; Scholten et al., 2001). The $F_{2\,km}C_{org}$ percentage is also very high in the OMEX-1 and -2 and L2-B sites that were measured repeatedly near the OMEX moorings at 47.8°N, 19.8°E in 1996 and 1997 (Kuss and Kremling, 1999). The maximum T% of $F_{2\,km}C_{inorg}$ is also found at a 2-km-deep TS-trap deployed at the L-1 Station in the Atlantic (40°N, 22°E in 1998) in the NAST Province. The combination at that station is 28:*66*:7 (a ternary % in this paper often does not add up to 100 due to rounding; Table 3) (original data from Scholten et al., 2001). The T% of $F_{2\,km}Si_{bio}$ at this station is one of the smallest found so far. The T% of all POOZ moorings (Southern Ocean) presents an extremely large $F_{2\,km}Si_{bio}$ T%. The combination with the maximum $F_{m/b}$ Si_{bio} T% is 7:7:*87* from the M-2 Station TS-trap set 1.3 km deep in the Indian Ocean sector (original data from Tréguer, 2003, personal communication) (Fig. 8D). The T% points of AZ samples are all remote from the global average point and strongly skewed to the Si_{bio}, and thus unique in the world ocean.

We examined the interannual variability in ternary percentages of fluxes at several stations. In a 3-year record from one of the Nordic Sea mooring sites occupied from 1985 to 1988 by von Bodungen et al. (1995) at 72.5°N, 8°E, T% $F_{2\,km}C_{org}$ was small during a 3-year period (between two points that are connected by a thin line in Fig. 8A). At the Pacific Aleutian BERS station at 53.5°N, 177°E, the annual ternary ratios from 1990 to 1994 were close (Fig. 8B) (data from Takahashi et al., 1997; Takahashi et al., 2000). The annual T% ratio during 1997 and 1998 at a PSAG-W station at 50°N, 165°W was also very close (data from Honda, 2001). However, the annual % ratios vary extensively from year to year at Station P in PSAG-E at 50°N, 145°E. The 6-year annual T% plot from 1983 to 1993 was scattered widely in the Silica Range and migrated to the Carbonate Range in 1983 (Fig. 8B; data from Wong et al., 1994).

Mean molar T% ratios are calculated from the 152 TS-trap samples moored from 1 to 3.5 km deep with FC_{org} normalized at 2 km (Table 3) (High Arctic data in Table 3 are excluded). Despite the strong provincialism and some interannual differences of T%, the ternary mol-ratios of POC, PIC, and biogenic Si at 2 km in the world ocean are very close—35:32:33, indicated as a red dot in Fig. 8E. The global average of binary ratios for the three elements calculated from the parameterization model (Section 9) are all approximately 1 and support the global T% ratios discussed above.

9. Global parameterizations of settling fluxes

Based on the observations of elemental export fluxes of carbon and biogenic Si at the mesopelagic/bathypelagic boundary, we developed several parameterizations to approximate the annual global distribution of particles in molar fluxes: $F_{m/b}C_{org}$, $F_{m/b}C_{inorg}$, and $F_{m/b}Si_{bio}$. For these parameterizations, we used the 153 TS-trap data sets listed in Table 3. The parameterizations are based on the least-squares fits of measured fluxes to surface hydrographic data. As the result of this parameterization, we obtain a global grid

(250 km × 250 km grid cell) for $F_{m/b}C_{org}$, $F_{m/b}C_{inorg}$, and $F_{m/b}Si_{bio}$. Global total fluxes of POC, carbonate and opal, their global ratios, and their average fluxes in the pelagic ocean were calculated by totaling all the grid cells that cover ocean areas deeper than 2 km (except the Arctic Ocean).

9.1. Regional models

Different models were used for determining the $F_{m/b}C_{org}$, $F_{m/b}C_{inorg}$, and $F_{m/b}Si_{bio}$ in different oceanic regions. Equations for computing the carbonate and opal fluxes ($F_{m/b}C_{inorg}$ [in $gCaCO_3\ m^{-2}\ yr^{-1}$] and $F_{m/b}Si_{bio}$ [in $gSiO_2\ m^{-2}\ yr^{-1}$]) are based on sea surface temperature (SST, in°C), primary production (in $gC\ m^{-2}\ yr^{-1}$), and/or winter surface dissolved SiO_2 (in $\mu mol\ kg^{-1}$). These are subsequently converted to molar fluxes. $F_{m/b}C_{org}$ fluxes are estimated using the Francois et al. (2002) equation and scaled to molar fluxes thereafter. Different models have been developed for the following regions:

1. The Trade Wind Domain: An area without significant seasonality, this region includes observations from all JGOFS-EqPac, MANOP, German Warm Water Pool program, and Panama Basin experiments. Fluxes estimated from these parameterizations are applied to the area bordered by 25°N to 18°S and 120°E to 70°W, where the annual primary production (Behrenfeld and Falkowski, 1997) is more than 8.3 molC m^{-2} (100 gC m^{-2}).
2. The Arabian Sea: This includes the Indo-German Arabian Sea Program (IGAS) and JGOFS-Arabian Sea Expedition (ASE). Parameterizations for this area are applied between the latitudes of 30°N to 25°S, longitudes of 70°W to 120°E, and where PP is more than 8.3 molC m^{-2}.
3. Southern Ocean: This model includes data from JGOFS-AESOPS, French (Tréguer, 2003, personal communication), and American Prydz Bay (Pilskaln et al., 2004) stations. It is subdivided into two regions: (1) the POOZ (AZ) region located between mean annual SST temperature contours of 2 °C and 8 °C, and (2) the ACC (ANTA and SANTA in the Atlantic sector) bounded on the north by the 2 °C SST isotherm and on the south by the 2000-m isobath.
4. All other areas (or "default"): These include 74 stations for $F_{m/b}C_{inorg}$ and 78 stations for $F_{m/b}Si_{bio}$ curve fitting from all other provinces including the Westerlies Domain (Longhurst et al., 1995).

9.2. Biomineral ballast parameterizations

9.2.1. Parameterization of PIC ($F_{m/b}C_{inorg}$)

EqPac:

$$F_{m/b}C_{inorg} = 0.281 \times PP - 14.6\ [gCaCO_3\ m^{-2}\ yr^{-1}] \quad (1)$$

Twelve stations are used, $R^2 = 0.59$. Mean error is 48 mmolC $m^{-2}\ yr^{-1}$.

Arabian Sea:

$$F_{m/b}C_{inorg} = 0.105 \times PP + 5.1\ [gCaCO_3\ m^{-2}\ yr^{-1}] \quad (2)$$

Seven stations are used, $R^2 = 0.60$. Mean error is 76 mmolC $m^{-2}\ yr^{-1}$.

Southern Ocean:

$$F_{m/b}C_{inorg} = 2.928 \times SST - 3.0\ [gCaCO_3\ m^{-2}\ yr^{-1}] \quad (3)$$

Seven stations are used to parameterize $F_{m/b}C_{inorg}$ in POOZ. It is represented by a simple linear function of SST, where R^2 is 0.50, and mean error = 56 mmolC $m^{-2}\ yr^{-1}$. Within the ACC, detailed spatial structure cannot be discerned from the station distribution; thus, a mean value of 15 mmolC $m^{-2}\ yr^{-1}$ (with std = 18 mmolC $m^{-2}\ yr^{-1}$) determined from eight stations is applied to the area.

Default:

$$F_{m/b}C_{inorg} = PP \times (0.0017 \times SST + 0.03)\ [gCaCO_3\ m^{-2}\ yr^{-1}] \quad (4)$$

The algorithm to cover the rest of world is determined using data from 74 stations by combining a linear function of PP and SST, where R^2 equals 0.33 and mean error is 69 mmolC m^{-2} yr^{-1}.

9.2.2. Parameterization of biogenic Si ($F_{m/b}Si_{bio}$)

EqPac:

$$F_{m/b}Si_{bio} = 0.179 \times PP - 13.3 \ [gSiO_2\ m^{-2}\ yr^{-1}] \quad (5)$$

Twelve stations are used, R^2 is 0.50. Mean error is 62 mmolSi m^{-2} yr^{-1}.

Arabian Sea:

$$F_{m/b}Si_{bio} = 0.0532 \times PP - 2.1 \ [gSiO_2\ m^{-2}\ yr^{-1}] \quad (6)$$

Twelve stations are used, R^2 is 0.68. Mean error is 54 mmolSi m^{-2} yr^{-1}.

Southern Ocean:

$$F_{m/b}Si_{bio} = -6.1615 \times SST + 59.6 \ [gSiO_2\ m^{-2}\ yr^{-1}] \quad (7)$$

To parameterize $F_{m/b}Si_{bio}$ in POOZ, seven stations are used. It is represented by a simple linear function of SST, where R^2 is 0.71, and mean error = 126 mmolSi m^{-2} yr^{-1}. In the ACC, an average value of 159 mmolSi m^{-2} yr^{-1} (std = 144 mmolSi m^{-2} yr^{-1}) from eight stations is used.

Default:

$$F_{m/b}Si_{bio} = 1.36e^{0.1114\times(Ws-Si)} \ [gSiO_2\ m^{-2}\ yr^{-1}] \quad (8)$$

For all other areas, using 78 stations in the Westerlies Domain, the winter surface dissolved SiO_2 (Louanchi and Najjar, 2000) best expressed the $F_{m/b}Si_{bio}$, with R^2 equal to 0.40 and mean error of 252 mmolSi m^{-2} yr^{-1}.

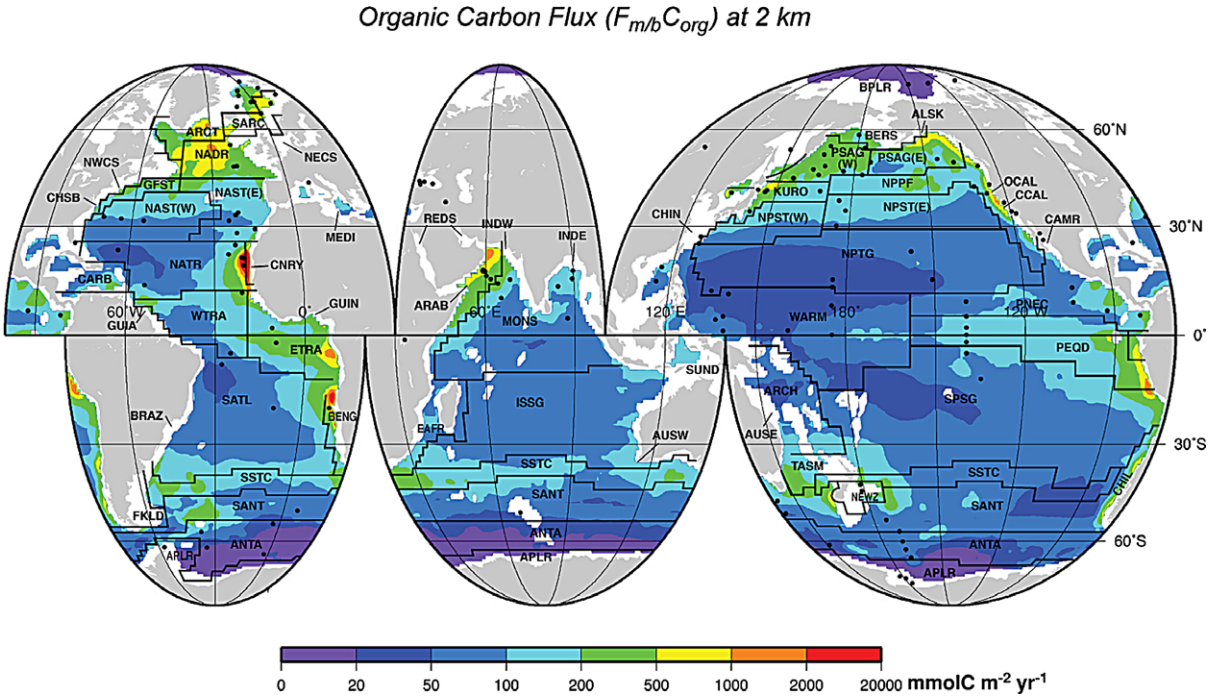

Fig. 9. Global parameterization of $F_{2\ km}C_{org}$ in mmolC m^{-2} yr^{-1} based on individual TS-trap data sets from four model domains—the Trade Wind Domain (as in Longhurst et al., 1995), the Arabian Sea Region, the Antarctic Zone, and data from default stations—projected on the geography of biogeochemical provinces and stations that were used for analyzing the data presented in this paper.

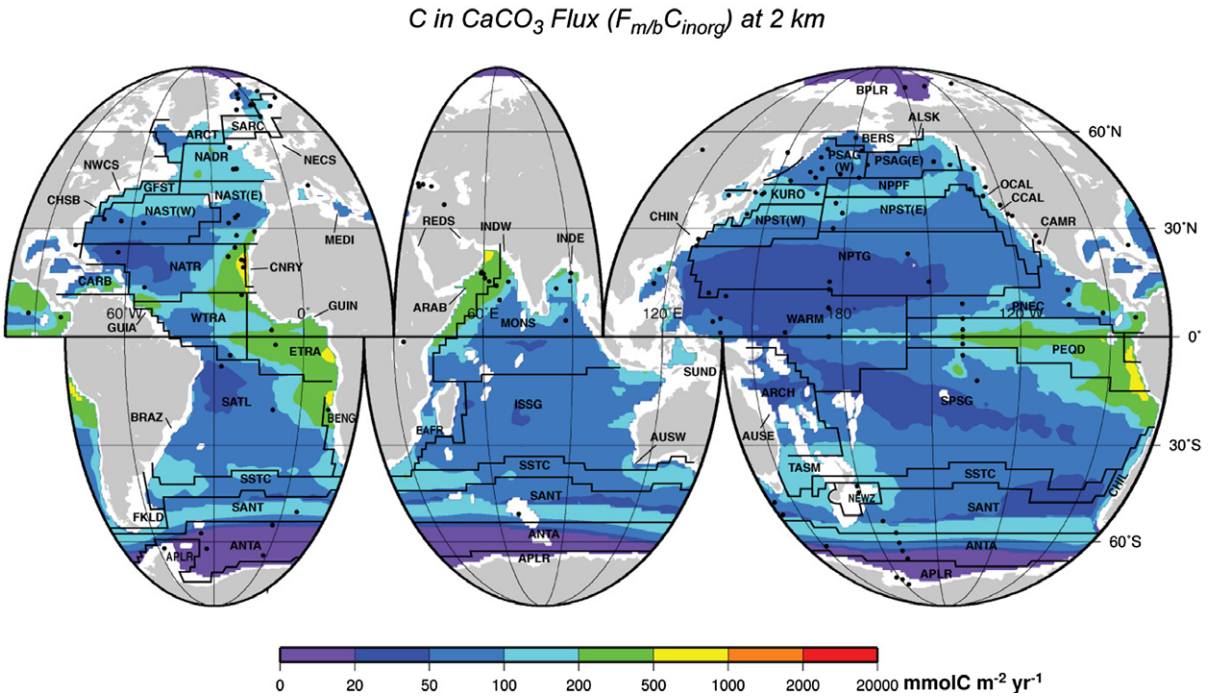

Fig. 10. Global parameterization of $F_{m/b}C_{inorg}$ in mmolC m^{-2} yr^{-1} based on individual TS-trap data sets from four model domains as in Fig. 9.

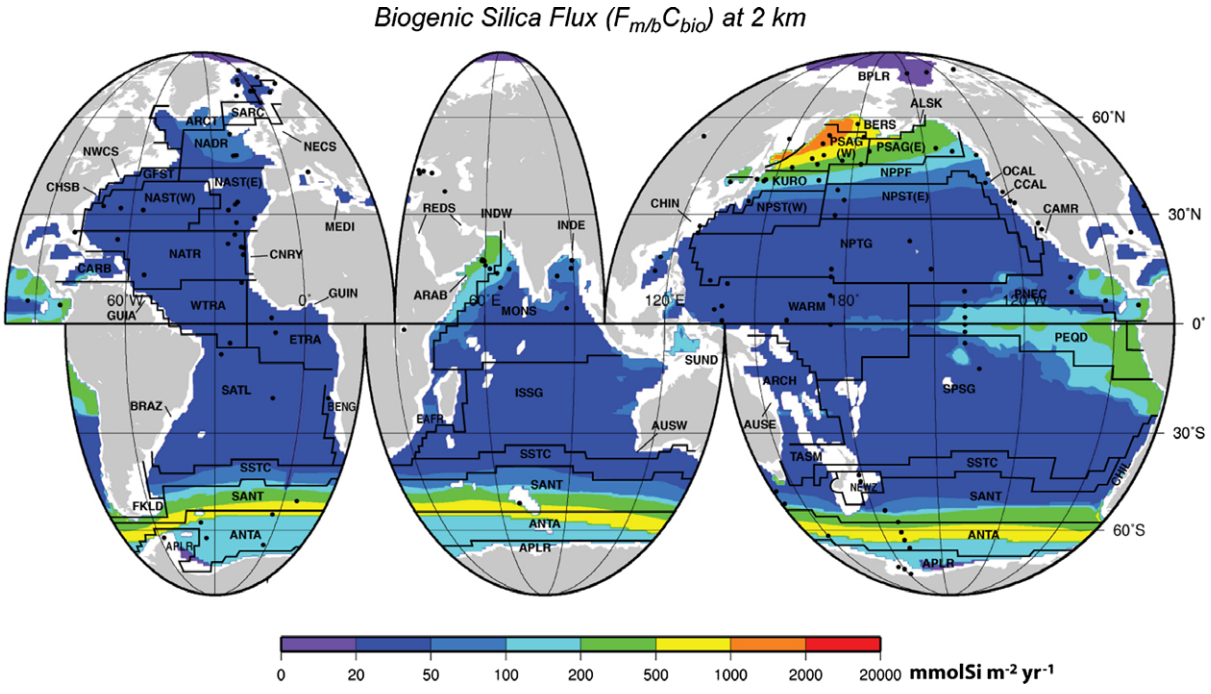

Fig. 11. Global parameterization of $F_{m/b}Si_{bio}$ in mmolSi m^{-2} yr^{-1} based on individual TS-trap data sets from four model domains as in Fig. 9.

9.3. Parameterization of global organic carbon fluxes

Francois et al. (2002) defined the transfer efficiency of organic carbon to the deep sea (T_{eff}) as the ratio of POC flux measured with sediment traps deployed at the mesopelagic/bathypelagic boundary zone (normalized here as 2 km depth) to the export production (EP) at the same site estimated from a satellite-derived PP model (Behrenfeld and Falkowski, 1997), and EP derived from a pelagic ecosystem model (Laws et al., 2000) (Table 2):

$$T_{\mathrm{eff}} = F_{\mathrm{m/b}}\mathrm{C}_{\mathrm{org}}/\mathrm{EP}. \tag{9}$$

Multiple linear regression (Francois et al., 2002) indicates that the transfer efficiency of organic carbon to the deep sea by the biological pump can be predicted to a large degree from the flux of carbonate, the f-ratio, and the water depth.

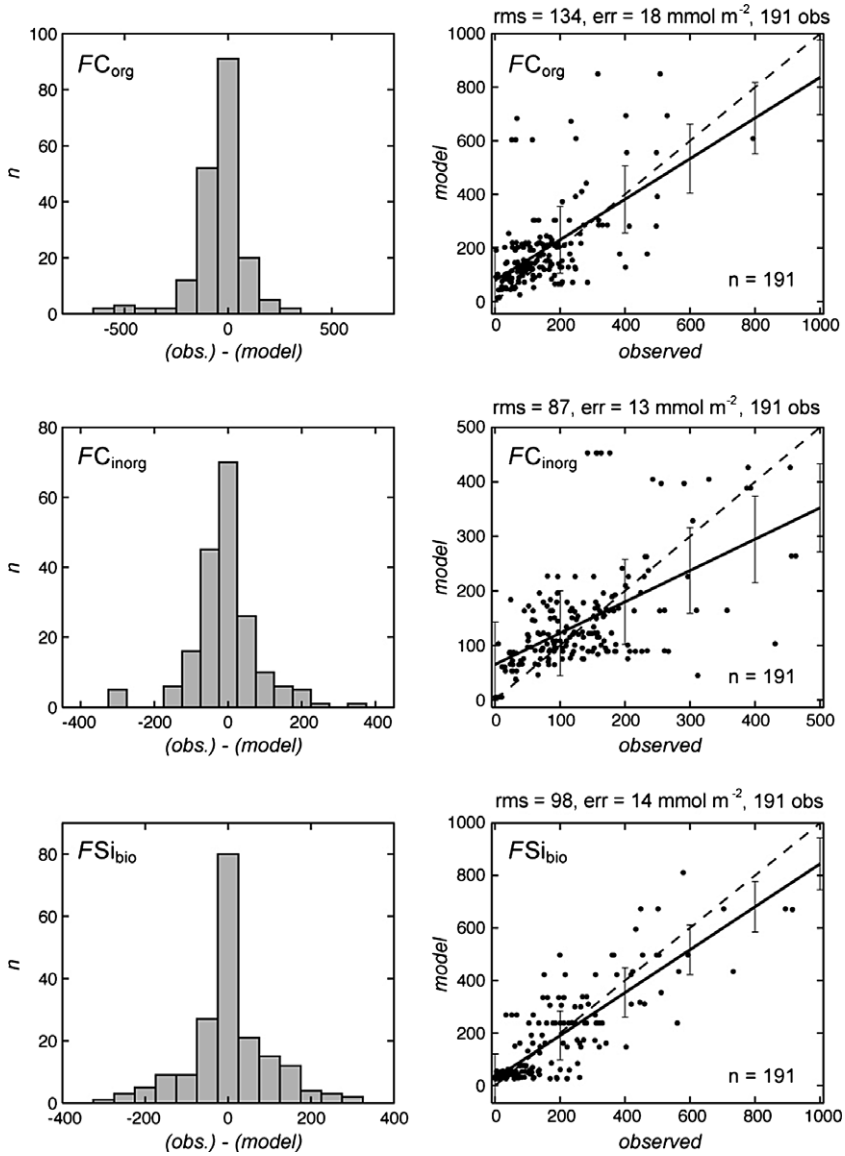

Fig. 12. Comparison of the parameterized model fluxes with observational $F_{\mathrm{m/b}}\mathrm{C}_{\mathrm{org}}$ (top panels), $F_{\mathrm{m/b}}\mathrm{C}_{\mathrm{inorg}}$ (middle panels), and $F_{\mathrm{m/b}}\mathrm{Si}_{\mathrm{bio}}$ (bottom panels). The histograms in the left-hand column show differences in how the deviations are normally distributed. The right-hand column plots show observations vs. model values with straight-line fit and error bars.

$$T_{\mathrm{eff}} = [2.15 \times 10^{-3} F\mathrm{CaCO_3}] + [102.4Z^{-1}] - [0.096\text{f-ratio}] + 0.0092. \quad (10)$$

The standard deviation of the difference between TS-trap-data-based $F_{\mathrm{m/b}}C_{\mathrm{org}}$/EP and "calculated" T_{eff} is 0.0166, 9% of the measured $F_{\mathrm{m/b}}C_{\mathrm{org}}$/EP range (0.18). At a 95% confidence level, our simple model Eq. (10) thus explains 82% of the T_{eff} variability in the global open ocean.

9.4. Global maps of $F_{m/b}C_{org}$, $F_{m/b}C_{inorg}$, and $F_{m/b}Si_{bio}$

Grids of $F_{\mathrm{m/b}}C_{\mathrm{org}}$ at 250-km resolution are produced in Fig. 12 by applying Eq. (10) using grid averages of annual PP (Behrenfeld and Falkowski, 1997), EP (Laws et al., 2000), and modeled carbonate fluxes. The gridded fluxes of $F_{\mathrm{m/b}}C_{\mathrm{inorg}}$ and $F_{\mathrm{m/b}}Si_{\mathrm{bio}}$ are obtained by applying Eqs. (1)–(8) to the grid averages of annual PP, winter surface dissolved SiO_2, and annual SST data and using the parameterization derived for each of the regions delineated at the beginning of this section.

Considering the statistical funnel through which particles sink before reaching a sediment trap (Siegel and Deuser, 1997), the export data were plotted at the mesopelagic/bathypelagic boundary in 250 km × 250 km grids with the following rationale: With an eddy kinetic energy of 10 $\mathrm{cm^2\ s^{-2}}$, and a mean particle sinking rate of 200 m $\mathrm{dy^{-1}}$ (Honjo, 1996), the spatial averaging scale at the surface (Lx) for a TS-trap deployed at 4000 m depth is approximately 60 km. Assuming a Gaussian collection probability density, the radius around the trap site from which 90% of the collected particles (R_c) would originate is:

$$R_c = (-2\ln(0.1) \times Lx)^{0.5}.$$

Thus, funnel diameter is approximately 250 km.Based on this calculation we reconstructed the global contours of $F_{\mathrm{m/b}}C_{\mathrm{org}}$ (Fig. 9), $F_{\mathrm{m/c}}C_{\mathrm{inorg}}$ (Fig. 10), and $F_{\mathrm{m/b}}Si_{\mathrm{bio}}$ (Fig. 11) and their binary ratios (Table 2). Boundaries between model areas are statistically smoothed.

The spread, or sample standard deviation, of our model estimates versus the observations are determined by taking the root-mean-square differences between the observed samples and the model estimated parameters (Fig. 12). Using 151 of the observations, the sample standard deviation is 87 mmolC $\mathrm{m^{-2}\ yr^{-1}}$ for $F_{\mathrm{m/b}}C_{\mathrm{inorg}}$, 98 mmolSi $\mathrm{m^{-2}\ yr^{-1}}$ for $F_{\mathrm{m/b}}Si_{\mathrm{bio}}$, and 134 mmolC $\mathrm{m^{-2}\ yr^{-1}}$ for $F_{\mathrm{m/b}}C_{\mathrm{org}}$. Assuming that the error is uniform across the model, that each observation is independent, that the parameters are time invariant, and that the deviations are normal, 95% confidence intervals for the climatologic mean values represented by the model were determined based on a statistical cumulative t distribution using the equation proposed by Emery and Thomson (1997):

$$2 \times (\text{sample std})/(\text{number of samples})^{0.5}.$$

Based on the derived sample standard deviations, there is a 95% probability that

(1) modeled values of $F_{\mathrm{m/b}}C_{\mathrm{inorg}}$ bracket the true values by ±13 mmolC $\mathrm{m^{-2}\ yr^{-1}}$,
(2) modeled values of $F_{\mathrm{m/b}}Si_{\mathrm{bio}}$ bracket the true values by ±14 mmolSi $\mathrm{m^{-2}\ yr^{-1}}$, and
(3) modeled values of $F_{\mathrm{m/b}}C_{\mathrm{org}}$ bracket the true values by ±18 mmolC $\mathrm{m^{-2}\ yr^{-1}}$.

10. Global total fluxes of POC, ballast particles, and biogeochemical ratios

The annual fluxes of $F_{\mathrm{m/b}}C_{\mathrm{org}}$, $F_{\mathrm{m/b}}C_{\mathrm{inorg}}$, and $F_{\mathrm{m/b}}Si_{\mathrm{bio}}$ in the global ocean can be calculated by integrating the flux estimates in each grid. The global annual export flux (Global F or G-F, Table 5) thus obtained at the mesopelagic/bathypelagic boundary are: POC (G-$F_{\mathrm{m/b}}C_{\mathrm{org}}$: 36.2 ± 4.5 teramolC $\mathrm{yr^{-1}}$ or 0. 43 Gt $\mathrm{yr^{-1}}$), PIC (G-$F_{\mathrm{m/b}}C_{\mathrm{inorg}}$: 33.8 ± 3.8 teramolC $\mathrm{yr^{-1}}$ or 0.41 Gt $\mathrm{yr^{-1}}$), and biogenic Si (34.4 ± 2.6 teramolSi $\mathrm{yr^{-1}}$ or 0.97 Gt $\mathrm{yr^{-1}}$) from the ocean area deeper than 2 km that is 301.3 $\mathrm{Mkm^2}$ (Table 5). The mean export fluxes (M-) at the mesopelagic/bathypelagic boundary per unit section (1 $\mathrm{m^2}$) of the global water column over 301.3 million $\mathrm{km^2}$ for M-$F_{\mathrm{m/b}}C_{\mathrm{org}}$, M-$F_{\mathrm{m/b}}C_{\mathrm{inorg}}$, and M-$F_{2\,\mathrm{km}}Si_{\mathrm{bio}}$ are 120 mmolC $\mathrm{m^{-2}\ yr^{-1}}$, 112 mmolC $\mathrm{m^{-2}\ yr^{-1}}$, and 114 mmolSi $\mathrm{m^{-2}\ yr^{-1}}$, respectively. In metric, these fluxes are 1.4 gC $\mathrm{m^{-2}\ yr^{-1}}$, 1.3 gC $\mathrm{m^{-2}\ yr^{-1}}$, and 3.2 gSi $\mathrm{m^{-2}\ yr^{-1}}$, respectively.

The global mean ratios of the three constituents are thus all about one. Broadly speaking, while 1 mol of POC is pumped to the bottom of the mesopelagic zone, one mole of PIC and one mole of biogenic Si settle together in the world ocean on average. The ternary % ratio of mole fluxes of these three elements, independently calculated from individual TS-trap data, are also very close: 35:32:33 T%, respectively (Section 8.2). This export flux similarity for POC and biominerals at the mesopelagic/bathypelagic boundary is stunning considering that $F_{m/b}C_{org}$, $F_{m/b}C_{inorg}$, and $F_{m/b}Si_{bio}$ differ by three to four orders of magnitude. However, we are unable to offer an explanation for this intriguing observation.

Our global POC flux estimate is very close to that in Jahnke's early result, which utilized particulate vertical flux and water depth correlations to estimate the global rain rate of POC at the seafloor as 33 teramolC yr^{-1}; this is very close to our estimate at 2 km of about 36 teramolC yr^{-1} (Jahnke, 1996). When Jahnke's seafloor flux is normalized to 2 km, the flux appears larger than our estimate. This discrepancy may stem from the fact that Jahnke's estimate includes data from the high-flux, deep continental margin regions while these data are, for the most part, excluded from the TS-trap analysis presented here (Section 5.3). Lampitt and Antia (1997) normalized sediment trap data at 2 km and calculated total global flux of POC at 26.7 teramolC yr^{-1}, which is close to our result, that is, approximately 74% of our flux estimate in this paper. These co-authors were limited by a shortage of geographically distributed data, particularly from the Silica Ocean, including the Pacific Boreal Gyres and all the pelagic Southern Ocean.

An estimate of PIC flux based on mass balance of continental input and oceanic deposition by Milliman (1993) was roughly 60 teramolC yr^{-1}. Our global estimation of the annual biogenic Si flux at the mesopelagic/bathypelagic boundary is close to the estimate of the delivery rate of opal to the oceanic interior and the global ocean floor made by Tréguer et al. (1995) based on the primary production of Si and a dissolution rate for opal of 29.1 teramolSi yr^{-1}. This is 85% of our estimate.

11. Remineralization of POC and formation of the mesopelagic $\sum CO_2$ sink

11.1. Global remineralization of POC in the mesopelagic zone

The difference between two fluxes, the export production and the flux of POC at the mesopelagic/bathypelagic boundary (defined in Section 2),

$$\Delta F_m = [EP - F_{m/b}C_{org}](\text{in molC m}^{-2}\text{ yr}^{-1}),$$

is the total rate of the mineralized POC that becomes $\sum CO_2$ as POC settles through the mesopelagic zone in areas where a conventional biological pump operates, that is, in virtually the entire world pelagic ocean (Table 2 and Figs. 13 and 14). An estimate of global ΔF_m is then 441 teramolC yr^{-1}, assuming the global export production (G-EP) is 477 teramolC yr^{-1} (Fig. 14) to the pelagic ocean below 2 km (calculated from the model by Laws et al., 2000). This estimate is based on the assumption that the downward transport of POC by the zooplankton community terminates at approximately 1.5 km, and the biological pump is then driven by gravity in deeper waters. Estimated global transfer efficiency of POC at the mesopelagic/bathypelagic zone (Eq. (9), Section 9.3) is 7.6% (Table 5), and 1.2% of the ocean's primary production POC is delivered to the mesopelagic/bathypelagic boundary (Tables 2 and 5, Figs. 13 and 14, calculated from the model by Behrenfeld and Falkowski, 1997).

We examined characteristics of ΔF_m in the several basins and regions exhibiting contrasting biological pump characteristics, including carbonate vs. silica ocean conditions (Table 4). However, there is an inherent difficulty in applying ΔF_m (that is, $EP - F_{m/b}C_{org}$) to examining the scale of the mesopelagic biological pump: there is a significant difference, three orders of magnitude, in observational precision between ocean-color-based EP and the annual $F_{m/b}C_{org}$ based on the TS-trap method. In practice, PP and EP are presented in molC m^{-2} yr^{-1} (e.g., Behrenfeld and Falkowski, 1997; Laws et al., 2000), while mmolC m^{-2} yr^{-1} is a better unit for expressing TS-trap based $F_{m/b}C_{org}$, as we have done in this paper. At many stations, $F_{m/b}C_{org}$ may even be much smaller than statistical errors in the estimates of EP. At least all ΔF_m values remain positive at all normalized locations in Table 2 (excluding the High Arctic stations), though that could be merely incidental. Therefore, ΔF_m data should be regarded as semi-quantitative information, and we refrain from further statistical manipulations such as calculating a global average for ΔF_m. In the following sections, we offer some

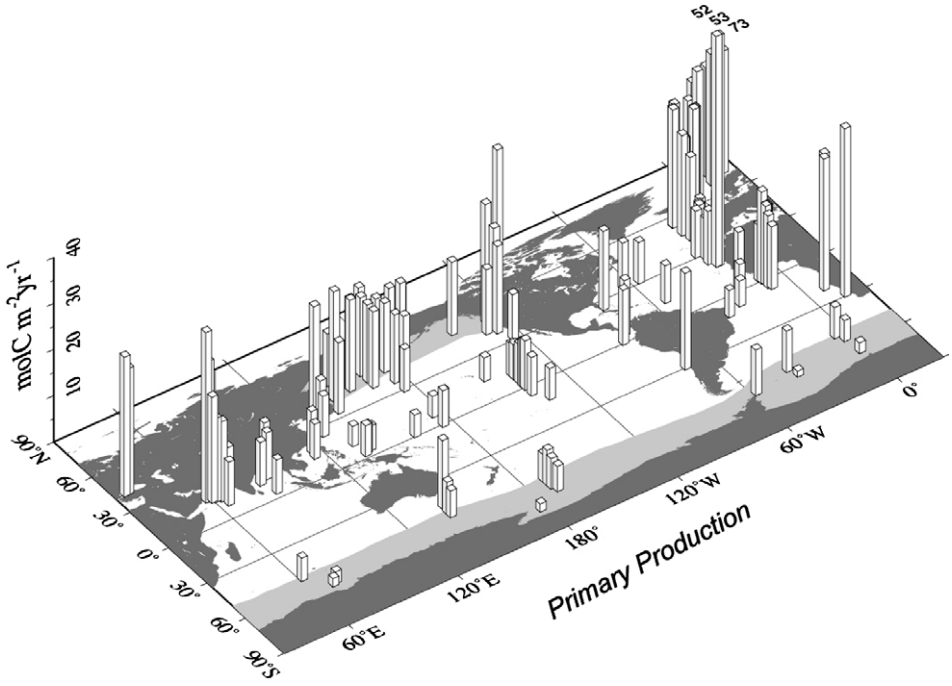

Fig. 13. Annual primary production (PP) in molC m^{-2} yr^{-1} averaged from the 250 km × 250-km grid boxes drawn around the TS-trap moorings where the annual mol-fluxes of three biogenic components and their ratios at the mesopelagic/bathypelagic boundary were calculated (Table 2, Fig. 1) from the ocean-color-based model of Behrenfeld and Falkowski (1997). Note extremely high PP in the Nordic Seas, up to 73 molC m^{-2} yr^{-1}, which may be unrealistic.

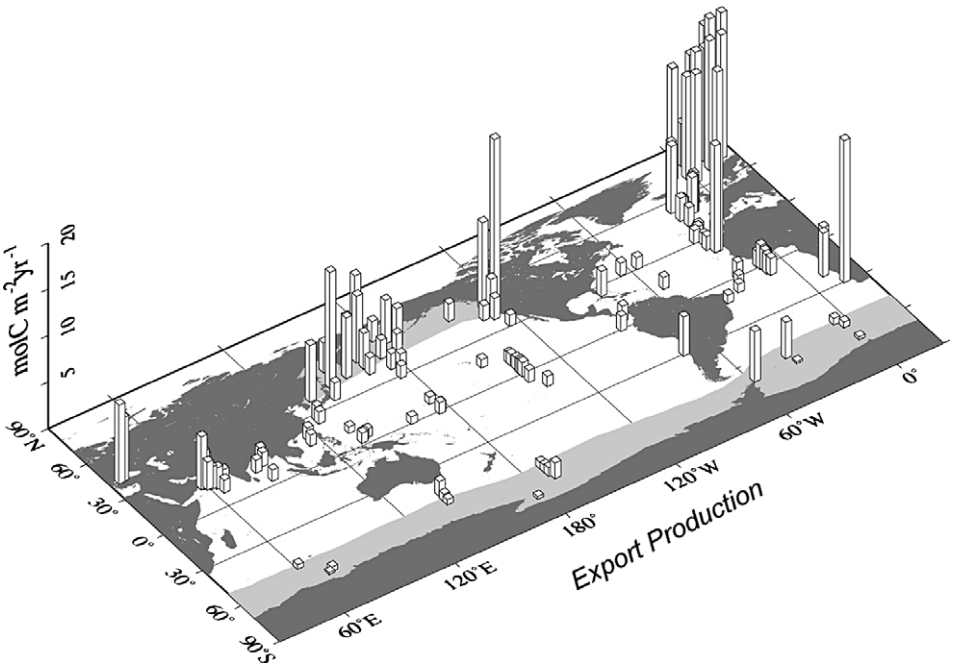

Fig. 14. Annual export production (EP) in molC m^{-2} yr^{-1} at stations where the annual mol-fluxes of three biogenic particles and their ratios at the mesopelagic/bathypelagic boundary were calculated (Table 2; Fig. 1) from Laws et al. (2000). The extremely large EP that covers the Nordic Seas reflects an apparently inflated PP estimate in the same area (Fig. 13).

Table 4
Biological pump indices in selected regions and areas with notable biogeochemical characteristics

Name of area/region	BGC province	# Sta.	PP (molC m^{-2} yr^{-1})	EP (molC m^{-2} yr^{-1})	EP/PP (%)	$F_{m/b}C_{org}$ (mmolC m^{-2} yr^{-1})	ΔFm (molC m^{-2} yr^{-1})	T_{eff} (%)	$F_{m/b}C_{inorg}$ (mmolC m^{-2} yr^{-1})	$F_{m/b}Si_{bio}$ (mmolSi m^{-2} yr^{-1})	Co/Ci	Si/Ci	Bio-pump
Nordic Seas	ARCT, SARC	9	21.9 (6.3)	12.6 (3.5)	58	61.4 (37.6)	12.5 (3.5)	0.48 (0.24)	54.9 (30.1)	32.8 (21.2)	1.3 (0.9)	0.7 (0.4)	Ca
North Atlantic Drift	NADR	13	22.8 (2.8)	3.6 (1.9)	16	171.1 (109.6)	3.4 (2.0)	5.73 (3.39)	136.3 (66.7)	60.1 (34.7)	1.3 (0.8)	0.4 (0.2)	Ca
North Atlantic Subtrop. Gy.	NAST	11	11.0 (2.4)	1.5 (0.4)	14	72.9 (23.9)	1.4 (0.4)	5.06 (1.75)	96.4 (40.2)	21.6 (12.1)	0.9 (0.4)	0.2 (0.1)	Ca
Cape Verde	SE-NAST	3	59.2 (11.8)	14.1 (3.1)	24	233.4 (9.1)	13.9 (4.6)	1.75 (0.43)	287.1 (0.0)	60.1 (34.7)	0.8 (0.0)	0.2 (0.1)	Ca
Guinea Basin	ETRA	2	12.4 (0.04)	1.7 (0.0)	14	117.7 (7.9)	1.6 (0.01)	6.78 (0.48)	130.6 (0.7)	47.6 (5.9)	0.9 (0.0)	0.4 (0.0)	Ca
Eastern Tropical Atlantic	S-ETRA	10	14.4 (4.5)	1.9 (0.5)	13	62.4 (18.8)	1.9 (0.5)	3.36 (1.00)	82.4 (30.0)	16.1 (6.3)	0.9 (0.3)	0.2 (0.0)	Ca
Arabian Sea (Divergent)	ARAB	3	26.6 (6.5)	3.4 (0.9)	13	552.7 (55.3)	2.8 (0.9)	17.5 (6.8)	423.7 (34.4)	264.5 (10.5)	1.3 (0.0)	0.7 (0.1)	Ca
Bay of Bengal	INDE, MONS	4	9.7 (1.8)	1.5 (0.2)	16	220.6 (55.3)	1.2 (0.2)	15.6 (5.4)	152.6 (28.7)	152.3 (41.7)	1.4 (0.2)	1.0 (0.3)	Si
North Pacific Si Ocean	BERS, PSAG	14	17.3 (3.7)	5.1 (3.1)	30	213.8 (69.5)	4.9 (3.1)	5.5 (3.1)	122.5 (28.3)	578.0 (269.6)	1.9 (0.9)	5.0 (2.4)	Si
North Pacific Ca Ocean	S-KURO, NPTG, WARM	7	5.7 (1.5)	0.9 (0.2)	16	39.2 (16.7)	0.9 (0.2)	4.1 (0.9)	62.9 (56.2)	18.9 (13.3)	0.6 (0.4)	0.4 (0.1)	Ca
Equatorial Pacific	PNEC, PEQD	5	10.3 (1.3)	1.5 (0.1)	14	143.0 (40.0)	1.3 (0.1)	9.5 (2.0)	226 (62.7)	165.3 (106.1)	0.6 (0.1)	0.7 (0.3)	Ca
Southern Ocean	ANTA, APLR	9	4.9 (2.0)	0.7 (0.4)	14	69.0 (30.7)	0.6 (0.4)	10.7 (3.1)	58 (48.3)	408.7 (251.1)	3.1 (4.0)	15.6 (16.3)	Si

Sta.: Number of stations in the area or region used to provide averages in the following columns (standard deviations are in parentheses). PP: Average annual primary production in the 250 × 250-km areas above time-series sediment trap (TS-trap) moorings calculated from the ocean-color-based model in molC m^{-2} yr^{-1} by Behrenfeld and Falkowski (1997). EP: Average annual export production in the 250 × 250-km areas above TS-trap moorings in molC m^{-2} yr^{-1} calculated from an ecosystem model by Laws et al. (2000). ΔF_m: the difference between EP and $F_{m/b}C_{org}$. T_{eff}: % C_{org}/EP (transfer efficiency). *Bio. Pump*: Types of biological pump: Ca = Carbonate Ocean, Si = Silica Ocean.

of our observations (Table 4) and preliminary interpretations of ΔF_m in the ocean areas with prominently operating biological pumps.

11.2. The North Pacific Silica Ocean and North Pacific Carbonate Ocean

Table 4 shows that the annual EP at 14 stations in the North Pacific Silica Ocean is five times larger than that at seven stations in the North Pacific Carbonate Ocean: 5.1 vs. 0.9 molC m^{-2} yr^{-1}. The EP/PP ratio in NPSO is about 30%, the largest among regions analyzed here. (The EP/PP at nine stations in the Nordic Seas is 58%, but ocean-color-based PP in this area may be overestimated [e.g., Francois et al., 2002].) The average $F_{m/b}C_{org}$ in the North Pacific Silica Ocean is 214 mmolC m^{-2} yr^{-1}. The average ΔF_m is thus estimated as 4.9 molC m^{-2} yr^{-1}, the largest rate in the world pelagic ocean, exceeded only by a more coastal setting near the Cape Verde region as further discussed below. The ΔF_m is 13.9 from three stations in Wefer and Fischer (1993b) (Table 4). In contrast, $F_{m/b}C_{org}$ in the North Pacific Carbonate Ocean is only 39 mmolC m^{-2} yr^{-1}. This suggests that a small EP of 0.9 molC m^{-2} yr^{-1} as mentioned above, equivalent to the Southern Ocean EP, is almost entirely remineralized before arriving at the mesopelagic/bathypelagic boundary zone. A compilation of several GOSECS meridional sections in the Pacific roughly along the Date Line (Bainbridge, 1979) shows high O_2 content in the surface of the North Pacific Silica Ocean (greater than 300 μmolO kg^{-1}) that drops to 50 μmolO kg^{-1} at approximately 400 m, and there is a substantial minimum O_2 layer at approximately 1800 m. Dissolved O_2 is depleted to less than 20 μmolO kg^{-1} in some parts of this O_2-minimum tongue. Attempts to link particle flux events directly with the interior ocean chemistry, such as dissolved O_2 concentration, are not always appropriate unless one deals with entire world values or an averaged characteristic over a large region because of deep-water advection.

11.3. Upwelling and divergent regions in the continental margins

The divergent Arabian Sea is also one of the most active biological pump areas with a high PP of 27 molC m^{-2} yr^{-1} (Table 4). The model-based annual EP of the divergent Arabian Sea is 3.4 molC m^{-2} yr^{-1}, surprisingly small compared to the Cape Verde area (14 molC m^{-2} yr^{-1}) and comparable to or smaller than the North Atlantic Silica Ocean (5 molC m^{-2} yr^{-1}). The Arabian Sea Process Study's EP estimates using the ^{234}Th method at 100 m (Buesseler et al., 1998) at the nearby stations combined with the annual EP estimate adopting annual variability of PP by Dickey et al. (1998) and Kinkade et al. (1999) are also $<$3.5 molC m^{-2} yr^{-1}. A significant characteristic of the divergent Arabian Sea biological pump is that 17.5% of EP reaches the mesopelagic/bathypelagic boundary. This means 434 mmolC m^{-2} yr^{-1} of organic carbon penetrates the oxygen-depleted mesopelagic layer and pumps substantial POC fluxes to the Central Arabian Sea bathypelagic zone. This provides a partial explanation for very high (and consistent) $\sum CO_2$ concentrations (2315–2350 μmolC kg^{-1}) throughout the bathypelagic water column of the Arabian Sea (Millero et al., 1998a), although the link between POC flux and water column chemistry must be further explored. The upwelling zone in the western equatorial Pacific is critical to understanding the global CO_2 system because it may contribute a significant portion of the ocean's new production (Chavez and Barber, 1987). The US JGOFS EqPac program provided an annual time series of biological pump operation along 140°W with a meridional transect of deep mooring stations (Honjo et al., 1995). However, there is no data available from east of the EqPac transect, and we are unable to offer a discussion on the role of ΔF_m in this significant region.

A vigorous upwelling region between the Mauritania–Senegal coast and the Cape Verde Islands is one of the most productive ocean areas known (e.g., Wefer and Fischer, 1993b). For the 250 × 250-km grid square drawn for this study around the sediment trap moorings in the area, PP calculated from ocean-color-based productivity estimates by Behrenfeld and Falkowski (1997) averages nearly 60 molC m^{-2} yr^{-1} (Table 4). This estimate is twice as large as that for the divergent Arabian Sea and four times larger than that for the North Pacific Silica Ocean (Table 4). The EP in the Cape Verde area is 14 molC m^{-2} yr^{-1}, several times larger than in average ocean regions. The ΔF_m (13.9 molC m^{-2} yr^{-1}) is statistically indistinguishable from the EP (14.1 molC m^{-2} yr^{-1}), and the C_{org}/EP is as small as 1.7%, which can be interpreted as nearly complete remineralization of POC within the mesopelagic zone of the Cape Verde area. The GEOSECS Leg 9 profile shows 50 μmolO kg^{-1} contours from 400 m to 1000 m,while the bathypelagic zone off the Cape Verde area is well

oxygenated, up to 250 μmolO kg^{-1}. However, because the distribution of dissolved CO_2 in the water column is controlled by complex kinetics and thermodynamics, direct comparison should be done with caution. Highly elevated $F_{2\,km}C_{org}$, up to 429 mmolC m^{-2} yr^{-1}, is also found at North Benguela-Walvis Bay TS-trap stations around 20°S, 9°W (Wefer and Fischer, 1993b; Fischer et al., 2000). The R/V *Meteor* Expedition Report for March–April 1927, as recompiled by Wattenberg (1992), illustrates a similar extensive O_2-minimum layer for the Cape Verde Basin and Walvis Bay area. $F_{m/b}C_{org}$ are large over the western margin of Africa where the western boundary current prevails. This may be the result of high PP and EP due to upwelling, and it may also be strongly influenced by the influx of lithogenic particles (e.g., Fischer et al., 2000) from the dry land and deserts immediately to the east.

11.4. The Southern Ocean

Average PP from nine Southern Ocean TS-trap stations is as small as 4.9 molC m^{-2} yr^{-1} with std of 2.0 molC m^{-2} yr^{-1}, nearly equivalent to the North Pacific Carbonate ("desert") Ocean (Section 11.1), where it is 5.7 with std of 1.5 molC m^{-2} yr^{-1}. The ΔF_m in the Southern Ocean is extremely small, 0.6 molC m^{-2} yr^{-1} at nine pelagic stations. The C_{org}/EP at the Southern Ocean stations is about 11%. The POC pumping mechanism is unique in the Southern Silica Ocean where there are no coccolithophorids (Section 2.2). Available zooplankton $CaCO_3$ ballast particles are very small (58 mmolC m^{-2} yr^{-1}), and the majority of PIC is contained in pteropod shells (large shells that are ineffective as ballast; Honjo, 2004). A hypothetical explanation for the unique AZ biological pump is that settling of POC is strongly enhanced by a massive flux of diatom frustules (408 mmolSi m^{-2} yr^{-1}) that, perhaps, form "falling mats" (sensu Lampitt, 1985), which engulf suspended particles and aggregates as they descend, particularly during the Antarctic bloom (Section 2.2). This hypothesis is based on observations of particles collected by TS-traps and contained in sediment samples (Honjo, 2004). A POC settling rate enhanced by falling mats of diatoms could result in a small ΔF_m and no significant O_2-minimum or $\sum CO_2$-maximum layer, as observed in the AZ transect along the New Zealand sector.

Table 5
Critical properties that drive the global biological pump

Global primary production (G-PP)	2931	TeramolC yr^{-1}	1
Global biogenic carbonate production	67–117	TeramolC yr^{-1}	2
Global biogenic silica production	100–140	TeramolSi yr^{-1}	3
Global export production (G-EP)	477	TeramolC yr^{-1}	4
G-EP/G-PP × 100	16.3	%	
Global $F_{m/b}C_{org}$	36.2 ± 4.5	teramolC yr^{-1}	7
Global $F_{m/b}C_{inorg}$	33.8 ± 3.8	TeramolC yr^{-1}	7
Global $F_{mb}Si_{bio}$	34.4 ± 2.6	teramolSi yr^{-1}	7
$F_{2\,km}C_{org}$/G-PP × 100	1.2	%	5
$F_{2\,km}C_{org}$/G-EP × 100	7.6	%	5
ΔF_m; [G-EP–G-$F_{2\,km}C_{org}$]	441	TeramolC yr^{-1}	6
G-C_{org}/C_{inorg}	1.07	Mole ratio	7
G-C_{org}/Si_{bio}	1.05	Mole ratio	7
G-Si_{bio}/C_{inorg}	1.02	Mole ratio	7
Global Ternary Ratio: T%(Co:Ci:Si)	35:32:33	Ternary%	8
G-mean $F_{2\,km}C_{org}$ from model	120	mmolC m^{-2} yr^{-1}	9
G-mean $F_{m/b}C_{inorg}$ from model	112	mmolC m^{-2} yr^{-1}	9
G-mean $F_{m/b}Si_{bio}$ from model	114	mmolSi m^{-2} yr^{-1}	9

Annotation for numbers in right-hand column: (1): Global annual primary production over the ocean area deeper than 2 km (301.3 M km^2) calculated from the model by Behrenfeld and Falkowski (1997). (2): From Lee (2001) and Iglesias-Rodriguez et al. (2002). (3): From Tréguer et al. (1995) and Nelson et al. (1995). (4): Calculated global export production (EP) from the model by Laws et al. (2000) over the same area as (1), (5), (6), and (7). Total of each biological pump element's annual fluxes at the mesopelagic/bathypelagic boundary and binary ratios from 250 × 250-km grids. (8): Nonweighted global average of ternary ratios among the three elements in the individual TS-traps at the mesopelagic/bathypelagic boundary as presented in Table 3. (9): Global mean annual fluxes of the three biological pump elements at the mesopelagic/bathypelagic boundary in one square meter over the ocean area deeper than 2 km (301.3 M km^2).

12. Remineralization of particulate inorganic carbon (PIC): impact of the biological pump on ocean alkalinity

12.1. Ocean surface alkalinity and the biological pump

The fluxes of POC, PIC, and opal-Si at the mesopelagic/bathypelagic boundary appear to be related to global surface ocean alkalinity. The pattern of total alkalinity normalized to salinity (NTA), as in Millero et al. (1998b), particularly Fig. 13, p. 127, reflects the Si_{bio}/C_{inorg} distribution in Fig. 7. The TS-trap stations exhibiting high $F_{m/b}Si_{bio}$ (Fig. 4) are located in high alkalinity regions. The boundary between the North Pacific Silica Ocean and the North Pacific Carbonate Ocean (Section 8.1) overlaps the North Pacific Polar Front, with closely spaced NTA contours that demarcate the areas with higher surface alkalinity to the north. It appears that the NTA of 2330–2340 μmol kg^{-1} marks the boundary between the North Pacific Silica and Carbonate Oceans. The Antarctic Zone Silica Ocean is also demarcated by a 2340 μmol kg^{-1} contour with the Southern Carbonate Ocean to the north, and this contour approximates the Antarctic Polar Front. This boundary is less sharp compared with its northern Pacific counterpart, perhaps because of the frequent meandering of the Antarctic Polar Front. The Indian Ocean is a Carbonate Ocean with low NTA (2290 μmol kg^{-1}), similar to the bulk of the Atlantic. The NTA in the Labrador Sea is as high as in NPSO (>2340 μmol kg^{-1}), and this small parcel of ocean could be the only Silica Ocean in the Atlantic (except for the Southern Ocean). However, no TS-trap data is available for this area.

12.2. Supply of alkalinity to the mesopelagic layer and supralysoclinal dissolution

12.2.1. Estimate of total mesopelagic dissolved PIC by mass balance

As we estimate in Section 10, the global ocean flux of biogenic $CaCO_3$–C (PIC) at the mesopelagic/bathypelagic boundary ($F_{m/b}C_{inorg}$) is 33.8 ± 3.8 teramolC yr^{-1} (generally rounded to 34 teramolC yr^{-1} in this section) (Section 10) while the global oceanic production of biogenic $CaCO_3$ is estimated as 67 to 117 teramolC yr^{-1} (0.8–1.4 petagC yr^{-1}) (Lee, 2001; Iglesias-Rodriguez et al., 2002; Takahashi, 2004). Thus, 49–71% of the PIC produced, 36–86 teramolC yr^{-1}, must dissolve in the upper 2 km. This estimate is comparable to the mass balance calculation by Milliman et al. (1999) and the estimate of carbonate dissolution rates from alkalinity measurements by Feely et al. (2004). Total mesopelagic dissolution of opal, between 66 and 106 teramolSi yr^{-1}, is similarly estimated by the difference between the global export production of opal Si, 100–140 teramolSi yr^{-1} (Nelson et al., 1995; Tréguer et al., 1995), and our estimate of the global flux of opal Si at the mesopelagic/bathypelagic boundary, 34.4 teramolSi yr^{-1} (Table 5).

12.2.2. Supralysoclinal dissolution of metastable carbonates

It is generally believed that dissolved carbonate in the water column originates from metastable skeletal $CaCO_3$ (e.g., Berner and Honjo, 1981), including pteropod shells (e.g., Berner and Berner, 1976; Berner, 1977) and a large variety of algal biominerals that include aragonite and Mg-calcite from shallow benthic ecosystems, particularly mid-ocean coral reefs (e.g., Milliman, 1974) as well as falling epibionts of pelagic epiphytes (Pestana, 1985). The depth of the chemical horizon where the waters are supersaturated with calcite lies deeper than 2 km,except in the North Pacific (Bering Sea to approximately 10°S; Takahashi, 1975). In many ocean areas, the waters at 2 km are undersaturated with respect to aragonite. However, the dissolution of mineral particles in the undersaturated water requires exposed surface areas and time to react with seawater.

The recent attention to the upper mesopelagic zone of the world ocean where alkalinity is significantly elevated (Feely et al., 2004; Sabine et al., 2004) requires assuming the dissolution of carbonate particles in the water column (Fiadeiro, 1980), particularly in the upper mesopelagic zone, that is, supralysoclinal dissolution of carbonate (e.g., Milliman et al., 1999). The apparent massive export of pelagic pteropod shells to the mesopelagic water column offers investigators an attractive source for the alkalinity budget of the North Pacific (e.g., Fiadeiro, 1980; Betzer et al., 1984; Byrne et al., 1984). Adult pteropod shells are relatively large (typically on the order of a mm), and empty shells settle at high speed (Vinogradov, 1961; Byrne et al., 1984), on the order of km dy^{-1}, so they remain only for a matter of hours in the upper mesopelagic water column. Byrne et al. (1984) indicate that only about 20% of Trade Wind Domain species' shells dissolve during descent to

2 km,though the dominant pteropod shells in the Westerlies Domain lose approximately 50% of their mass during their descent to 2 km.

A first-order approach to this complicated question, though not conclusive, might compare the production rate in the world ocean and the flux of aragonite-PIC in the mesopelagic zone. Estimation of pelagic pteropod production is extremely challenging, and a literature search for this subject yields only a pioneering work at Ocean Station P (50°N, 145°E, Station # 73, Table 2; PSAG-E) by Farby (1989). The result shows a pteropod-shell, aragonite-PIC production rate during July 1985 of 66–133 mmolC m^{-2} yr^{-1}. The 10-year average total PIC flux at 2000 m at this time-series station (including 1985) is 131 mmolC m^{-2} yr^{-1}, suggesting a significant loss of aragonite PIC in the mesopelagic zone. Annual aragonite PIC flux in the lower mesopelagic zone in the literature shows a wide range: 0.4–1.7 (Nordic Seas; Meinecke and Wefer, 1990), 13.0 (Lofoten Basin; Meinecke and Wefer, 1990), 6.1 (ES/JS; Hong and Chen, 2002), and >10 mmolC m^{-2} yr^{-1} (Arabian Sea; Mohan et al., 2006). However, depth-series pteropod fluxes at 500-, 1500-, and 3200-m traps in the Sargasso Sea are consistent regardless of depth, and they are extremely large compared to the other stations mentioned above (Farby and Deuser, 1991).

Shells of pteropods (also heteropods), common marine snails, are not only chemically metastable but also constructed delicately (Milliman, 1974; Lalli and Gilmer, 1989). The shells of living pteropods are thin and transparent, exhibit a poorly developed protective periostracum, and appear to have only a nacreous (aragonite) layer that consists of needle-like microcrystals. Therefore, these shells, particularly the veligers and juvenile shells, may be highly susceptible to disintegration and dissolution (Fiadeiro, 1980). Indeed, in examining TS-trap samples under SEM, we observe sequences of pteropod-shell dissolution and disintegration that range from white or "frosted" shells (Vinogradov, 1961) to nacreous layers that disassemble into aragonite needles (SEM photomicrographs in Honjo, 1978, 1980; Honjo et al., 1988; Honjo and Erez, 1978; Plate II in Meinecke and Wefer, 1990). Honjo and Erez (1978) observed that when weight loss is about 25%, the specific surface area increased very rapidly, suggesting that increase in surface area itself becomes an important factor in determining the dissolution rates as dissolution proceeds. This self-perpetuating process, superimposed on other surface chemistry factors that control the kinetics of dissolution may cause extremely sharp pteropod-aragonite lysocline.

Mg-calcite, produced in large quantities along with aragonite in coral reef environments (e.g., Milliman, 1993), is another biogenic carbonate mineral exhibiting a high rate of solubility. Even a small leak of reef material, such as descent of reef boulders into the pelagic environment, could have a considerable impact on the carbonate budget particularly in the Pacific (Berner and Berner, 1976; Berner, 1977; Pilskaln et al., 1989). Coral reef destruction correlates strongly with today's elevated seawater temperatures and seawater alkalinity. One potentially important pelagic source of Mg-calcite in the Atlantic Ocean may be epibionts, benthic and shallow water communities that live among floating *Sargassum* and other epiphyte colonies in the North Atlantic subtropical gyre (e.g., Pestana, 1985; Farby and Deuser, 1991). Pestana (1985) estimates that 0.4–1.0 million tons of $CaCO_3$ (9–12 mol% $MgCO_3$) are associated with *Sargassum* in the Sargasso Sea. Fragments of *Sargassum* and other epiphytes, often on the order of 10 mm long, along with traces of epibionts were collected in traps deployed at 372–389 m depth in the central Sargasso Sea (31.5°N, 55.9°W) (Honjo, 1980).

12.2.3. Stable biogenic carbonate: calcite

In contrast to aragonite and Mg-calcite (metastable carbonate) mineral dissolution, we are not convinced by arguments in favor of extensive calcite dissolution in the upper water column (Honjo, 1977). If a significant portion of calcite PIC, particularly of coccoliths, one of the most ubiquitous and arguably the most ideal type of ballast particle for POC transport (Section 2.2), were dissolved in the upper mesopelagic zone, the biological pump in the world pelagic ocean would become dysfunctional through loss of the major gravitational transport mechanism for POC. A number of publications on deep ocean sediment have observed that coccoliths are more dissolution resistant than foraminifera (e.g., McIntyre and McIntyre, 1971; Honjo, 1977). *In situ* dissolution experiments with six common species of coccoliths and foraminiferal assemblages at depths of 3.6 km, 4.8 km, and 5.5 km in the central North Atlantic using the *in situ* dissolution chamber (ISWAC; *In situ* Water Circulator; Honjo and Erez, 1978) showed no detectable dissolution after 79 days of non-stagnant exposure in the chamber at the two shallower depths. Both coccoliths and foraminiferal tests showed approx-

imately 35% dissolution at 5.5 km. Pteropod shell loss was 2.4%, 45%, and 73% at these depths (Honjo and Erez, 1978). Berelson (2002) estimates that the settling velocity of particles increases by 15–60% between 2000 and 3500 m and explains this by loss of POC, although calcite particles remain more intact and available as ballast.

For example, scanning electron micrographs of deep trap-collected fecal pellets show that they are often packed with coccoliths, whose delicate architecture is preserved (Section 2.2). In particular, a monograph by Steinmetz (1991) showed that the microstructure of coccolithophorid species such as *Syracosphaera pulchra* and *Rhabdosphaera clavigera* was intact in 4280-m and 2770-m trap samples from the Equatorial Pacific station (NPTG) (Station #103, Table 2) where the water column is significantly undersaturated with calcite. The same monograph shows that *Florisphaera profunda*, one of the smallest and most poorly calcified coccoliths produced at the bottom of the euphotic zone, was perfectly preserved in a sample from the 5068-m trap in the Equatorial Atlantic (NATR) station (Station #37, Table 2). Suspended coccoliths in the bathypelagic zone often exhibit strong dissolution (Honjo, 1975). Broerse (2000) found coccoliths and coccospheres generally intact in many mesopelagic JGOFS samples but not in very deep traps. The same author found clear evidence of *E. huxleyi* dissolution in a trap deployed at 258 m. Further, >90% of robustly constructed coccoliths of *C. pelagicus* exhibited etching at 1061 m. These findings deserve further investigation.

Elevated acidity in the gut of metazoan grazers has been proposed as a possible mechanism for epipelagic dissolution of calcite. However, transmission micrographs of calanoid crustacean fecal pellets in deep-sea sediment showed intact coccospheres and coccoliths (Gowing and Wishner, 1986). Laboratory feeding experiments with a few common Atlantic calanus species failed to show dissolution of coccolith architecture or lab-synthesized aragonite microcrystals (Honjo and Roman, 1978). Many pellets produced by mesozooplankton are covered by a pellicle (peritrophic membrane) (e.g., Gauld, 1957). Thus, pellet interiors may maintain chemical and microbial environments different from those of the gut and of seawater. However, EM observations and laboratory experiments are critical, but not sufficient, to prove the hypothesis that biogenic calcite particles do not dissolve in mesopelagic waters. Further investigation of *in situ* water-column dissolution of calcite particles based on, for example, better controlled dissolution and calcification experiments and mass balance modeling efforts are needed to obtain answers to this long-standing question.

13. Summary of global TS-trap observations

The North Pacific Silica Ocean develops in the Pacific Boreal Gyres on the pole side of the North Pacific Polar Front. This area yields an average $F_{m/b}C_{org}$ of 214 mmolC m^{-2} yr^{-1} that is twice as large as the global average $F_{m/b}C_{org}$ of 120 mmolC m^{-2} yr^{-1}. A smaller Atlantic counterpart is found in the North Atlantic Drift. The most $F_{m/b}C_{org}$-depleted basin among the world's oceans contains the Pacific Subtropical and Tropical Gyres, particularly the Pacific Warm Pool (mean 39 mmolC m^{-2} yr^{-1}), while its large Atlantic counterpart yields a larger POC flux (averaging 62 mmolC m^{-2} yr^{-1}). The $F_{m/b}C_{org}$ in the Southern Ocean is about equal to the global average north of the Antarctic Front, but is reduced by about half in the pelagic Antarctic Zone (AZ; Fig. 2). Biological pump studies in the High Arctic Seas are yet to be undertaken; FC_{org} measured successfully at only two deep sea traps was even smaller than that in the AZ, <10% of the global average. The largest annual $F_{m/b}C_{org}$ so far measured is that in the Arabian Sea. The average $F_{m/b}C_{org}$ in this monsoon-controlled divergent ocean is 553 mmolC m^{-2} yr^{-1}, nearly five times larger than the global average. $F_{m/b}C_{org}$ is also elevated in western boundary current and vigorous upwelling zones. As an example, $F_{m/b}C_{org}$ is as large as 233 mmolC m^{-2} yr^{-1} in the Cape Verde area. There are three orders of magnitude difference between the maximum and the minimum average $F_{m/b}C_{org}$ among regions.

The $F_{m/b}C_{inorg}$ distribution generally imitates the $F_{m/b}C_{org}$, but with less geographic diversity (Fig. 3). The maximum $F_{m/b}C_{inorg}$ occurs in the divergent Arabian Sea (averaging 424 mmolC m^{-2} yr^{-1}) followed by the Cape Verde upwelling area (averaging 287 mmolC m^{-2} yr^{-1}), repeating the pattern of the $F_{m/b}C_{org}$. The North Pacific Subarctic Gyre and the North Atlantic Drift yielded larger average $F_{m/b}C_{inorg}$ (123 and 136 mmolC m^{-2} yr^{-1}, respectively) than the global average of 112 mmolC m^{-2} yr^{-1}. The most $F_{m/b}C_{inorg}$-depleted region spans the North Pacific Subtropical and Tropical Gyres, particularly the Warm Pool province (WARM), which yields only 27 mmolC m^{-2} yr^{-1}, less than one-third of the global average $F_{m/b}C_{inorg}$. The

average pan-Atlantic $F_{m/b}C_{inorg}$ from pelagic stations, excluding the NADR and the Atlantic Southern Ocean, appear to be about half (62 mmolC m^{-2} yr^{-1}) of the global average.

Several provinces to the north of the North Pacific Polar Front are characterized by $F_{m/b}Si_{bio}$ as large as 578 mmolSi m^{-2} yr^{-1} on average, which is more than five times the global average of 114 mmolSi m^{-2} yr^{-1}. The $F_{m/b}C_{org}$ and $F_{m/b}C_{inorg}$ are also large in this region—about 200% and 20% larger than the global average, respectively. The divergent Arabian Sea is a truly significant high-export area in regard to all three biological pump components; not only are the annual $F_{m/b}C_{org}$ and $F_{m/b}C_{inorg}$ high, as mentioned above, but the average $F_{m/b}Si_{bio}$ is as large as 266 mmolSi m^{-2} yr^{-1}, 2.3 times the global average. From the Antarctic Polar Front to the Antarctic Circumpolar Current, the $F_{m/b}Si_{bio}$ increases abruptly to 915 mmolSi m^{-2} yr^{-1}, eight times the global average, while the $F_{m/b}C_{inorg}$ diminishes to a trace amount, indicating that the biological pump in this area is driven almost exclusively by opal as ballast. In the Atlantic, the $F_{m/b}Si_{bio}$ is about half of the global average as is the $F_{m/b}C_{org}$ in areas such as the NARD and the Cape Verde basin. Average flux of $F_{m/b}Si_{bio}$ is merely 19 mmolSi m^{-2} yr^{-1}, 17% of the global average, in the North Pacific Subtropical and Tropical Gyres that abut the North Pacific Front to their south. It is remarkable that the $F_{m/b}Si_{bio}$ is strongly depleted in the Atlantic compared to other major basins, and it is also remarkable that the pan-Atlantic mean is merely 29 mmolSi m^{-2} yr^{-1}, except in the NARD and the few productive areas mentioned above (Table 4; the fluxes from the Atlantic Antarctic Zone are not included in the averages). A dramatic longitudinal transition of the fluxes of the three elements is observed along the equator in the Pacific Ocean. The $F_{m/b}C_{org}$ and the ballast particle fluxes at WARM are very small throughout the equatorial TTS. Moving east along 140°E, the annual $F_{m/b}C_{org}$ increases by 50–100%, and the $F_{m/b}C_{inorg}$ and $F_{m/b}Si_{bio}$ are two to three times greater than the global average. Because of the scarcity of mooring stations to the east of 140°W, we have little knowledge of biological pump activity in most of the huge east equatorial Pacific divergent zone that encompasses most of PENC and PEQD, except for our parameterization (Figs. 9–11).

The global variability of annual $F_{m/b}C_{inorg}$ generally follows the $F_{m/b}C_{org}$. Therefore, the variability of the C_{org}/C_{inorg} is modest, with little deviation from the global average ratio of 1.07 (Table 5) except in the Antarctic Zone (Fig. 4). On the other hand, annual Si_{bio}/C_{inorg} varies hugely from the global average of 1.02, following the large variability of $F_{m/b}Si_{bio}$ in the world ocean (Fig. 4). Particularly in the Southern Ocean, the average annual C_{org}/C_{inorg} and Si_{bio}/C_{inorg} are as large as 3 and 16, respectively. Mean annual C_{org}/C_{inorg} and Si_{bio}/C_{inorg} in the North Pacific Silica Ocean are notably large, 1.9 and 5.0, respectively. In this area, not only is the annual $F_{m/b}Si_{bio}$ extremely large, but the $F_{m/b}C_{inorg}$ is also larger than the global average, resulting in an elevated ΔF_m rate over an extensive region of the North Pacific. The pan-Atlantic average of annual C_{org}/C_{inorg} and Si_{bio}/C_{inorg} are <1 and 0.4, respectively. These ratios in the Pacific Subtropical and Tropical Gyres are 0.9 and 0.4, indicating that the biological pump functions similarly in both regions.

14. Conclusions

We investigated the flux of biogenic particles (POC, PIC, biogenic silica) from 134 locations where international investigators have collected settling materials with bottom-tethered, time-series sediment traps (TS-traps) since 1983 (Fig. 1). As one of the essential conclusions of this study, we find that the vertical biological pump operates ubiquitously in the pelagic world ocean (except, perhaps, in relatively small, sea-ice-covered areas of the High Arctic Seas) (Fig. 2).

The annual mole fluxes reported here as $F_{m/b}C_{org}$, $F_{m/b}C_{inorg}$, and $F_{m/b}Si_{bio}$ in mmolC or Si m^{-2} yr^{-1} are normalized to an ocean depth of 2 km, the approximate boundary between the mesopelagic and bathypelagic domains, where POC is in "terminal gravitational transport mode" with minimal influence from the zooplankton ecosystem. These three fluxes are essential components of the biological pump system as $CaCO_3$ and biogenic silica provide ballast for removing light and metastable POC from the epipelagic zone to the CO_2 sink in the interior ocean. Vertical transport of POC by the oceanic ecosystem, particularly by diel migrating zooplankton, is crucial in the mesopelagic zone.

We determined that the fluxes of each biogenic constituent vary among oceanic regions by two to three orders of magnitude (Table 3). $F_{m/b}C_{org}$ at sea-ice-free locations, ranging from a minimum of 25 mmolC m^{-2} yr^{-1} in the Pacific Warm Pool to a maximum of 605 mmolC m^{-2} yr^{-1} in the divergent zone of the Arabian Sea. Likewise, $F_{m/b}C_{inorg}$ ranges from 15 mmolC m^{-2} yr^{-1} in the Pacific Warm Pool to 459 mmolC m^{-2} yr^{-1} in the Ara-

bian Sea. $F_{m/b}Si_{bio}$ varies the most geographically, from 6 mmolSi m^{-2} yr^{-1} under the North Atlantic Drift and 7 mmolSi m^{-2} yr^{-1} in the Pacific Warm Pool to 1118 mmolSi m^{-2} yr^{-1} at a North Pacific Subarctic Gyre station and 915 mmolSi m^{-2} yr^{-1} under the Antarctic Circumpolar Current (Table 3).

The polar sides of the North Pacific Polar Front and the Bering Sea are characterized by a very large $F_{m/b}Si_{bio}$ (averaging 578 mmolSi m^{-2} yr^{-1}) (Fig. 4) and a relatively modest $F_{m/b}C_{inorg}$ (averaging 123 mmolC m^{-2} yr^{-1}) (Fig. 3) that are still larger than the global mean flux (Table 5) and that transport a large $F_{m/b}C_{org}$ (averaging 214 mmolC m^{-2} yr^{-1}, twice the global mean) to the mesopelagic/bathypelagic boundary. In this region, the average ratio of $F_{m/b}Si_{bio}$ to $F_{m/b}C_{inorg}$ (Si_{bio}/C_{inorg}) and $F_{m/b}C_{org}$ to $F_{m/b}C_{inorg}$ (C_{org}/C_{inorg}) are 5.0 and 1.9, respectively. Si_{bio}/C_{inorg} is particularly large in the Antarctic Zone, while $F_{m/b}C_{inorg}$ is small and $F_{m/b}Si_{bio}$ is very large. The average Si_{bio}/C_{inorg} in AZ is as high as 26 (Table 2, Fig. 7).

The Silica Ocean is thus defined as the area where the Si_{bio}/C_{inorg} and the C_{org}/C_{inorg} ratios are >1 (approximately 20% of the world pelagic ocean; see shaded area in Figs. 2–7). The rest is the Carbonate Ocean where Si/Ci and Co/Ci are <1. These Silica and Carbonate oceans are clearly separated from each other by two major oceanographic fronts, the North Pacific Polar Front and the Antarctic Polar Front. The Carbonate Ocean covers all the Atlantic (except the Weddell Sea) and the Pacific Trade Wind Domain. POC is more efficiently pumped to the interior of the Silica Ocean than to the interior of the Carbonate Ocean.

A unique combination of ballast particles in the North Pacific Silica Ocean results in a $F_{m/b}C_{org}$ that is twice as large as the global mean, with a very large $F_{m/b}Si_{bio}$ that is five times the global average and a $F_{m/b}C_{inorg}$ about 10% larger than the global average. This finding suggests that regions with such "hybrid ballast" may drive a unique biological pump to remove POC to the interior ocean with a relatively small loss of alkalinity at the surface. In contrast to the North Pacific Silica Ocean where the $F_{m/b}Si_{bio}$ is extremely large, the $F_{m/b}C_{inorg}$ is very small in the Antarctic Zone Silica Ocean where $F_{m/b}C_{org}$ is modest (averaging 69 mmolC m^{-2} yr^{-1}, about 60% of the global average). This $F_{m/b}C_{org}$ is marginally larger than that of the pan-Atlantic and twice as large as that of the Pacific Carbonate Ocean (Table 4). Highly elevated $F_{m/b}C_{org}$ and $F_{m/b}Si_{bio}$ are found at several stations in areas with intense divergence or western boundary currents in the Carbonate Ocean. Examples include the Arabian Sea, the Cape Verde Basin, and the Pacific Equatorial Divergence (Table 4).

In order to geographically interpolate the measured TS-trap annual fluxes of the three elements at the mesopelagic/bathypelagic boundary and calculate global mean fluxes, four regional algorithms were developed by parameterization to correlate measured flux to grid (250 × 250 km) surface-water properties (T, S, and nutrient concentrations) (Figs. 9–11). We estimated total global annual export fluxes of POC, PIC, and biogenic Si at the mesopelagic/bathypelagic boundary by summing the fluxes in each grid. They are unexpectedly close at 36.2 and 33.8 teramolC yr^{-1} and 34.4 teramolSi yr^{-1} (0.43 and 0.41 GtC yr^{-1} and 0.97 GtSi yr^{-1}), respectively, and the average fluxes from these statistics (ocean area deeper than 2 km = 301.3 Mkm^2) are 120 and 112 mmolC m^{-2} yr^{-1}, and 114 mmolSi m^{-2} yr^{-1} (Table 5). Thus, the global mole ratios among the three elements at the mesopelagic/bathypelagic boundary are virtually equal to one (Table 5).

The world average ternary % among the $F_{m/b}C_{org}$, $F_{m/b}C_{inorg}$, and $F_{m/b}Si_{bio}$ calculated from 152 individual T-S trap data sets (Table 3) is 35:32:33 (Fig. 8E) and supports the estimation from the parameterization model. This indicates that the global biological pump works at one mole part of PIC and one part of biogenic Si in order to remove one part of POC to the mesopelagic/bathypelagic boundary zone where the terminal gravitational transport mode of POC prevails (Section 2.5).

An ocean-color-based estimate of global primary production (PP) in the pelagic ocean deeper than 2 km is approximately 2930 teramolC yr^1 (about 35.17 petagC yr^1, calculated from Behrenfeld and Falkowski, 1997). The global export production (EP) covering the same area as PP, using Laws et al., 2000, is 477 teramolC yr^1 (5.36 petagC yr^1) (Table 5). Thus, 2454 teramolC (29.45 petagC yr^1) of POC is remineralized annually in the world epipelagic layer, and the resulting $\sum CO_2$ is recycled to the epipelagic CO_2 pool. The POC, equivalent to the EP, that penetrates the pycnocline by both gravity and diel migratory zooplankton supports part of the metabolic demands of the mesopelagic community. In the upper mesopelagic zone, directly below the epipelagic, removal of POC is driven by a highly complex ecosystem of diel migrators interlaced with gravitational transport of ballasted aggregates and repacked fecal pellets.

This vigorous zooplankton activity is most likely a major cause of unpredictable and inconsistent POC flux and low $^{230}Th/^{231}Pa$ trapping efficiency in this zone, and we must separate these ecosystem effects from turbulence. The remineralization rate for settling POC slows down in the lower mesopelagic zone with diminishing zooplankton and lower temperature. Below the zooplankton habitat, in the mesopelagic/bathypelagic boundary zone (1.5–2 km), vertical transport of POC is more exclusively driven by ballasted aggregates, and microbial metabolism is responsible for further remineralization of POC in submesopelagic zones.

Where a conventional biological pump operates in the global ocean, the difference between two fluxes, the EP and the flux of POC at the mesopelagic/bathypelagic boundary, expressed as ΔF_m, is the total annual rate of POC mineralized to $\sum CO_2$ as POC settles through the mesopelagic zone. An estimate of global ΔF_m is then 441 teramolC yr^{-1}, assuming the global annual export production is 477 teramolC yr^{-1} to the pelagic ocean below 2 km.Thus, calculated regional ΔF_m in molC m^{-2} yr^{-1} is 13.9 in the Cape Verde upwelling region, 4.9 in the North Pacific Silica Ocean, 3.4 in the North Atlantic Drift, 1.4 in the North Atlantic Subtropical Gyres, 0.9 in the North Pacific Carbonate Ocean, and 0.6 in the Southern Ocean. The divergent Arabian Sea, where the world's largest $F_{2\,km}C_{org}$ (553 mmolC m^{-2} yr^{-1}) is recorded, yields a modest ΔF_m of 2.8 molC m^{-2} yr^{-1} compared to an annual EP of 3.4. This indicates that as much as 18% of EP escapes mineralization while settling through the anoxic mesopelagic water column and thus supplies unusually large POC to the bathypelagic zone. In contrast, the EP and ΔF_m are about the same value in the North Pacific Silica Ocean (5.1 and 4.9 molC m^{-2} yr^{-1}, respectively) and the Cape Verde region (14.1 and 13.9, respectively), indicating that virtually all EP is mineralized to $\sum CO_2$ within the mesopelagic zone (Table 4).

Subtracting our global $F_{m/b}C_{inorg}$ estimation (34 teramolC yr^{-1}) from the global oceanic production of biogenic $CaCO_3$ estimated at 67 to 117 teramolC yr^{-1} by Lee (2001) and Iglesias-Rodriguez et al. (2002), the supply rate of dissolved $CaCO_3$ to the mesopelagic zone is 33–83 teramolC yr^{-1}. We suspect the source of this alkalinity to be supralysoclinal dissolution of metastable $CaCO_3$ in the upper mesopelagic zone. Further study of the origins and supply scheme of this hypothetical metastable $CaCO_3$ will bring greater understanding of global ocean alkalinity.

We recognize that zooplankton play a key role in the biological pump as they, along with gravity-driven aggregates, transport the products of primary production from the euphotic zone to the deep ocean and remineralize POC. Further understanding and constraint of the animal community's effects on both their contribution to the vertical transport of POC and their capacity to modify the biogeochemical setting of the ocean interior will be an important next step in biological pump investigation. Combining study of the dynamic animal community with more traditional, regimented approaches calls for a new, broader view on the part of physicists, chemists, and those studying the biogeochemistry of the ocean.

Acknowledgements

We are indebted to all the international colleagues who have published volumes of valuable open-ocean sediment trap data and their interpretations especially during the last two decades. Their efforts made this synthesis possible. In particular, our thanks are due to many long-time colleagues who generously shared ideas and seagoing opportunities, including: the late Derek Spencer, the late Yoshi Nozaki, the late Jack Dymond, Venu Ittekkot, C.S. Wong, Scott Doney, Gerald Wefer, Peter Wiebe, Rich Harbison, Jonathan Erez, Cindy Pilskaln, Kozo Takahashi, and E. Yu. Paul Tréguer generously shared his unpublished Southern Ocean data with us. Ken Doherty, McLane Research Laboratories Inc., John Kemp, and Rick Trask and the WHOI Mooring and Rigging Shop have contributed to the design and development of highly engineered TS-traps and mooring systems that have been used both by us and by international colleagues. We thank Julie Palmieri, Lary Ball, Margaret Goreau, and many other able marine technicians, sample analysts, and microscopists who have always put forth their very best efforts both at sea and in laboratories ashore. In preparing this paper, we take pleasure in acknowledging Trish White, Vicky Cullen, John Furfey, Roger Goldsmith, Jack Cook, and Cyndy Chandler, who made significant contributions to editing, data management, graphics, and library support. We are deeply indebted to anonymous reviewers who provided us insightful reviews and innumerable constructive suggestions. We are grateful for the continuing support of the Woods Hole Oceanographic Institution (WHOI), the National Science

Foundation (NSF) and the ocean science community at large, particularly to the US JGOFS Export Production Study Program since 1983. This synthesis program at WHOI was supported by the US JGOFS-Synthesis and Modeling Program (SMP): NSF grant # OCE 9986766 (Marine Chemistry). This is US JGOFS contribution # 1057.

References

Alldredge, A.L., 1976. Discarded appendicularian houses as sources of food, surface habitats, and particulate organic matter in planktonic environments. Limnology and Oceanography 21, 14–23.

Alldredge, A.L., Cox, J.L., 1982. Primary productivity and chemical composition of marine snow in surface waters of the Southern California Bight. Journal of Marine Research 40, 517–527.

Alldredge, A.L., Silver, M.W., 1988. Characteristics, dynamics and significance of marine snow. Progress in Oceanography 20, 41–82.

Alldredge, A.L., Granata, T.C., Gotschalk, C.C., Dickey, T.D., 1990. The physical strength of marine snow and its implications for particle disaggregation in the ocean. Limnology and Oceanography 35, 1415–1428.

Altabet, M.A., Deuser, W.G., Honjo, S., Stienen, C., 1991. Seasonal and depth-related changes in the source of sinking particles in the North Atlantic. Nature 345, 136–139.

Altabet, M.A., 1996. Nitrogen and carbon isotopic tracers of the source and transformation of particles in the deep Sea. In: Ittekkot, V., Schäfer, P., Honjo, S., Depetris, P.J. (Eds.), Particle Flux in the Ocean. John Wiley & Sons, New York, pp. 155–184.

Altabet, M.A., 2006. Isotopic tracers of the marine nitrogen cycle. In: Volkman, J. (Ed.), Marine Organic Matter: Chemical and Biological Markers. The Handbook of Environmental Chemistry. Springer-Verlag, Berlin, pp. 251–293.

Anderson, R.F., Bacon, M.P., Brewer, P.G., 1983. Removal of 230-Th and 231-Pa from the open ocean. Earth and Planetary Science Letters 62, 7–23.

Angel, M.V., 1989a. Does mesopelagic biology affect the vertical flux? In: Berger, W.H., Smetacek, V.S., Wefer, G. (Eds.), Productivity of Oceans, Past and Present (Dahlem Konferenzen, 1989), Life Science Research Report 44. John Wiley & Sons, New York, pp. 155–173.

Angel, M.V., 1989b. Vertical profiles of pelagic communities in the vicinity of the Azores Front and their implications to deep ocean ecology. Progress in Oceanography 22, 1–46.

Angel, M.V., Baker, A.De.C., 1982. Vertical distribution of the standing crop of plankton and micronekton at three stations in the northeast Atlantic. Biological Oceanography 2, 1–30.

Angel, M.V., Hargreaves, P., Karkpatric, P., Domansky, P., 1982. Low variability in planktonic and micronektonic population s at 1000 m depth in the vicinity of 42N, 17W; evidence against diel migratory behavior in the majority of species. Biological Oceanography 1, 287–319.

Antia, A.N., von Bodungen, B., Peinert, R., 1999. Particle flux across the mid-European continental margin. Deep Sea Research Part I 46, 1999–2024.

Antia, A.N., Maaßen, J., Herman, P., Voß, M., Scholten, J., Groom, S., Miller, P., 2001a. Spatial and temporal variability of particle flux at the N.W. European gocontinental margin. Deep Sea Research Part II 48, 3083–3106.

Antia, A., Koeve, W., Fischer, G., Blanz, T., Schulz-Bull, D., Scholten, J., Neuer, S., Kremling, K., Kuss, J., Peinert, R., Hebbeln, D., Bathmann, U., Conte, M., Fehner, U., Zeitzschel, B., 2001b. Basin-wide particulate carbon flux in the Atlantic Ocean: regional export patterns and potential for atmospheric CO_2 sequestration. Global Biogeochemical Cycles 15, 845–862.

Antoine, D.M., 1996. Oceanic primary production 1: adaptation of a spectral light-photosynthesis model in view of application to satellite chlorophyll observations. Global Biogeochemical Cycles 10, 43–55.

Archer, D.E., Maier-Reimer, E., 1994. Effect of deep-sea sedimentary calcite preservation on atmospheric CO_2 concentration. Nature 367, 260–264.

Archer, D., Aiken, J., Balch, W., Barber, D., Dunne, J., Flament, P., Gardner, W., Garside, C., Goyet, C., Johnson, E., Kirchman, D., McPhaden, M., Newton, J., Pelzer, E., Welling, L., White, J., Yoder, J., 1997. A meeting place of great ocean currents: shipboard observations of a convergent front at 2 degrees N in the Pacific. Deep Sea Research Part II 44, 1827–1849.

Arístegui, J., Duarte, C.M., Agustí, S., Doval, M., Álvarez-Salgado, X.A., Hansel, D.A., 2002. Dissolved organic carbon support of respiration in the dark ocean. Science 298, 1967.

Arístegui, J., Duarte, C.M., Gaso, J.M., Alonso-Sáez, L., 2005. Active mesopelagic prokaryotes support high respiration in the subtropical northeast Atlantic Ocean. Geophysical Research Letters 32, doi:10.1029/2004GLO21863.

Armstrong, R.A., Lee, C., Hedges, J.I., Honjo, S., Wakeham, S.G., 2001. A new, mechanistic model for organic carbon fluxes in the ocean based on the quantitative association of POC with ballast minerals. Deep Sea Research Part II 49, 219–236.

Asper, V.L., 1987. Measuring the flux and sinking speed of marine snow aggregates. Deep Sea Research 34, 1–17.

Asper, V.L., Honjo, S., Orsi, T.H., 1992. Distribution and transport of marine snow aggregates in the panama basin. Deep Sea Research Part I 39, 939–952.

Bainbridge, A.E., 1979. GEOSECS Atlantic Expedition, vol. 1. International Decade of Ocean Sciences, National Science Foundation. US Government Printing Office, Washington, DC.

Baker, E.T., Milburn, H.B., Tennant, D.A., 1988. Field assessment of sediment trap efficiency under varying flow conditions. Journal of Marine Research 46, 573–592.

Bé, A.W.H., Gilmer, R.W., 1977. A zoogeographic and taxonomic review of euthecosomatous Pteropda. In: Ramsey, A.T.S. (Ed.). Oceanic Micropaleontology, vol. 1. Academic Press, London, pp. 733–808.

Beaumont, K., Nash, G.V., Davidson, A.T., 2002. Ultra structure, morphology and flux of microzooplankton faecal pellets in an east Antarctic fjord. Marine Ecology Progress Series 245, 133–148.

Behrenfeld, M.J., Falkowski, P.G., 1997. Photosynthetic rates derived from satellite-based chlorophyll concentration. Limnology and Oceanography 42, 1–20.

Belkin, I., Krishfield, R., Honjo, S., 2002. Decadal variability of the North Pacific polar Front: subsurface warming versus surface cooling. Geophysical Research Letters 29. doi:10.1029/2001GL013806.

Benfield, M.C., Grosjean, P., Culverhouse, P., Irigoien, X., Sieracki, M.E., Lopez-Urrutia, A., Dam, H.G., Hu, Q., Davis, C.S., Hansen, A., Pilskaln, C.H., Riseman, E., Schultz, H., Utgoff, P.E., Gorsky, G., 2007. G. RAPID: research on automated plankton identification. Oceanography Magazine 20, 12–26.

Berelson, W.M., 2001. Particle settling rates increase with depth in the ocean. Deep Sea Research Part II 49, 237–251.

Berelson, W.M., 2002. The flux of particulate organic carbon into the ocean interior: a Comparison of four US JGOFS regional studies. Oceanography 14, 59–67.

Berger, W.H., 1989. Global maps of ocean productivity. In: Berger, W.H., Smetacek, V.S., Wefer, G. (Eds.), Productivity of Oceans, Past and Present (Dahlem Konferenzen, 1989), Life Science Research Report 44. John Wiley & Sons, New York, pp. 429–455.

Berger, W.H., Piper, D.J., 1972. Planktonic foraminifera: differential settling, dissolution and reproduction. Limnology and Oceanography 17, 275–287.

Berger, W.H., Fischer, K., Lai, C., Wu, G., 1987. Ocean productivity and organic carbon flux. Part 1. Overview and Maps of Primary Production and Export Production. University of California, San Diego (SIO Reference 87-30).

Berner, R.A., 1977. Sedimentation and dissolution of pteropods in the ocean. In: Malahoff, A., Anderson, N.R. (Eds.), The Fate of Fossil Fuel CO_2 in the ocean. Plenum Press, New York, pp. 243–268.

Berner, R.A., Berner, E.K., 1976. Aragonite dissolution on the Bermuda Pedestal: its depth and geochemical significance. Earth & Planetary Science Letters 30, 169–178.

Berner, R.A., Honjo, S., 1981. Pelagic sedimentation of aragonite: its geochemical significance. Science 211, 940–942.

Bernstein, R.E., Betzer, P.R., Feely, R.A., Byrne, R.H., Lamb, M.F., Michaels, A.F., 1987. Acantharian fluxes and strontium to chlorinity ratios in the north Pacific Ocean. Science 237, 1490–1494.

Betzer, P.R., Byrne, R.H., Acker, J.G., Lewis, C.S., Jolley, R.R., 1984. The oceanic carbonate system: a reassessment of biogenic controls. Science 226, 1074–1077.

Bishop, J.K.B., 1989. Regional extremes in particulate matter composition and flux: effects on the chemistry of ocean floor. In: Berger, W.H., Smetacek, V.S., Wefer, G. (Eds.), Productivity of Oceans, Past and Present (Dahlem Konferenzen, 1989), Life Science Research Report 44. John Wiley & Sons, New York, pp. 117–137.

Bishop, J.K.B., Davis, R.E., Sherman, J.T., 2002. Robotic observations of dust storm enhancement of carbon biomass in the North Pacific. Science 298, 817–821.

Bray, S., Trull, T., Manganini, S. 2000. SAZ Project Moored Sediment Traps: Results of the 1997–1998 Deployments. Technical Report, Cooperative Research Centre for Antarctica and the Southern Ocean, Hobart, Australia.

Brewer, P.G., Nozaki, Y., Spencer, D.W., Fleer, A.F., 1980. Sediment trap experiments in the deep North Atlantic: isotopic and elemental fluxes. Journal of Marine Research 38, 703–728.

Broecker, W., 1971. Calcite accumulation rates and glacial and interglacial changes in oceanic mixing. In: Turekian, K.K. (Ed.), Late Cenozoic Glacial Ice Age. Yale University Press, New Haven, pp. 239–265.

Broerse, A.T.C., 2000. Coccolithophore export production in selected ocean environments: seasonality, biogeography and carbonate production. Doctoral thesis publication accepted by Vrije University on January 20, 2000. Vrije University, Amsterdam, 185 pp.

Buat-Ménard, P., Davies, J., Remoudaki, E., Miquel, J.C., Bergametti, G., Lambert, C.E., Ezat, U., Quetel, C., La Rosa, J., Fowler, S.W., 1989. Non-steady-state biological removal of atmospheric particles from Mediterranean surface waters. Nature 340, 131–134.

Buesseler, K.O., 1991. Do upper-ocean sediment traps provide an accurate record of particle flux? Nature 353, 420–423.

Buesseler, K.O., Livingston, H.D., Honjo, S., Hay, B.J., Manganini, S.J., Degens, E.T., Ittekkot, I., Konuk, T., 1987. Chernobyl radionuclides in a Black Sea sediment trap. Nature 329, 825–828.

Buesseler, K., Michaels, A.F., Siegel, D.A., Knap, A.H., 1994. A three dimensional time-dependent approach to calibrating sediment trap fluxes. Global Biogeochemical Cycles 8, 179–193.

Buesseler, K., Ball, L., Andrews, J., Benitez-Nelson, C., Belastock, R., Chai, F., Chao, Y., 1998. Upper ocean export of particulate organic carbon in the Arabian Sea derived from thorium-234. Deep Sea Research Part II 45, 2461–2487.

Buesseler, K.O., Steinberg, D.K., Michaels, A.F., Johnson, R.J., Andrews, J.E., Valdes, J.R., Price, J.F., 2000. A comparison of the quantity and composition of material caught in a neutrally buoyant versus surface-tethered sediment trap. Deep Sea Research Part I 47, 277–294.

Buesseler, K.O., Lamborg, C.H., Boyd, P.W., Lam, P.L., Trull, T.W., Bidigare, R.R., Bishop, J.K.B., Casciotti, K.L., Dehairs, F., Elskens, M., Honda, M., Karl, D.M., Siegel, D.A., Silver, M.W., Steinberg, D.K., Valdes, J., Van Mooy, B., Wilson, S., 2007. Revisiting carbon flux through the ocean's "twilight zone". Science 316, 567–570.

Butman, C.A., 1986. Sediment trap biases in turbulent flows: results from a laboratory flume study. Journal of Marine Research 44, 645–693.

Byrne, R.H., Acker, J.G., Betzer, P.R., Feely, R.A., Cates, M.H., 1984. Water column dissolution of aragonite in the Pacific Ocean. Nature 321, 321–326.

Calvert, S., 1983. Sedimentary geochemistry of silicon. In: Aston, S.R. (Ed.), Silicon Geochemistry and Biochemistry. Academic Press, London, pp. 143–186.

Caron, D.A., Michaels, A.F., Swanberg, N.R., Howse, F.A., 1995. Primary productivity by symbiont-bearing planktonic sarcodines (Acantharia, Radiolaria, Foraminifera) in surface waters near Bermuda. Journal of Plankton Research 17, 103–129.

Cauwet, G., 2002. In: Hansell, D.A., Carlson, C.A. (Eds.), Biogeochemistry of Marine Dissolved Organic Matter. Academic Press, San Diego, CA, pp. 597–609.

Chavez, F.P., Barber, R.T., 1987. An estimate of new production in the equatorial Pacific. Deep Sea Research 34, 1229–1243.

Christensen, J.P., 2000. A relationship between deep-sea benthic oxygen demand and oceanic primary productivity. Oceanologica Acta 23, 65–82.

Church, J.A., 2007. A change in circulation? Science 317, 908–909.

Cobler, R.J.D., Dymond, D., 1980. Sediment trap experiment on the Galapagos spreading center, equatorial Pacific. Science 209, 801–803.

Cole, J.J., Honjo, S., Caraco, N., 1985. Seasonal variation in the flux of algal pigments to a deep-water site in the Panama Basin. Hydrobiology 122, 193–197.

Cole, J.J., Honjo, S., Erez, J., 1987. Benthic decomposition of organic matter at a deep-water site in the Panama Basin. Nature 327, 703–704.

Collier, R., Dymond, D., Honjo, S., Manganini, S.J., Francois, R., Dunbar, R., 2000. The vertical flux of biogenic and lithogenic material in the Ross Sea: moored sediment trap observations 1996–1998. Deep Sea Research Part II 47, 3491–3520.

Conte, M.H., Deuser, W., Ralf, N., Ross, E.H., 2001. Seasonal and interannual variability in deep ocean particle fluxes at the Oceanic Flux Program (OFP), Bermuda Atlantic Time-Series (BAT) site in the Western Sargasso Sea near Bermuda. Deep Sea Research Part II 48, 1471–1505.

Cota, G.F., Pomeroy, L.R., Harrison, W.G., Jones, E.P., Peters, F., Sheldon, W.M., Weingartner, T.R., 1996. Nutrients, primary production and microbial heterotrophy in the southern Chukchi Sea: Arctic summer nutrient depletion and heterotrophy. Marine Ecology Progress Series 135, 242–258.

Davis, D.L., Pilskaln, C.H., 1993. Measurements with underwater video: camera field width calibration and structured lightning. Marine Technology Society Journal 26, 13–19.

Deuser, W.G., 1987. Variability of hydrography and particle flux: transient and long-term relationships. In: Degens, E.T., Izdar, E., Honjo, S. (Eds.), Particle Flux in the Ocean. SCOPE/UNEP, vol. 62, Hamburg, pp. 179–193.

Deuser, W.G., 1996. Temporal variability of particle flux in the deep Sargasso Sea. In: Ittekkot, V., Schäfer, P., Honjo, S., Depetris, P.J. (Eds.), Particle Flux in the Ocean. John Wiley & Sons, New York, pp. 185–198.

Deuser, W.G., Jickells, T.D., King, P., Commeau, J.A., 1995. Decadal and annual changes in biogenic opal and carbonate fluxes to the deep Sargasso Sea. Deep Sea Research Part I 42, 1923–1932.

Dickey, T., Marra, J., Sigurdson, D.E., Weller, R.A., Kinkade, C.S., Zedler, S.E., Wiggert, J.D., Langdon, C., 1998. Seasonal variability of bio-optical and physical properties in the Arabian Sea: October 1994–October 1995. Deep Sea Research Part II 45, 2001–2025.

Diercks, A.R., Asper, V.L., 1997. In situ settling speeds of marine snow aggregates below the mixed layer: Black Sea and Gulf of Mexico. Deep Sea Research Part I 44, 385–398.

Doval, M.D., Hansell, D.A., 2000. Organic carbon and apparent oxygen utilization in the western South Pacific and the central Indian Oceans. Marine Chemistry 68, 249–264.

Duce, R.A., Liss, P.S., Merrill, J.T., Atlas, E.L., Buat-Ménard, P., Hicks, B.B., Miller, J.M., Prospero, J.M., Arimoto, R., Church, T.M., Ellis, W., Galloway, J.N., Hansen, L., Jickells, T.D., Knap, A.H., Reinhardt, K.H., Schneider, B., Soudine, A., Tokos, J.J., Tsunogai, S., Wollast, R., Zhou, M., 1991. Atmospheric input of trace species to the world ocean, global biogeochemical changes. International Journal of Global Change 5, 193–259.

Dymond, J.R., Collier, R.W., 1988. Biogenic particle fluxes in the Equatorial Pacific: evidence for both high and low productivity during 1982–1983 El Nino. Global Biogeochemical Cycles 2, 129–137.

Dymond, J., Lyle, M., 1985. Flux comparisons between sediments and sediment traps in the eastern tropical Pacific: implications for atmospheric CO_2 variations during the Pleistocene. Limnology and Oceanography 30, 699–712.

Emery, W.J., Thomson, R.E., 1997. Data Analysis Methods in Physical Oceanography. Pergamon Press, New York.

Etcheber, H., Heussner, S., Weber, O., Dinet, A., Durrieu de Madron, X., Monaco, A., Buscail, R., Miquel, J.C., 1996. Organic carbon fluxes and sediment biogeochemistry on the French Mediterranean and Atlantic margins. In: Ittekkot, V., Schäfer, P., Honjo, S., Depetris, P.J. (Eds.), Particle Flux in the Ocean. John Wiley & Sons, New York, pp. 223–241.

Fahl, K., Nöthig, E-M., 2007. Lithogenic and biogenic particle fluxes on the Lomonosove Ridge (central Arctic Ocean) and their relevance for sediment accumulation: vertical vs. lateral transport. Deep Sea Research Part I 54, 1256–1272.

Farby, V.J., 1989. Aragonite production by pteropod molluscs in the subarctic Pacific. Deep Sea Research 36, 1735–1751.

Farby, V.J., Deuser, W.G., 1991. Aragonite and magnesium calcite fluxes to the deep Sargasso Sea. Deep Sea Research 38, 713–728.

Favorite, F.A., Dodimead, J., Nasu, K., 1976. Oceanography of the Subarctic Pacific region. Bulletin of the International North Pacific Fisheries Commission 33, 187.

Feely, R.A., Sabine, C.L., Lee, K., Berelson, W., Kleypas, J., Fabry, V.J., Millero, F.J., 2004. Impact of anthropogenic CO_2 on the $CaCO_3$ system in the oceans. Science 305, 362–366.

Fiadeiro, M., 1980. The alkalinity of the deep Pacific. Earth and Planetary Science Letters 49, 499–505.
Findlater, J., 1974. The low-level cross-equatorial air current of the Western Indian Ocean during the northern summer. Weather 29, 411–416.
Fischer, G., Wefer, G., 1996. Seasonal and interannual particle fluxes in the Eastern Equatorial Atlantic from 1989 to 1991: ITCZ migrations and upwelling. In: Ittekkot, V., Schäfer, P., Honjo, S., Depetris, P.J. (Eds.), Particle Flux in the Ocean. John Wiley & Sons, New York, pp. 199–214.
Fischer, G., Donner, B., Ratmeyer, V., Davenport, R., Wefer, G., 1996. Distinct year-to-year particle flux variations off Cape Blanc during 1988–1991: relation to $d^{18}O$-deduced sea-surface temperatures and trade winds. Journal of Marine Research 54, 73–98.
Fischer, G., Ratmeyer, V., Wefer, G., 2000. Organic carbon fluxes in the Atlantic and the Southern Ocean: relationship to primary production compiled from satellite radiometer data. Deep Sea Research Part II 47, 1961–1997.
Fischer, G., Wefer, G., Romero, O., Dittert, N., Ratmeyer, V., Donner, B., 2003. Transfer of particles into the deep Atlantic and the global ocean: control of nutrient supply and ballast production. In: Wefer, G., Mulitza, S., Ratmeyer, V. (Eds.), The South Atlantic in the Late Quaternary: reconstruction of Material Budgets and Current Systems. Springer-Verlag, Berlin, pp. 12–46.
Francois, R., Honjo, S., Krishfield, R., Manganini, S., 2002. Factors controlling the flux of organic carbon to the bathypelagic zone of the ocean. Global Biogeochemical Cycles 16, 1087.
Gagosian, R., Nigrelli, G.E., Volkman, J.K., 1983. Vertical transport and transformation of biogenic organic compounds from a sediment trap experiment off the coast of Peru. In: Suess, E., Thiede, J. (Eds.), Coastal Upwelling It's Sediment Record. Part A: responses of the Sedimentary Regime to Present Coastal Upwelling. Plenum Press, New York, pp. 241–272.
Gardner, W.D., 1980. Sediment trap dynamics and calibration: a laboratory evaluation. Journal of Marine Research 38, 17–39.
Gardner, W.D., 1989. Baltimore Canyon as a modern conduit of sediment to the deep sea. Deep Sea Research 36, 323–358.
Gardner, W.D., Sullivan, L.G., 1981. Benthic storms: temporal variability in a deep-ocean nepheloid layer. Science 213, 329–331.
Gardner, W.D., Walsh, I.D., 1990. Distribution of macroaggregates and find grained particles across continental margin and their potential role in fluxes. Deep Sea Research 37, 401–411.
Gardner, W.D., Hinga, K.R., Marra, J., 1983. Observations on the degradation of biogenic material in the deep ocean with implications on accuracy of sediment trap fluxes. Journal of Marine Research 41, 195–214.
Gardner, W.D., Richardson, M.J., Smith, J.W.O., 2000. Seasonal patterns of water column particulate organic carbon and fluxes in the Ross Sea, Antarctica. Deep Sea Research Part II 47, 3423–3449.
Gauld, D.T., 1957. A peritrophic membrane in calanoid copepods. Nature 179, 325–326.
Gorsky, G., Fisher, N.S., Gowler, S.W., 1984. Biogenic debris from the pelagic tunicate, *Oikopleura diocia*, and its role in the vertical transport of a transuranium elements. Estuarine, Coastal and Shelf Science 18, 13–23.
Gosselin, M., Levasseur, M., Wheeler, P.A., Horner, R.A., Booth, B.C., 1997. New measurement of phytoplankton and ice algal production in the Arctic Ocean. Deep Sea Research Part II 44, 1623–1644.
Gowing, M.M., Coale, S.L., 1989. Fluxes of living radiolarians and their skeletons along a Northeast pacific transect from coastal upwelling to open ocean waters. Deep Sea Research 36, 561–579.
Gowing, M.M., Silver, M.W., 1985. A new and abundant size class of marine fecal pellets. Journal of Marine Research 43, 395–418.
Gowing, M.M., Wishner, K.F., 1986. Trophic relationships of deep-sea calanoid copepods from the benthic boundary layer of the Santa Catalina Basin, California. Deep Sea Research A 33, 939–961.
Guieu, C., Roy-Barman, M., Leblond, N., Jeandel, C., Souhaut, M., Le Cann, B., Dufour, A., Bournot, C., 2005. Vertical particle flux in the northeast Atlantic Ocean (POMME experiment). Journal of Geophysical Research 110, 1029–2004.
Haake, B., Ittekkot, V., Rixen, T., Ramaswamy, V., Nair, R.R., Curry, W.B., 1993. Seasonality and interannual variability of particle fluxes to the deep Arabian Sea. Deep Sea Research Part I 40, 1323–1344.
Haake, B., Rixen, T., Reemtsma, T., Ramaswamy, V., Ittekkot, V., 1996. Processes determining seasonality and interannual variability of settling particle fluxes to deep Arabian Sea. In: Ittekkot, V., Schäfer, P., Honjo, S., Depetris, P.J. (Eds.), Particle Flux in the Ocean. John Wiley & Sons, New York, pp. 251–270.
Handa, N., 1989. Flux of organic matter at Japan Trench Sites (JT-01 and 02). Kaiyo Monthly 21, 197–202.
Handa, N., Hosokawa, A., Masuzawa, Tsunogai, S., 1997. Studies on vertical flux of particulate carbon and silica in the ocean and factors controlling the chemical fluxes. In: Tsunogai, S. (Ed.), Biogeochemical Processes in the North Pacific. Japan Marine Science Foundation, Tokyo, pp. 249–255.
Hansell, D.A., Carlson, C.A., 1998. Net community production of dissolved organic carbon. Global Biogeochemical Cycles 12, 443–453.
Hansell, D.A., Carlson, C.A., 2001. Biogeochemistry of total carbon and nitrogen in the Sargasso Sea: control by convective overturn. Deep Sea Research Part II 48, 1648–1649.
Hansell, D.A., Kadko, D., Bates, N.R., 2004. Degradation of terrigenous dissolved organic carbon in the western Arctic Ocean. Science 304, 858–861.
Harbison, G.R., Gilmer, R., 1986. Effects of animal behavior on sediment trap collections: implications for the calculation of aragonite fluxes. Deep Sea Research 33, 1017–1024.

Harbison, G.R., McAlister, V.L., 1979. The filter-feeding rates and particle retention efficiencies of three species of Cyclosalpa (Tunicata, Thaliacea). Limnology and Oceanography 24, 875–892.
Hardy, A.C., Bainbridge, R., 1954. Experimental observations on the vertical migration of plankton animals. Journal of the Marine Biological Association of the United Kingdom 33, 409–448.
Hargrave, B.T., von Bodungen, B., Stoffyn-Egli, P., Mudie, P.J., 1993. Seasonal variability in particle sedimentation under permanent ice cover in the Arctic Ocean. Continental Shelf Research 14, 279–293.
Hay, B.J., Honjo, S., 1989. Particle decomposition in the present and the Holocene Black Sea. Oceanography 2, 26–61.
Hay, B.J., Honjo, S., Kempe, S., Ittekkot, V., Degans, E., Konuk, T., Izdar, E., 1990. Interannual variability in particle flux in the southwestern Black Sea. Deep Sea Research 37, 911–928.
Hebbeln, D., Wefer, G., 1991. Effects of ice coverage and ice-rafted material on sedimentation in the Fram Strait. Nature 350, 409–411.
Hebbeln, D., Marchant, M., Wefer, G., 2000. Seasonal variations of the particle flux in the Peru–Chile current at 30°S under normal and El Niño conditions. Deep Sea Research II 47, 2101–2128.
Hedges, J.I., Lee, C., Wakeham, S.G., Hernes, P.J., Peterson, M.L., 1993. Effects of poisons and preservatives on the fluxes and elemental compositions of sediment trap material. Journal of Marine Research 51, 651–668.
Hedgpeth, J.W., 1957. Classification of marine environments. Geological Society of America, Memoir 67 (1), 17–28.
Heinmiller, Jr., R.H., 1979. Mooring operations techniques of the buoy project at the Woods Hole Oceanographic Institution. WHOI Technical Reports 76-69, Woods Hole Oceanographic Institution, Woods Hole.
Honda, M., 2001. Sediment trap experiments and a study of carbon cycle in the North Western Pacific Ocean. Ph.D. thesis submitted and accepted at the Department of Earth Environment Studies, Hokkaido University. Sapporo, March, 2001, 193 pp. (unpublished).
Honda, M., Kusakabe, M., Nakabayashi, S., Honjo, S., Manganini, S., 1997. The efficiency of biological pump in the western North Pacific. In: Tsunogai, S. (Ed.), Biogeochemical Processes in the North Pacific. Japan Marine Science Foundation, Tokyo, pp. 249–255.
Honda, M.C., Imai, K., Nojiri, Y., Hoshi, F., Sugawara, T., Kusakabe, M., 2002. Biological pump in the northwestern North Pacific based on fluxes and major component of particulate matter obtained by sediment trap experiments (1997–2000). Deep Sea Research Part II 49, 5595–5625.
Hong, G.H., Chen, C.T.A., 2002. Aragonitic pteropod flux to the interior of the East Sea (Sea of Japan). TAO 13, 205–210.
Hong, G.H., Choe, S.M., Suk, M.S., Na, J.Y., Sin, I.C., Chang, S.C., Kim, S.H., 1997. Annual biogenic particle fluxes to the interior of the East/Japan Sea, a large marginal sea of the Northwest Pacific. In: Tsunogai, S. (Ed.), Biogeochemical Processes in the North Pacific. Japan Marine Science Foundation, Tokyo, pp. 300–321.
Honjo, S., 1975. Dissolution of suspended coccoliths in the deep-sea water column and sedimentation of coccolith ooze. In: Sliter, W.V., Bé, A.H., Berger, W.H. (Eds.), Dissolution of Seep-Sea Carbonates. Cushman Foundation Foraminifera Research, Special Publication, 13, Washington, DC, pp. 114–128.
Honjo, S., 1976. Coccoliths: production, transportation, and sedimentation. Marine Micropaleontology 1, 65–79.
Honjo, S., 1977. Biogenic carbonate particles in the ocean; Do they dissolve in the water column? In: Andersen, N.R., Marahoff, A. (Eds.), The Fate of Fossil Fuel CO_2 in the Oceans. Plenum Press, New York, pp. 269–294.
Honjo, S., 1978. Sedimentation of materials in the Sargasso Sea at a 5367 m deep station. Journal of Marine Research 36, 469–492.
Honjo, S., 1980. Material fluxes and modes of sedimentation in the mesopelagic and bathypelagic zones. Journal of Marine Research 38, 53–97.
Honjo, S., 1982. Seasonality and interaction of biogenic and lithogenic particulate flux at the Panama Basin. Science 218, 883–884.
Honjo, S., 1990. Particle fluxes and modern sedimentation in the Polar Oceans. In: Smith, W.O. (Ed.), Polar Oceanography, Part B: Chemistry, Biology, and Geology. Academic Press, New York, pp. 687–739.
Honjo, S., 1996. Fluxes of particles to the interior of the open oceans. In: Ittekkot, V., Schäfer, P., Honjo, S., Depetris, P.J. (Eds.), Particle Flux in the Ocean. John Wiley & Sons, New York, pp. 91–154.
Honjo, S., 1997a. The Northwestern Pacific Ocean, a crucial ocean to understand global change: rationale for new international collaborative investigations. In: Tsunogai, S. (Ed.), Biogeochemical Processes in the North Pacific. Japan Marine Science Foundation, Tokyo, pp. 233–248.
Honjo, S., 1997b. The rain of ocean particles and Earth's carbon cycle. Oceanus 40, 4–7.
Honjo, S., 2004. Export fluxes and act of biological pump in the Southern Ocean. Antarctic Science 16, 501–516.
Honjo, S., Doherty, K.W., 1988. Large aperture time-series sediment traps; design objectives, construction and application. Deep Sea Research 35, 133–149.
Honjo, S., Erez, J., 1978. Dissolution rates of calcium carbonate in the deep ocean; an in situ experiment in the North Atlantic Ocean. Earth and Planetary Sc ience Letters 40, 287–300.
Honjo, S., Manganini, S.J., 1987. Particle Fluxes, North-Eastern Nordic Seas: 1983–1986. Nordic Seas Sedimentation Data File, vol. 1. WHOI Technical Report 87-17, Woods Hole Oceanographic Institution, Woods Hole.
Honjo, S., Manganini, S.J., 1993. Annual biogenic particle fluxes to the interior of the North Atlantic ocean; studied at 34°N 21°W and 48°N 21°W. Deep Sea Research 40, 587–607.
Honjo, S., Roman, M.R., 1978. Marine copepod fecal pellets: production, preservation and sedimentation. Journal of Marine Research 36, 45–57.
Honjo, S., Weller, R.A., 1997. Monsoon winds and carbon cycles in the Arabian Sea. Oceanus 40, 24–28.

Honjo, S., Connell, J.F., Sachs, P., 1979. Construction of PARFLUX Mark II Sediment Trap; Engineering Report, Technical Report, 79-80, Woods Hole Oceanographic Institution, 49 pp.
Honjo, S., Manganini, S.J., Cole, J.J., 1982. Sedimentation of biogenic matter in the deep ocean. Deep Sea Research 29, 609–625.
Honjo, S., Manganini, S.J., Karowe, A., Woodward, B.L., 1987. Particle fluxes, Northeastern Nordic seas: 1983–1986 (Nordic Seas Sedimentation Data File, vol. 1). Technical Report, Woods Hole Oceanographic Institution, WHOI-87-17.
Honjo, S., Doherty, K.W., Agrawal, Y.C., Asper, V.L., 1984. Direct optical assessment of macroscopic aggregates in the deep ocean. Deep Sea Research 31, 67–76.
Honjo, S., Manganini, S.J., Wefer, G., 1988. Annual particle flux and a winter outburst of sedimentation in the northern Norwegian Sea. Deep Sea Research 35, 1223–1234.
Honjo, S., Spencer, D.W., Gardner, W.D., 1992. A sediment trap intercomparison experiment in the Panama Basin, 1979. Deep Sea Research 39, 333–358.
Honjo, S., Dymond, J., Collier, R., Manganini, S.J., 1995. Export production of particles to the interior of the equatorial Pacific Ocean during the 1992 EqPac experiment. Deep Sea Research 42, 831–870.
Honjo, S., Dymond, J., Prell, W.L., Ittekkot, V., 1999. Monsoon-controlled export fluxes to the interior of the Arabian Sea. Deep Sea Research Part II 46, 1859–1902.
Honjo, S., Francois, R., Manganini, S., Dymond, J., Collier, R., 2000. Particle fluxes to the interior of the Southern Ocean in the Western Pacific sector along 170°W. Deep Sea Research Part II 47, 3521–3548.
Hurd, D.C., 1983. Physical and chemical properties of siliceous skeletons. In: Aston, S.R. (Ed.), Silicon Geochemistry and Biogeochemistry. Academic Press, London, p. 248.
Hwang, J., Eglinton, T.I., Manganini, S., Honjo, S., Krishfield, R., Proshutinsky, A., 2007. Radiocarbon evidence for lateral supply of organic carbon to the deep Canada Basin (unpublished).
Iglesias-Rodriguez, D., Armstrong, R., Feely, R., Hood, R., Kleypas, J., 2002. Progress made in study of ocean's calcium carbonate budget. EOS 83, 374–375 (see also p. 365).
Itou, M., Noriki, S., 1997. Temporal changes of particulate flux observed in the northern Japan Trench. In: Tsunogai, S. (Ed.), Biogeochemical Processes in the North Pacific. Japan Marine Science Foundation, Tokyo, pp. 262–266.
Ittekkot, V., 1991. Particle flux studies in the Indian Ocean. EOS 72, 527–530.
Ittekkot, V., Nair, R.R., Honjo, S., Ramaswamy, V., Bartsch, M., Manganini, S., Desai, B.N., 1991. Enhanced particle fluxes in the Bay of Bengal induced by injection of fresh water. Nature 351, 385–387.
Izdar, E., Konuk, T., Honjo, S., Asper, V.L., Manganini, S.J., Degens, E.T., Ittekkot, V., Kempe, S., 1984. First data on sediment trap experiment in black sea deep water. Naturwissenschaften 71, 478–479.
Jahnke, R.A., 1996. The global ocean flux of particulate organic carbon: a real distribution and magnitude. Global Biogeochemical Cycles 10, 71–88.
Jennerjahn, T.C., Ittekkot, V., Carvalho, C.E.V., 1996. Preliminary data on particle flux off the Sao Francisco River, Eastern Brazil. In: Ittekkot, V., Schäfer, P., Honjo, S., Depetris, P.J. (Eds.), Particle Flux in the Ocean. John Wiley & Sons, New York, pp. 215–222.
Jickells, T.D., Newton, P.P., King, P.L.R.S., Boutle, C., 1996. A comparison of sediment trap records of particle fluxes from 19 to 48 degrees N in the Northeast Atlantic and their relation to surface water productivity. Deep Sea Research 43, 971–986.
Kawahata, H., Suzuki, A., Ohta, H., 1997. Sinking particles between the Equatorial and Subarctic regions (0°N–46°N) in the Central Pacific. Official Report, North Pacific Carbon Cycle Study (NOPACCS). Release form Marine Geology Division, Geological Survey of Japan, Tsukuba.
Kawahata, H., Yamamuro, M., Ohta, H., 1999. Seasonal and vertical variations of sinking particle fluxes in the West Caroline Basin. Oceanologica Acta 21, 521–532.
Kawahata, H., Suzuki, A., Ohata, H., 2000. Export fluxes in the Western Pacific warm pool. Deep Sea Research Part I 47, 2061–2091.
Kawahata, H., Nishimura, A., Gagan, M.K., 2002. Seasonal change in foraminiferal production in the western equatorial Pacific warm pool: evidence from sediment trap experiments. Deep Sea Research Part II 49, 2783–2800.
Kempe, S., Knaack, H., 1996. Vertical particle flux in the western Pacific below the north Equatorial Current and the Equatorial Counter Current. In: Ittekkot, V., Schäfer, P., Honjo, S., Depetris, P.J. (Eds.), Particle Flux in the Ocean. John Wiley & Sons, New York, pp. 313–323.
Kempe, S., Schaumburg, M., 1996. Vertical particle flux in Lake Baikal. In: Ittekkot, V., Schäfer, P., Honjo, S., Depetris, P.J. (Eds.), Particle Flux in the Ocean. John Wiley & Sons, New York, pp. 325–354.
Kemp, A.E.S., Pearce, R.B., Koizumi, I., Pike, J., Rance, S.J., 1999. The role of mat-forming diatoms in the formation of Mediterranean sapropels. Nature 398, 57–61.
Kikuchi, T., Omori, M., 1985. Vertical distribution and migration of oceanic shrimps at two locations off the Pacific coast of Japan. Deep Sea Research 32, 837–851.
Kinkade, C.S., Marra, J., Dickey, T.D., Langdon, C., Sigurdson, D.E., Weller, R., 1999. Diel bio-optical variability observed from moored sensors in the Arabian Sea. Deep Sea Research Part II, 46–1813–1831.
Klaas, C.A., Archer, D.E., 2002. Association of sinking organic matter with various types of mineral ballast in the deep sea: implications for the rain ratio. Global Biogeochemical Cycles 16, 1–16.
Klaveness, D., Paasche, E., 1971. Pysiology of coccolithophorids, third ed. In: Levadowski, M., Hunter, S.H. (Eds.). Biochemistry and Physiology of Protozoa, vol. 1 Academic Press, San Diego, pp. 191–213.

Knauer, G.A., Martin, J.H., Bruland, K.W., 1979. Fluxes of particulate carbon, nitrogen, and phosphorus in the upper water column of the northeast Pacific. Deep Sea Research 26A, 97–108.

Knauer, G.A., Karl, D.M., Martin, J.H., Hunter, C.N., 1984. In situ effects of selected preservatives on total carbon, nitrogen, and metals collected in sediment traps. Journal of Marine Research 42, 445–462.

Kuss, J., Kremling, K., 1999. Particulate trace element fluxes in the deep northeast Atlantic Ocean. Deep Sea Research 46, 149–169.

Lalli, C.M., Gilmer, R.W., 1989. Pelagic Snails: The Biology of Holoplanktonic Gastropod Mollusks. Stanford University Press, Stanford.

Lampitt, R.S., 1985. Evidence for the seasonal deposition of detritus to the deep-sea floor (Porcupine Bight, NE Atlantic) and its subsequent resuspension. Deep Sea Research 32, 885–897.

Lampitt, R.S., Antia, A.N., 1997. Particle flux in the deep seas: regional characteristics and temporal variability. Deep Sea Research Part I 44, 1377–1403.

Lampitt, R.S., Wisher, K.F., Turley, C.M., Angel, M.V., 1993. Marine snow studies in the Northeast Atlantic: distribution, composition and role as a food source for migrating plankton. Marine Biology 116, 689–702.

Lane, P.V.Z., Smith, S.L., Biscay, P.E., 1994. Carbon flux and recycling associated with zooplankton fecal pellets on the shell of the Middle Atlantic Bight. Deep Sea Research 41, 437–457.

Laws, E.A., Falkowski, P.G., Smith, W.O., Ducklow, H., McCarthy, J.J., 2000. Temperature effects on export production in the open ocean. Global Biogeochemical Cycles 14, 1231–1246.

Lee, K., 2001. Global net community production estimated from the annual cycle of surface water total dissolved inorganic carbon. Limnology and Oceanography 46, 1287–1297.

Lee, C., Wakeham, S.G., Hedges, J.I., 1988. The measurement of oceanic particle flux – are "swimmers" a problem? Oceanography 1, 34–36.

Lee, C., Hedges, J.I., Wakeham, S.G., Zhu, N., 1992. Effectiveness of various treatments in retarding microbial activity in sediment trap material and their effects on the collection of swimmers. Limnology and Oceanography 37, 117–130.

Lee, C., Murray, D.W., Barber, R.T., Buesseler, K., Dymond, J., Hedges, J.I., Honjo, S., Manganini, S.J., Marra, J., Moser, C., Peterson, M.L., Prell, W.L., Wakeham, S.G., 1998. Particulate organic carbon fluxes: compilation of results from the 1995 US JGOFS Arabian Sea Process Study. Deep Sea Research Part II 45, 2489–2501.

Longhurst, A., Harrison, W.G., 1988. Vertical nitrogen flux from the oceanic photic zone by diel migrant zooplankton and nekton. Deep Sea Research 35, 881–889.

Longhurst, A., Sathyendranath, S., Platt, T., Caverhill, C., 1995. Estimate of global primary production in the ocean from satellite radiometer data. Journal of Plankton Research 17, 1245–1271.

Louanchi, F., Najjar, R.G., 2000. A global monthly climatology of phosphate, nitrate, and silicate in the upper ocean: Spring-summer export production and shallow remineralization. Global Biogeochemical Cycles 14, 957–977.

Lyle, M., Zahn, R., Prahl, F., Dymond, J., Collier, R., Pisias, N., Suess, E., 1992. Paleoproductivity and carbon burial across the California Current: the multitracers transect, 42°N. Paleoceanography 7, 251–272.

Macdonald, R.W., Carmack, E.C., 1991. Age of Canada Basin deep waters: a way to estimate primary production for the Arctic Ocean. Science 254, 1348–1350.

Madin, L.P., 1982. Production, composition and sedimentation of salp pellets in oceanic waters. Marine Biology 67, 39–45.

Madin, L.P., Kremer, P., Wiebe, P.H., Purcell, J.E., Horgan, E.H., Nemazie, D.A., 2006. Periodic swarms of the salp Salpa aspera in the Slope Water off the NE United States: Biovolume, vertical migration, grazing, and vertical flux. Deep Sea Research Part I 53, 804–819.

Mahowald, N., Kohfeld, K., Hansson, M., Balkanski, Y., Harrison, S.P., Prentice, I.C., Schulz, M., Rodhe, H., 1999. Dust sources and deposition during the last glacial maximum and current climate: a comparison of model results with paleodata from ice cores and marine sediments. Journal of Geophysical Research 104, 15895–15916.

Manganini, S., Honjo, S., 1992. Biogenic particle fluxes at the 34°N 21°W and 48°N 21°W Stations, 1989–1990: methods and analytical data compilation. WHOI Technical Report 92-15. Woods Hole Oceanographic Institution, Woods Hole.

Manganini, S.J., Chandler, C., Honjo, S., 2003. Global data base of export production measured by TS-traps since 1983. US JGOFS Website, JGOFS Office. WWW Page, <http://usjgofs.whoi.edu/mzweb/data/sed_traps.html>. Woods Hole Oceanographic Institution, Woods Hole.

Marshall, S.M., Orr, A.P., 1972. The Biology of a Marine Copepod. Springer-Verlag, Berlin, New York.

Martin, J.H., Knauer, G.G., Karl, D.M., Broenkow, W.W., 1987. VERTEX: carbon cycling in the northeast Pacific. Deep Sea Research 34, 267–285.

Matsueda, H., Handa, N., Inoue, I., Takano, H., 1986. Ecological significance of salp fecal pellets collected by sediment traps in the eastern north Pacific. Marine Biology 91, 421–431.

McCave, I.N., Hall, I.R., Antia, A.N., Chou, L., Dehairs, F., Lampitt, R.C., Thomsen, L., van Weering, T.C.E., Wollast, R., 2001. Distribution, composition and flux of particulate material over the European margin at 47°–50°. Deep Sea Research Part II 48, 3107–3139.

McGowan, J.A., 1971. Oceanic biogeography of the Pacific. In: Funnell, B.M., Riedel, W.R. (Eds.), The Micropaleontology of Oceans. Cambridge University Press, Cambridge, pp. 3–74.

Miller, C.B., Frost, B.W., Batchelder, H.P., Clemons, M.J., Conway, R.E., 1984. Life histories of large, grazing copepods in a subarctic ocean gyre: *Neocalanus plumchrus*, *Neocalanus cristatus*, and *Eucalanus bungii* in the Northeast Pacific. Progress in Oceanography 13, 201–243.

Millero, F.J., Lee, K., Roche, M., 1998a. Distribution of alkalinity in the surface waters of the major oceans. Marine Chemistry 60, 111–130.

Millero, F.J., Degler, E.A., O'Sullivan, D.W., Goyet, C., Eischeid, G., 1998b. The carbon dioxide system in the Arabian Sea. Deep Sea Research Part II 45, 2225–2252.

Milliman, J.D., 1974. Marine Carbonates. Springer-Verlag, New York.

Milliman, J.D., 1993. Production and accumulation of calcium carbonate in the ocean: budget of a nonsteady State. Global Biogeochemical Cycles 7, 927–957.

Milliman, J.D., 1995. Sediment discharge to the ocean from small mountainous rivers: the New Guinea example. Geo-Marine Letters 15 (3–4), 126–133.

Milliman, J.D., Syvitski, J.P.M., 1992. Geomorphic/tectonic control of sediment discharge to the ocean: the importance of small mountainous rivers. Journal of Geology 100, 520–540.

Milliman, J.D., Manheim, F.T., Pratt, R.M., Zarudzki, E.F.K., 1967. Alvin dives on the continental margin off the Southwestern United States, July 2–13, 1967. Technical Report, Woods Hole Oceanographic Institution, 67-80, Woods Hole, MA, 64 pp.

Milliman, J.D., Troy, P.J., Balch, W.M., Adams, A.K., Li, Y.H., Mackenzie, F.T., 1999. Biologically mediated dissolution of calcium carbonate above the chemical lysocline? Deep Sea Research Part I 46, 1653–1669.

Miquel, J.C., Fowler, S.W., La Rosa, J., Buat-Ménard, P., 1994. Dynamics of the downward flux of particles and carbon in the open northwestern Mediterranean Sea. Deep Sea Research Part I 41, 243–261.

Mohan, R., Verma, K., Mergulhao, L.P., Sinha, D.K., Shanvas, S., Guptha, M.V.S., 2006. Seasonal variation of pteropods from the Western Arabian Sea sediment trap. Geo-Marine Letters 26, 265–273.

Monaco, A., Courp, T., Heussner, S., Carnonne, J., Fowler, S.W., Deniaux, B., 1990. Seasonality and composition of particulate fluxes during ECOMARGE-I, western Gulf of Lions. Continental Shelf Research 10, 959–987.

Mortlock, R.A., Froelick, P.N., 1989. A simple method for the rapid determination of biogenic opal in pela SGIC marine sediments. Deep Sea Research 36, 1425–1426.

Murray, J.W., Johnson, E., Garside, C., 1995. A US JGOFS process study in the Equatorial Pacific (EqPac): introduction. Deep Sea Research Part II 42, 275–293.

Nair, R.R., Ittekkot, V., Manganini, S.J., Ramaswamy, V., Haake, B., Degens, E.T., Desai, B.N., Honjo, S., 1989. Increased particle flux to the deep ocean related to monsoons. Nature 338, 749–751.

National Astronomical Observatory, Japan, 2006. Diel migration of marine zooplankton (Table 6.4.6., p. 182). In: Anon. (Ed.), Chronological Scientific, Environment, Maruzen, Tokyo, 373 pp.

Nelson, D.M., Tréguer, P., Brzezinski, M.A., Leynaert, A., Queguiner, B., 1995. Production and dissolution of biogenic silica in the ocean: revised global estimated, comparison with regional data and relationship to biogenic sedimentation. Global Biogeochemical Cycle 9, 359–372.

Neuer, S., Ratmeyer, D., Davenport, R., Fischer, G., Wefer, G., 1997. Deep water particle flux in the Canary Island region: seasonal trends in relation to long-term satellite derived pigment data and lateral sources. Deep Sea Research Part I 44, 1451–1466.

Noriki, S., Tsunogai, S., 1986. Particulate fluxes and major components of settling particles from sediment trap experiments in the Pacific Ocean. Deep Sea Research 33, 903–912.

Noriki, S., Iyoda, K., Sasaki, K., 1997. Biogenic particle flux in the western North Pacific. In: Tsunogai, S. (Ed.), Biogeochemical Processes in the North Pacific. Japan Marine Science Foundation, Tokyo, pp. 256–261.

Norris, R.E., 1971. Extant calcareous nannoplankton from the Indian Ocean. In: Farinacci, A. (Ed.), Proceedings of the Second Plankton Conference. Tecnoscineza, Roma, pp. 899–910.

Nöthig, E.-M., Shevchenko, V., 2004. Laptev Sea and Lomonosov Ridge. In: Stein, E., Macdonald, R.W. (Eds.), The Organic Carbon Cycles in the Arctic Ocean. Springer, Berlin, pp. 117–118.

Nozaki, Y., 1989. Radionuclide fluxes obtained by the recent successful deployment of super-deep time-series sediments. Kaiyo Kenkyu 21, 187–191.

Nozaki, Y., Oba, T., 1995. Dissolution of calcareous tests in the ocean and atmosphere carbon dioxide. In: Sakai, H., Nozaki, Y. (Eds.), Biogeochemical Processes and Ocean Flux in the Western Pacific. Terra Scientific Publishing, Tokyo, pp. 83–92.

O'Brien, M.C., Macdonald, R.W., Melling, H., Iseki, K., 2006. Particle fluxes and geochemistry of Canadian Beaufort Shelf: importance for sediment transport and deposition. Continental Shelf Research 26, 41–81.

Okada, H., Honjo, S., 1973. The distribution of oceanic coccolithophorids in the Pacific. Deep Sea Research 20, 335–374.

Okada, H., McIntyre, A., 1979. Seasonal distribution of modern coccolithophores in the Western North Atlantic Ocean. Marine Biology 54, 319–328.

Olafsson, J., Ostermann, D.R., Curry, W.B., 2001. Unpublished.

Orr, W.N., Conley, S., 1976. Siliceous dinoflagellates in the northeast Pacific rim. Micropaleontology 22, 92–99.

Pena, M.A., Denman, K.L., Calvert, S.E., Thomson, R.E., Forbes, J.R., 1999. The seasonal cycle in sinking particle fluxes off Vancouver Island, British Columbia. Deep Sea Research Part II 46, 2969–2992.

Pestana, H., 1985. Carbonate sediment production by *Sargassum* epibionts. Journal of Sedimentary Petrology 55, 184–186.

Peterson, M.L., Wakeham, S.G., Lee, C., Meaghan, A.A., Miquel, J.C., 2005. Novel technique for collection of sinking particles in the ocean and determining their settling rates. Limnology and Oceanography, Methods 3, 520–532.

Pilskaln, C.H., 2004. Seasonal and interannual particle export in an African Rift Valley Lake: a five-year record from Lake Malawi, southern East Africa. Limnology and Oceanography 49, 964–977.

Pilskaln, C.H., Honjo, S., 1987. The fecal pellet fraction of biogeochemical particle fluxes to the deep-sea. Global Biogeochemical Cycles 1, 31–48.

Pilskaln, C.H., Neumann, A.C., Bane, J.M., 1989. Periplatform carbonate flux in the northern Bahamas. Deep Sea Research 36, 1392–1406.

Pilskaln, C.H., Paduan, J.B., Chavez, F.P., Anderson, R.Y., Berelson, W.M., 1996. Carbon export and regeneration in the coastal upwelling system of Monterey Bay, central California. Journal of Marine Research 54, 1149–1178.

Pilskaln, C.H., Lehmann, C., Paduan, J.B., Silver, M.W., 1998. Spatial and temporal dynamics in marine aggregate abundance, sinking rate and flux: Monterey Bay, central California. Deep Sea Research Part II 45, 1803–1837.

Pilskaln, C.H., Manganini, S.J., Trull, T.W., Armand, L., Howard, W., Asper, V.L., Massom, R., 2004. Geochemical particle fluxes in the Southern Indian Ocean seasonal ice zone: Prydz Bay region, East Antarctica. Deep Sea Research Part I 51, 307–332.

Prospero, J.M., 1996. The atmospheric transport of particles to the ocean. In: Ittekkot, V., Schäfer, P., Honjo, S., Depetris, P.J. (Eds.), Particle Flux in the Ocean. John Wiley & Sons, New York, pp. 19–52.

Ramaswamy, V., Gaye, B., 2006. Regional variations in the fluxes of foraminifera carbonate, coccolithophorid carbonate and biological opal in the northern Indian Ocean. Deep Sea Research Part I 53, 271–293.

Ratmeyer, V., Fischer, G., Wefer, G., 1999. Lithogenic particle fluxes and grain size distributions in the deep ocean off northwest Africa: implications for seasonal changes of aeolian dust input and downward transport. Deep Sea Research I 46, 1289–1337.

Rea, D.K., 1994. The paleoclimatic record provided by Eolian deposition in the deep-sea – the geologic history of wind. Reviews of Geophysics 32, 159–195.

Sabine, C.L., Feely, R.A., Gruber, N., Key, R.M., Lee, K., Bullister, J.L., Wanninkhof, R., Wong, C.S., Wallace, D.W.R., Tilbrook, B., Millero, F.J., Peng, T.H., Kozyr, A., Ono, T., Rios, A.F., 2004. The oceanic sink for anthropogenic CO_2. Science 305, 367–371.

Saito, C., Noriki, Y., Kodama, Y., Nozaki, Y., 1997. Fluxes of settling particles in the Japan Trench. In: Tsunogai, S. (Ed.), Biogeochemical Processes in the North Pacific. Japan Marine Science Foundation, Tokyo, pp. 270–276.

Sakshaug, E., 2004. Primary and secondary production in the Arctic Seas. In: Stein, E., Macdonald, R.W. (Eds.), The Organic Carbon Cycles in the Arctic Ocean. Springer, Berlin, pp. 57–81.

Sambrotto, R.N., Savidge, G., Robinson, C., Boyd, P., Takahashi, T., Karl, D.M., Langdon, C., Chipman, D., Marra, J., Godispoti, L., 1993. Elevated consumption of carbon relative to nitrogen in the surface ocean. Nature 363, 250–284.

Sarmiento, J.L., Gruber, N., Brzezinski, M.A., Dunne, J.P., 2004. High-latitude controls of thermocline nutrients and low latitude biological productivity. Nature 427, 56–60.

Schäfer, P., Ittekkot, V., Bartsch, M., Nair, R.R., Tiemann, J., 1996. Fresh water influx and particle flux variability in Bay of Bengal. In: Ittekkot, V., Schäfer, P., Honjo, S., Depetris, P.J. (Eds.), Particle Flux in the Ocean. John Wiley & Sons, New York, pp. 217–292.

Scholten, J.C., Fietzke, J., Vogler, S., Loeff, M.M.R., Mangini, A., Koeve, W., Waniek, J., Stoffers, P., Antia, A., Kuss, J., 2001. Trapping efficiencies of sediment traps form the deep eastern North Atlantic: the ^{230}Th calibration. Deep Sea Research Part II 48, 2383–2408.

Shanks, A.L., Trent, J.D., 1980. Marine snow: sinking rates and potential role in vertical flux. Deep Sea Research 27, 137–144.

Siegel, D.A., Deuser, W.G., 1997. Trajectories of sinking particles in the Sargasso Sea: modeling of statistical funnels above deep-ocean sediment traps. Deep Sea Research Part I 44, 1519–1541.

Silver, M.W., Gowing, M.M., 1991. The "particle" flux: origins and biological components. Progress in Oceanography 26, 75–113.

Small, L.F., Fowler, S.W., Unlu, M.L., 1979. Sink rates of natural copepod fecal pellets. Marine Biology 51, 233–241.

Smayda, T.J., 1971. Normal and accelerated sinking of phytoplankton in the sea. Marine Geology 11, 105–122.

Smith, K.L., Kaufmann, R.S., 1999. Long-term discrepancy between food supply and demand in the deep eastern north Pacific. Science 284, 1174–1177.

Smith, D.C., Simon, M., Alldredge, A.L., Azam, F., 1992. Intense hydrolytic enzyme activity on marine aggregates and implications for rapid particle dissolution. Nature 539, 139–142.

Smith, S.L., Codispoti, L.A., Morrison, J.M., Barber, R.T., 1998. The 1994–1996 Arabian Sea Expedition: an integrated, interdisciplinary investigation of the response of the northwestern Indian Ocean to monsoonal forcing. Deep Sea Research Part II 45, 1905–1915.

Smith, W.O., Anderson, R.F., Moore, K., Codispoti, L.A., Morrison, J.M., 2000. The US Southern ocean joint global ocean flux study: an introduction to AESOPS. Deep Sea Research Part II 47, 3073–3093.

Smith, K.L., Baldwin, R.J., Ruhl, H.A., Kahru, M., Mitchell, B.G., Kaufmann, R.S., 2006. Climate effect on food supply to depths greater than 4,000 meters in the northeast Pacific. Limnology and Oceanography 51, 166–176.

Staresenic, N., Farrington, J., Gagosian, R., Clifford, C.H., Hulbert, E.M., 1983. Downward transport of particulate matter in the Peru coastal upwelling: role of the anchoveta, *Engraulis ringense*. In: Suess, E., Thiede, J. (Eds.), Coastal Upwelling: It's Sediment Record. Part A: Responses of the Sedimentary Regime to Present Coastal Upwelling. Plenum Press, New York, pp. 225–241.

Stein, R., Macdonald, R.W., 2004. The organic carbon cycles in the arctic ocean. Springer, Berlin, pp. 363.

Steinberg, D.K., Goldthwait, S.A., Hansell, D.A., 2002. Zooplankton vertical migration and the active transport of dissolved organic and inorganic nitrogen in the Sargasso Sea. Deep Sea Research I 49, 1445–1461.

Steinmetz, J.C., 1991. Calcareous nannoplankton biocoenosis: sediment trap studies in the Equatorial Atlantic, Central Pacific, and Panama Basin. In: Honjo, S. (Ed.). Ocean Biocoenosis, Series 1. Marine Biological Laboratory Publishing, Woods Hole, pp. 1–85.

Suess, E., 1980. Particulate organic carbon flux in the oceans – surface productivity and oxygen utilization. Nature 288, 260–262.

Suzuki, N., Kato, K., 1953. Studies on suspended materials. Marine snow in the sea, part 1. Source of marine snow. Bulletin of the Faculty of Fisheries, Hokkaido University 4, 132–135.

Swift, J.H., 1986. The Arctic Waters. In: Hurdle, B.G. (Ed.), The Nordic Seas. Springer-Verlag, New York, pp. 129–153.

Takahashi, T., 1975. Carbonate chemistry of sea water and the calcite compensation depth in the oceans. In: Sliter, W.V., Bé, A.H., Berger, W.H. (Eds.), Dissolution of Deep-Sea Carbonates. Cushman Foundation Foraminifera Research, Special Publication, vol. 13, Washington, DC, pp. 11—26.

Takahashi, K., 1991a. Radiolaria: flux, ecology, and taxonomy in the Pacific and Atlantic. In: Honjo, S. (Ed.), Ocean Biocoenosis, Series 3. Marine Biological Laboratory Publishing, Woods Hole, pp. 1–303.

Takahashi, K., 1991b. Silicoflagellates and Actiniscus: vertical fluxes at Pacific and Atlantic sediment trap stations. In: Honjo, S. (Ed.), Ocean Biocoenosis, Series 2. Marine Biological Laboratory Publishing, Woods Hole, pp. 1–35.

Takahashi, T., 2004. The fate of industrial carbon dioxide. Science 305, 352–353.

Takahashi, K., Bé, A.W.H., 1984. Planktonic foraminifera: factors controlling sinking speeds. Deep Sea Research 31, 1477–1500.

Takahashi, K., Fujitani, N., Yanada, M., Maita, Y., 1997. Five year long particle fluxes in the Central Subarctic Pacific and the Bering Sea. In: Tsunogai, S. (Ed.), Biogeochemical Processes in the North Pacific. Japan Marine Science Foundation, Tokyo, pp. 249–255.

Takahashi, K., Fujitani, N., Yanada, M., Maita, Y., 2000. Long-term biogenic particle fluxes in the Bering Sea and the central subarctic Pacific Ocean, 1990–1995. Deep Sea Research Part I 47, 1723–1759.

Talley, L., 2003. Shallow, intermediate, and deep overturning components of the global head budget. Journal of Physical oceanography 33, 530–560.

Tanioka, Y., Ruff, L., Satake, K., 1996. The Sanriku-Oki, Japan, Earthquake of December 28, 1994 (Mw 7.7): Rupture of different asperity from a previous earthquake. Geophysical Research Letters 23, 1465–1468.

Tegen, I., Fung, I., 1994. Modeling of mineral dust in the atmosphere: sources, transport, and optical thickness. Journal of Geophysical Research 99, 22897–22914.

Thomsen, H.A., Buck, K.R., Coale, S.L., Garrison, D.L., Gowing, M.M., 1988. Nonnoplanktonic coccolithophorids (Prymnesiophyceae, Haptophyceae) from the Weddell Sea, Antarctica. Nordic Journal of Botany 8, 418–436.

Thunell, R., 1998a. Particle fluxes in a coastal upwelling zone: sediment trap results from Santa Barbara Basin, California. Deep Sea Research Part II 45, 1863–1884.

Thunell, R., 1998b. Seasonal and annual variability in particle fluxes in the Gulf of California: a response to climate forcing. Deep Sea Research Part I 45, 2059–2083.

Thunell, R., Pilskaln, C.H., Tappa, E., Sautter, L.R., 1994. Temporal variability in sediment fluxes in the San-Pedro Basin, Southern-California Bight. Continental Shelf Research 14, 333–352.

Thunell, R., Varela, R., Llano, M., Collister, J., Muller-Karger, F., Bohrer, R., 2000. Organic carbon fluxes, degradation, and accumulation in an Anoxic Basin: sediment trap results from the Cariaco Basin. Limnology and Oceanography 45, 300–308.

Thunell, R., Benitez-Nelson, C., Varela, R., Aster, Y., Muller-Karger, F., 2007. Particulate organic carbon fluxes along upwelling-dominated continental margins: rates and mechanisms. Global Biogeochemical Cycle 21, 1–12 (GB1029).

Tréguer, P., 2003. Unpublished.

Tréguer, P., Jaques, G., 1992. Dynamics of nutrients and phytoplankton, and fluxes of carbon, nitrogen and silicon in the Antarctic Ocean. Polar Biology 12, 149–162.

Tréguer, P., Nelson, D.M., Van Bennekom, A.J., DeMaster, D.J., Leynaert, A., Quéguiner, B., 1995. The silica balance in the world ocean: a re-estimate. Science 268, 375–379.

Trull, T.W., Bray, S.G., Manganini, S.J., Honjo, S., Francois, R., 2001. Moored sediment trap measurements of carbon export in the Subantarctic and Polar Frontal Zones of the Southern Ocean, south of Australia. Journal of Geophysical Research 106, 31489–31509.

Tsubota, H., Ishizuka, J., Nishimura, A., Watanabe, Y.W., 1999. Overview of NOPACCS (Northwest pacific Carbon Cycles Study). Journal of Oceanography 55, 645–653.

Tsujita, T., 1953. Studies on naturally occurring suspended organic matter in waters adjacent to Japan (II). On an application of suspended organic matters. Records of Oceanographic Works in Japan 2, 94–100.

Tsunogai, S., Noriki, S., 1987. Organic matter fluxes and the sites of oxygen consumption in deep water. Deep Sea Research 34, 755–767.

Urban-Rich, J.L., 1999. Release of dissolved organic carbon from copepod fecal pellets in the Greenland Sea. Journal of Experimental Marine Biology and Ecology 232, 124–197.

Urban-Rich, J.L., Hansell, D.A., Roman, M.R., 1998. Analysis of copepod fecal pellet carbon using a high temperature combustion method. Marin Ecology Progress Series 171, 199–208.

Usbeck, R., Schlitzer, R., Fischer, G., Wefer, G., 2003. Particle fluxes in the ocean: comparison of sediment trap data with results from inverse modeling. Journal of Marine Systems 39, 167–183.

US JGOFS Planning Committee, 1989. Sediment trap technology and sampling. US JGOFS Planning Report, No. 10. Woods Hole Oceanographic Institution, Woods Hole, 94 pp.

Vinogradov, M.E., 1961. Food sources of the deep-water fauna. Speed of decomposition of dead Pteropoda. Doklady of the Academy of Sciences, USSR, Oceanology Section, pp. 136–141 and 39–42.

Vinogradov, M.E., 1972. Vertical Migration of the Oceanic Plankton. Israel Program for Scientific Translations, Jeruselem.

Vinogradov, M.E., Tseitlin, V.B., 1983. Deep-sea pelagic domain (aspects of bioenergetics). In: Rowe, G.T. (Ed.), Deep-Sea Biology. John Wiley & Sons, New York, pp. 123–165.

Volk, T., Hoffert, M.I., 1985. Ocean carbon pumps: analysis of relative strength and efficiencies of in ocean-driven circulation atmospheric CO_2 changes. In: Sundquist, E.T., Broecker, W.S. (Eds.), The Carbon Cycle and Atmospheric CO_2: Natural Variation Archean to Present: AGU Monograph 32. American Geophysical Union, Washington, DC, pp. 99–110.

von Bodungen, B., Fischer, G., Nöthig, E.M., Wefer, G., 1987. Sedimentation of krill faces during spring development of phytoplankton in Bransfiled Strait, Antarctica. In: Degens, E.T., Izdar, E., Honjo, E. (Eds.), Particle Flux in the Ocean, SCOPE/UNEP vol. 62, pp. 243–257, University of Hamburg.

von Bodungen, B., Antia, A., Bauerfeind, E., Haupt, O., Reitmeier, S., Thomsen, C., Voss, M., Wunch, M., Zeller, U., Zeitzschel, B., 1995. Pelagic processes and vertical flux of particles: an overview of a long-term comparative study in the Norwegian Sea and Greenland Sea. Geologische Rundschau 84, 11–27.

Walsh, I.D., Gardner, D., 1992. A comparison of aggregate profiles with sediment trap fluxes. Deep Sea Research 39, 1817–1834.

Walsh, I.D., Gardner, W.D., Richardson, M.J., Chung, S.P., Plattner, C.A., Asper, V.L., 1997. Particle dynamics as controlled by the flow field of the eastern equatorial Pacific. Deep Sea Research II 44, 2025–2047.

Wattenberg, H., 1992. Atlas of the dissolved oxygen content of the Atlantic Ocean. Scientific results of the German Atlantic Expedition of the Research Vessel Meteor, 1925–27, vol. 9 – Atlas. Translated from German by National Science Foundation, OCE/NSF 85-00-002. Amerind Publishing Co.

Wefer, G., Fischer, G., 1988. Seasonal particle flux in the Bransfield Strait (Antarctica). Deep Sea Research 35, 891–898.

Wefer, G., Fischer, G., 1991. Annual primary production and export flux in the Southern Ocean from sediment trap data. Marine Chemistry 35, 599–613.

Wefer, G., Fischer, G., 1993a. Annual primary productivity and export flux in the Southern Ocean from sediment trap data. Marine Chemistry 35, 597–613.

Wefer, G., Fischer, G., 1993b. Seasonal patterns of vertical particle flux in equatorial and coastal upwelling areas of the eastern Atlantic. Deep Sea Research Part I 40, 1613–1645.

Wefer, G., Honjo, S., 1985. Seasonal particle flux in the Lofoten Basin, Norwegian Sea. Terra Cognita 5, 90.

Wefer, G., Suess, E., Balzer, W., Liebezeit, G., Muller, P.J., Ungerer, C.A., Zenk, W., 1982. Fluxes of biogenic components from sediment trap deployment in circumpolar waters of the Drake Passage. Nature 299, 145–147.

Wefer, G., Fischer, G., Fütterer, D.K., Gersonde, R., Honjo, S., Ostermann, D., 1990. Particle sedimentation and productivity in Antarctic Waters of the Atlantic Sector. In: Bleil, U., Thiede, J. (Eds.), Geological History of the Polar Oceans: Arctic Versus Antarctic. Kluwer Academic Publishers, pp. 363–379.

Wiebe, P.H., Boyd, S., Cox, J.L., 1975. Relationships between Zooplankton Displacement Volume, Wet Weight, Dry Weight. Carbon Fishery Bulletin 73, 777–786.

Wiebe, P.H., Madin, L., Haury, L., Harbison, G.R., Philbin, L., 1979. Diel vertical migration by salpa-aspera and its potential for large-scale particulate organic matter transport to the deep-sea. Marine Biology 53, 249–255.

Wiesner, M.G., Zheng, L., Wong, H.K., Wang, Y., Chen, W., 1996. Fluxes of particulate matter in the South China Sea. In: Ittekkot, V., Schäfer, P., Honjo, S., Depetris, P.J. (Eds.), Particle Flux in the Ocean. John Wiley & Sons, New York, pp. 293–312.

Williams, P.J.leB., 1995. Evidence for the seasonal accumulation of carbon rich dissolved organic material, its scale in comparison with changes in particulate material and the consequential effect on the net C/N assimilation ratios. Marine Chemistry 51, 17–29.

Wilson, S.E., Steinberg, D.K., Buesseler, K.O., 2006. Changes in fecal pellet characteristics with depths indicators of zooplankton repacking of particles in the mesopelagic zone. EOS, American Geophysical Union 87, 36.

Wishner, K.F., 1980. The biomass of deep-sea benthopelagic palankton. Deep Sea Research 27, 203–216.

Wollast, R., Chou, L., 2001. Ocean margin exchange in the Northern Gulf of Biscay: OMEX I. An introduction. Deep Sea Research Part II 49, 2971–2978.

Wong, C.S., Whitney, F.A., Tsoy, I., Bychkov, A., 1994. Opal pump and subarctic carbon removal. In: 1994 Sapporo IGBP Symposium (extended abstract), Sapporo.

Wong, C.S., Whitney, F.A., Crawford, D.W., Iseki, K., Matear, R.J., Johnson, W.K., Page, J.S., Timothy, D., 1999. Seasonal and interannual variability in particle fluxes of carbon, nitrogen and silicon from time series of sediment traps at Ocean Station P, 1982–1993: relationship to changes in subarctic primary productivity. Deep Sea Research Part II 46, 2735–2760.

Yang, T-N., Wei, K-Y., 2003. How many coccoliths are there in a coccosphere of the extant coccolithophorids? A compilation. Journal of Nanoplankton Research 25, 7–15.

Yoder, J.A., Ackleson, S.G., Barber, R.T., Flament, P., Balch, W.M., 1994. A Line in the Sea. Nature 371, 689–692.

Yu, E., Francois, R., Bacon, M., Honjo, S., Fleet, A., Manganini, S., Rutgers, M., Ittekkot, V., 2001. Trapping efficiency of bottom-tethered sediment traps estimated from the intercepted fluxes of ^{230}Th and ^{231}Pa. Deep Sea Research Part I 48, 865–889.

Zernova, V.V., Nöthig, E.-M., Shevchenko, V.P., 2000. Vertical microalgae flux in the northern Laptev Sea (from the data collected by the year-long sediment trap). Oceanology 40, 801–808.

Zhang, X., Dam, H.G., 1997. Downward export of carbon by migrant mesozooplankton in the central equatorial Pacific. Deep Sea Research Part II 44, 2192–2202.

Ziveri, P., Broerse, A.T.C., van Hinte, J.E., Honjo, S., 2000. The fate of coccoliths at 48°N 21°W, Northeastern Atlantic. Deep Sea Research Part II 47, 1853–1875.